Efficient and High-fidelity Finite Element Models for Fibre Composites

by

Qian Zhang

A thesis submitted in conformity with the requirements
for the degree of Doctor of Philosophy
Graduate Department of Aerospace Science and Engineering
University of Toronto

Abstract

Efficient and High-fidelity Finite Element Models for Fibre Composites

Qian Zhang
Doctor of Philosophy
Graduate Department of Aerospace Science and Engineering
University of Toronto
2019

Fibre reinforced composites are widely used as structural components in the aerospace industry. The fabrication of highly tailored fibre composite structures is enabled by advanced composite manufacturing methods, such as Automated Fibre Placement (AFP). AFP enables fibre tows to be placed at arbitrary fibre orientations, either straight or curved, and the local tailoring of composite properties significantly improves the mechanical performance. The conventional finite element approaches assume that the curved fibres are locally straight, and many small elements are needed to model the curved fibres accurately. This increases the computational expense of gradient-based fibre angle optimization as it requires repeated evaluations of the finite element model of the composite. Therefore, the goal of this research is to establish an accurate finite element (FE) model with good computational efficiency for composite structures with complex fibre configurations to be used for gradient-based optimization.

In this work, a novel finite element approach that enables the use of larger elements with the desired level of accuracy is formulated for a single-layer thin composite lamina with curved fibres. Fewer elements make the FE analysis more efficient as the dimension of the global stiffness matrices is reduced. The element model represents the real physical system more accurately, as the Gauss quadrature process is modified to capture the stiffness change caused by the fibre curvature in the calculation of element stiffness matrices. As a function of the orientation of fibres in adjacent elements, fibre curvature is calculated by minimizing the fibre discontinuity between adjacent elements given their average fibre orientation. This is a least square minimization problem and solved through

its normal equation. Finally, stiffness maximization for the single-layer thin composite lamina is performed using a gradient descent algorithm integrated with the finite element formulation with explicit fibre curvature. The fibre curvature is an intermediate variable to the objective function, and the total derivative of the objective function with respect to fibre orientation is calculated analytically using the adjoint method. The optimal solutions show that this new method gives the same results as optimization using conventional finite elements, but has much faster convergence.

Acknowledgements

I would like to give my sincerest gratitude to Professor Craig Steeves for his continuous support, help, and guidance in completing this thesis work. It was an invaluable opportunity and experience to work with him.

I would also like to thank the members of my DEC committee, Professor Prasanth Nair and Professor Jonathan Kelly for reviewing my thesis work and providing me with constructive feedback.

I would like to thank my parents and sister for their endless support on pursuing my goal. I can always feel their love and encouragement from thousand miles away. Thank you for believing in me and supporting me in numerous ways to accomplish another one of my dreams.

Last, but not least, thank my colleagues in the Advanced Aerospace Structures Lab, as well as other UTIAS friends, who have not only provided help when I've needed it but also for their warm friendship, and for making the studying environment full of enjoyment.

Contents

1 Introduction **1**

1.1 Motivation 1

1.2 Finite Element Formulation for Composite Laminates with Curved Fibres . . 3

1.2.1 Finite Element Formulation 3

1.2.2 Mesh Convergence for Composite Laminates with Curved Fibres . . 6

1.3 Parametrization of the Fibre Arrangement 8

1.4 Optimization of Composite Laminates with Curved Fibres 10

1.4.1 Topology Optimization 11

1.4.2 Fibre Angle Optimization 12

1.4.2.1 Conventional Composite Laminates 12

1.4.2.2 Composite Laminates with Curved Fibres 13

1.5 Thesis Layout 15

2 Interlayer Slip between Curved Fibres **19**

2.1 Introduction 19

2.2 Effective Axial Stiffness of A Two-layered Curved Beam 20

2.2.1 Interlayer Slip 20

2.2.2 Derivation of the Effective Axial Stiffness 22

2.3 Analytical Solution and Finite Element Verification 24

2.4 Concluding Remarks 27

3 Finite Element with Curved Fibres **29**

3.1 Introduction 29

3.2 Averaged Compliance Method 31
3.2.1 Element Verification 34
3.3 Finite Element with Explicit Fibre Curvature 38
3.3.1 Element Verification 41
3.4 Concluding Remarks 50

4 Curvature Generation **52**
4.1 Introduction 52
4.2 Analytical Expression for Fibre Angles in an Element 54
4.3 Calculation of Curvatures 56
4.3.1 Steepest Descent Method 57
4.3.2 The Normal Equation 59
4.3.3 Physical Interpretation of The Tolerance in The Pseudoinverse Calculation 61
4.4 Verification of The Calculation of Curvature 63
4.5 Concluding Remarks 72

5 Stiffness Optimization **74**
5.1 Introduction 74
5.2 Maximum Stiffness Design 76
5.3 Results 81
5.4 Concluding Remarks 92

6 Conclusions **94**
6.1 Contributions 96
6.2 Future Research Directions 96

List of Tables

3.1 The maximum relative error of the horizontal displacement on path A-B for the square region containing sinusoidal fibres between the three FE methods and the exact solution 42

5.1 Summary of the optimization results for the L- and T-shaped structures. The star sign denotes the compliance obtained by calculating the curvatures based on the optimized fibre orientations in the conventional optimization, and running the finite element with explicit curvature on the same mesh. 91

List of Figures

1.1 Definition of fibre orientation angle. (a) The fibres in an element are aligned parallel to the x- axis; (b) The global $x-y$ coordinate system rotates with an angle θ to a local $x'-y'$ coordinate system. The angle θ is the fibre orientation; (c) The x'-axis of the local $x'-y'$ coordinate system is the tangent line of the curved fibre. The radius of curvature is ρ and the fibre curvature $\kappa = 1/\rho$. . 4

1.2 A 1×1 single composite lamina with sinusoidal curved fibres. The fibre angle in the element centre is assigned as the orientation. The orientations vary due to variations both in mesh size and in position. The conventional finite element method is used to calculate the displacement on the right edge of the plate. 7

1.3 The strain energy of the plate with respect to the number of elements. The strain energy oscillates first as the number of elements increases, but eventually approaches convergence around 100 elements. 7

1.4 Flowchart of the gradient-based optimization for stiffness maximization of a thin single-layer composite lamina with curved fibres. Given an initial fibre configuration, the fibre curvature is generated by minimizing the discontinuity between elements. The finite element with explicit fibre curvature is formulated for the structure analysis and sensitivity analysis. Then the gradient of the objective function is calculated. The fibre orientation angles are updated and the values of objective function are recalculated until the convergence criterion is satisfied. 15

2.1 An initially curved beam as a circular arc: (a) geometry and coordinate system and (b) an infinitesimal element. The curved beam is fixed at two horizontal points A and B. Point A is constrained by a pinned boundary condition and point B is subjected to an axial load, P, while its vertical displacement is zero. The solid and dashed line represent the beam before and after deformation, respectively. f is the shear force between two beams. a and a_T are tangent angles at point A before and after deformation, respectively. 22
2.2 The finite element model of a three-layer simply supported curved beam. Layer 1 and 2 represent the single fibres or the fibre tows, and the thin layer between them is the resin. Both the geometric size of single fibres and fibre tows are tested in this FE model. 25
2.3 Analytical and FE solution for the stiffness of pairs of fibres or pairs of fibre tows as a function of the initial curvature. The effective stiffness of the three-layer curved beam system decreases as the initial curvature increases. The curvature greatly influences the compliance of the beam system. 26
2.4 Analytical and FE solution for the effective stiffness as a function of the slip modulus. The interlayer slip between fibre has little influence on the effective stiffness of two-layered curved beam. 27

3.1 A reference fibre path in a square element with curved fibres. The curve is the reference fibre path, which starts from the left edge and ends at the right edge. θ_0 and θ_1 are the orientation angle on the left and right edge, respectively. The orientation angle $\theta(x)$ is the angle between the x-axis and the tangent line to an arbitrary point on the path. 32
3.2 Geometric model of a curved fibre plate. The left edge of the plate is fixed, and the right edge is subjected to a uniform tensile distributed load, F=50000. The orientation angles at the left and right edges are $\frac{\pi}{10}$ and $-\frac{\pi}{10}$. Path A-B is the right edge of the plate. 35

3.3 Contour of the horizontal displacement from the Abaqus simulation. The blue and red color represents the minimum and maximum horizontal displacement on this plate. 36
3.4 Convergence of the Abaqus simulation for the displacement on path A-B. Three meshes, 160 (20×8), 640 (40×16) and 2560 (80×32) elements are used. The displacement on path A-B approaches convergence at the mesh of 2560 elements, which can be considered as the exact solution. 36
3.5 Comparison of displacement on path A-B of the exact solution, ACM (40 elements), conventional FE (40 and 160 elements). 38
3.6 A typical 8-node quadrilateral element in the natural coordinate system (ξ, η). The vector of element degrees of freedom is $d = (u_1, w_1, u_2, w_2, \cdots, u_8, w_8)^T$. The shape function N_1, N_2, $\cdots$, N_8 for this element in natural coordinates are given in Eq. (3.16). The red circles in the element are Gauss points. 40
3.7 1×1 square plate containing fibre with path defined by the sinusoidal curve $\theta = \sin(\pi x)$ and comparison of horizontal displacement from the Abaqus simulation, S8 CFE with 5 elements×5 elements, S8 with 5 elements×5 elements and S4 with 5 elements×5 elements on path A-B. The horizontal displacement obtained the S8 CFE is closest to the Abaqus calculation since the maximum relative error between the three finite element methods and Abaqus result are 0.4%, 1.8% and 3.8%, respectively. 43
3.8 1×1 square plate with sinusoidal curve $\theta = \sin(2\pi x)$ and comparison of horizontal displacement from the Abaqus simulation, S8 CFE with 5 elements×5 elements, S8 with 5 elements×5 elements and S4 with 5 elements×5 elements on path A-B. The horizontal displacement from S8 CFE is closest to the Abaqus convergent results since the maximum relative error between the three finite element methods and Abaqus result are 1.6%, 6.8% and 6.7%, respectively. 43

3.9 1×1 square plate with sinusoidal curve $\theta = \sin(4\pi x)$ and comparison of horizontal displacement from the Abaqus simulation, S8 CFE with 7 elements×7 elements, S8 with 7 elements×7 elements and S4 with 7 elements×7 elements on path A-B. More elements are used here as the fibre configuration is more complex. The horizontal displacement from S8 CFE is closest to the Abaqus convergent simulation since the maximum relative error between the three finite element method and Abaqus result are 0.8%, 6.9% and 6.8%, respectively. 44

3.10 Running time vs. relative error of displacement for 1×1 square plate with sinusoidal curve $\theta = \sin(\pi x)$ for three finite element method: S8 CFE, S8 and S4. The running time is the processing time of formulating the element stiffness matrix, assembling the global stiffness matrix and solving the FE equations. The numbers on each data points are the number of nodes used during the finite element process. The average relative errors are calculated based on Abaqus convergent solution using Eq. (3.20). S8 CFE is more efficient and accurate than the other two methods. 45

3.11 Running time vs. relative error of displacement of the right edge for 1×1 square plate with sinusoidal curve $\theta = \sin(2\pi x)$. 46

3.12 Running time vs. relative error of displacement of the right edge for 1×1 square plate with sinusoidal curve $\theta = \sin(4\pi x)$. 46

3.13 1×1 square plate with a set of circular concentric arcs and comparison of horizontal displacement from the Abaqus simulation, S8 CFE with 5 elements×5 elements, S8 with 5 elements×5 elements and S4 with 5 elements×5 elements on path A-B. The horizontal displacement from S8 CFE is closest to the Abaqus calculation since the maximum relative error between the three finite element method and Abaqus result are 0.1%, 0.3% and 10.5%, respectively. . 48

3.14 Running time vs. relative error of displacement for 1×1 square plate with a set of concentric arcs. The running time is the processing time of formulating the element stiffness matrix, assembling global stiffness matrix and solving FE equations. The numbers on each data points are the number of nodes used during the finite element process. The average relative errors are calculated based on Abaqus convergent solution using Eq. (3.20). 48
3.15 An L-shaped structure with top edge fixed and a point load in the middle of the right of the square hole. The contour of the horizontal displacement in Abaqus solution is in the right figure. 49
3.16 Convergence of Abaqus simulation for the displacement on path A-B. The Abaqus simulation with a mesh of 92, 368, 1472, 5888 and 9200 elements are performed, respectively. As the number of elements increases, the displacement on path A-B approaches convergence at the mesh of 9200 elements, which can be considered as the exact solution. 49
3.17 Running time vs error of displacement for an L-shaped structure with square hole. The running time is the processing time of formulating the element stiffness matrix, assembling global stiffness matrix and solving FE equations. The numbers on each data points are the number of nodes used during the FE process. The average relative errors are calculated based on Abaqus convergent solution using Eq. (3.20). 50

4.1 A geometric model of an element with curved fibres. The circular arcs represent the curved fibres and and centres of all the curved fibres are on the line L. Point O is the element centre with coordinate (0, 0) and M is an arbitrary point with coordinate (x,y). The normal vector $\boldsymbol{n}$ of line L starts at point O. The angles θ_0 and θ are between the x-axis and the tangent line of the fibre passing through the point O and M respectively. The orientation angle is between -90° and 90° . The radius of curvature is ρ and d is the distance from point M to line L. 55

4.2 Orientation angles and shared boundaries for a square region of 2 element by 2 element. The curvatures that entail the minimum discontinuity are obtained by the selection of the value of κ that minimize the angle difference between adjacent elements. It is noticed that this 2×2 region is the only case where its objective function will go to zero because the number of boundaries is same as the number of parameters. 58
4.3 Convergence for the objective function for a 2 element by 2 element region with different orientation angles. The orientation angles in element I−IV are 30°, 36°, 45° and 36°, respectively. 59
4.4 Contours of the curvature distribution obtained by the steepest descent method and the normal equation for a 10×10 square region. This region contains fibre with path defined as a set of concentric arcs. The square is meshed into 10 elements $\times$ 10 elements with straight fibres. The fibre orientations are represented as short lines. 65
4.5 Contours of curvature distribution from the analytical solution based on the trigonometric equation for the fibre paths and the numerical solution through the application of the normal equation. The square region contains fibres with paths defined by a sinusoidal function. 66
4.6 Contours of curvature distribution from analytical solution based on the quadratic equation for the fibre paths and the numerical solution through the application of the normal equation. The square region contains fibres with paths defined by a quadratic function. 67
4.7 Contour of curvature for a discretized 24×8 plate section meshed into $192(24 \times 8)$ elements. The short lines represent the fibre orientation from an optimization of eigenfrequency. 68
4.8 Geometric model of the L-shaped single-layer composite lamina. The fibre orientation in each element is same as the maximum principal stress for the relevant geometry with an isotropic material. 69
4.9 Contour of curvature and curved fibre orientations for the L-shaped structure. 69
4.10 Curved fibre orientations in the L-shaped domain using different tolerance. . 71

4.11 Plots of spatially varying curved fibres for the L-shaped structure. 71
4.12 The theoretical upper bound of curvatures generated and the actual maximum curvatures (semi-log scale) as a function of the tolerance for the L-shaped structure. 72

5.1 Flowchart of the fibre angle optimization for stiffness maximization of a thin single-layer composite lamina with curved fibres. 81
5.2 A square composite laminate with arbitrary fibre configuration. The Abaqus results on the right provide the solution of the maximum stiffness design problem for a square plate under an axial load. 83
5.3 The convergence comparison between two optimizations. Optimization B reduces the computation time by 95.3%. 84
5.4 Geometric model of the L-shaped structure. The Abaqus model uses a isotropic material and applies the same load and boundary conditions on the L-shaped structure. The maximum principal stress directions are exported and assigned as the initial fibre configuration. 86
5.5 Convergence for the stiffness maximization for the L-shaped structure using optimizations C and D. Optimization D reduces the computation time by 64.5%. 88
5.6 Fibre orientations before and after the stiffness maximization for the L-shaped composite thin plate using optimization D. The stiffness of this structure is improved by 3.9% after the optimization. 89
5.7 Geometric model of the T-shaped structure. The Abaqus model uses an isotropic material and apply the same load and boundary conditions on the T-shaped structure. Then the maximum principal stress direction are exported and assigned as the initial fibre orientation. 90
5.8 Convergence for the stiffness maximization for the T-shaped structure using optimization E and F. Optimization F reduces the computation time by 69.6%. 91
5.9 Fibre orientations before and after the stiffness maximization for the T-shaped structure using optimization F. The stiffness of this structure is improved by 5.6% after the optimization. 92

Chapter 1

Introduction

1.1 Motivation

Fibre reinforced polymer composites are widely used as structural components in the aerospace industry. They have outstanding stiffness- and strength-to-weight ratios, as well as excellent thermal properties and are highly resistant to corrosion [1]. Compared to conventional materials such as aluminum, steel or titanium, the primary benefits of composite components include reduced weight and improved design flexibility. Taking advantage of these properties, it is possible to manufacture lighter, stronger and stiffer aerospace structures.

In order to exploit the advantages of fibre composites fully, one needs to use complicated composite fibre arrangements, which allow for much greater capacity than conventional composite structures with straight fibres to tailor the structural properties both overall and locally. Complicated fibre arrangements make it possible to control the local mechanical properties of the structure and design the composite to have highly tailored structural performance such as maximum stiffness or a desirable vibrational frequency.

The major problem with using complicated composite fibre arrangements is that it is difficult to model accurately, and then use the model for optimization. If the composite model is used in an optimization scheme, it is generally necessary to evaluate the model repeatedly. The most reliable existing composite models are computationally very expensive [2–5], and hence their use for optimization is limited. Therefore, an efficient model that accurately

depicts the complicated composite fibre arrangements is necessary if such composites are to be exploited fully. The goal of this research is to establish a high-fidelity finite element model with good computational efficiency for composite structures with curved fibres, and integrate it into gradient-based fibre angle optimization.

Advanced composite manufacturing methods, such as Automated Fibre Placement (AFP) enable the fabrication of highly tailored fibre composite structures by allowing the fibre angle to vary within a single ply, so that fibres can always be in the orientation that most efficiently carries the desired loads. To achieve this, the fibres need to be curved. This is not convenient for conventional finite element approaches to composites, where the fibres are assumed to be locally straight. Many small elements are necessary to capture the overall configuration of the fibres for the accurate modeling. This increases the computational expense of gradient-based optimization as the optimization algorithm typically uses a large number of analysis iterations. The most economic way to mitigate this issue is to use fewer elements to make the FE analysis more efficient. Conventional finite elements, employing a model that assumes straight fibres within each element, experience rapid degradation in accuracy when the elements increase in size. In order to use larger elements, the element model must more accurately represent the real physical system. Hence, a finite element that accounts explicitly for the intra-element fibre curvature will be developed in this thesis.

In this work, a finite element with explicit fibre curvature is formulated for a single-layer thin composite lamina with curved fibres, which enables the use of larger elements with the desired level of accuracy. In the calculation of element stiffness matrices, the Gauss quadrature process is modified to collect information about fibre curvature rather than assigning a uniform orientation within an element. Because fibre curvature is a function of the orientation of fibres in adjacent elements, the curvature itself is not a design variable, but instead is calculated by minimizing the fibre discontinuity between adjacent elements given their average fibre orientation. This is considered as a least square minimization problem and solved through its normal equation. Finally, stiffness maximization for the single-layer thin composite lamina is performed using a gradient descent algorithm integrated with the finite element formulation with explicit fibre curvature. The sensitivity analysis is conducted using the adjoint method, so that the gradient of the objective with respect to fibre orientation is

derived analytically considering the influence of curvature. To accelerate the convergence, a good initial configuration is chosen: the initial fibre configuration in each element is orientated with the maximum principal stress for the relevant geometry with an isotropic material. The optimal solution is verified and compared to the results from gradient descent optimization using conventional finite elements.

1.2 Finite Element Formulation for Composite Laminates with Curved Fibres

1.2.1 Finite Element Formulation

Most fibre-reinforced composite materials have uniformly oriented fibres, which are placed in with a prescribed orientation angle [6]. The orientation angle is defined as an angle between the principal material axes and some reference coordinate axes, as shown in Fig. 1.1. Conventional finite element approaches are appropriate because they assume a uniform fibre orientation angle in each element. This is true for conventional composite fabrication approaches. As advanced composite manufacturing methods increase in popularity for the fabrication of complex composite structures, it becomes feasible to configure fibre tows in more desirable paths to improve the mechanical properties of the composite. An example of such technology is AFP. AFP is an automated composite manufacturing process that uses a robotic arm to place fibre tows and build a structure one ply at a time [7]. In the fibre-placement process, the fibre tows are impregnated with epoxy resin, fed to a heater and compaction roller on the fibre-placement head and placed onto a work surface as a single fibre band. This technology provides precise control of fibre orientations and makes laminates with curved fibres possible. The primary advantages of AFP include improved mechanical properties, repeatability of results, a seamless transition between design and manufacturing, and higher accuracy than manual layup. This technology enables highly tailored fibre composite structures for better performance, but inherently implies fibre curvature. Fibre curvature changes the local stiffness of the composite structure and reduces the accuracy of structural analysis using uniform orientation finite elements, unless many small elements are employed.

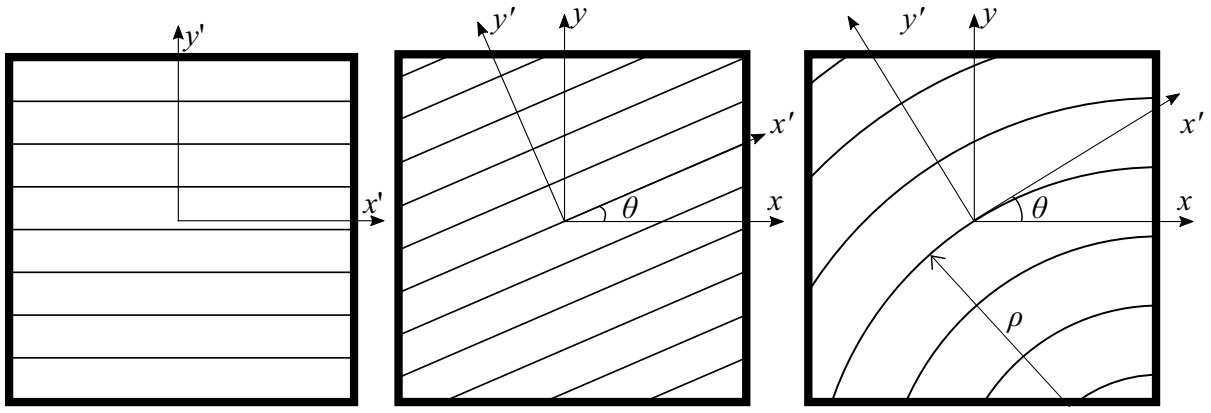

(a) An element with fibres aligned parallel to the x-axis.

(b) The fibre orientation for straight fibres.

(c) The fibre orientation for curved fibres.

Figure 1.1: Definition of fibre orientation angle. (a) The fibres in an element are aligned parallel to the x-axis; (b) The global $x-y$ coordinate system rotates with an angle θ to a local $x'-y'$ coordinate system. The angle θ is the fibre orientation; (c) The x'-axis of the local $x'-y'$ coordinate system is the tangent line of the curved fibre. The radius of curvature is ρ and the fibre curvature $\kappa = 1/\rho$.

Employing composite configurations with curved fibres can improve the mechanical properties of the composite, such as strength, stiffness and vibrational properties. The use of curved fibres in composite laminates result in the increase of the buckling load. Hyer and Charette [8] used a curvilinear fibre path near a hole in a composite laminate to study how such a design can increase the buckling capabilities. The tensile and compressive buckling loads were studied through the finite element method. Results show that the curvilinear designs improve the performance in tension. Abdalla et al. [9] also studied the effect of thermal residual stresses on the performance of laminate with curved fibres. They found that the use of curved fibres can increase the maximum buckling load, and the residual thermal stress of the curved fibre plate helps to reduce the stress resultant distribution near the centre of the plate. The buckling and first-ply failure responses were also analyzed on this same structure using Abaqus [10]. The manufacturing limits of tow-placement machines on the curved fibre panels were considered as well. It was found that tailoring the in-plane stiffness around the hole can reduce the stress concentrations, and the buckling and first-ply failure responses of the fibre-steered laminate were insensitive to the existence of a central hole.

The variation of fibre orientation in composite laminates also causes the change of natural frequencies and mode shapes. Honda and Narita [11] developed an analytical solution for the natural frequencies and vibration modes of composite laminates with curvilinear fibres.

They found that plates with curvilinear fibres give specific mode shapes that differ from the unidirectional laminates with straight fibres. Akhavan and Ribeiro [12] investigated the effects of using curvilinear fibres in laminated composite plates on the mode shapes and natural frequencies of vibration. They found that using curved fibres can change the mode shapes of vibration and may lead to a significant change in the natural frequencies.

Research also shows that composite laminates with curved fibres have higher resistance to damage than laminates with straight fibres. Lopes et al. [13] used Abaqus simulations to compare the buckling and first-ply failure responses of straight and curvilinear fibre composite plates subjected to compressive longitudinal load. The curved fibre and straight-fibre composite panels were analyzed in Abaqus, with a set of first-ply failure criteria implemented in the FE subroutine. The results showed that the composite panels with curved fibres have better resistance to the onset of damage than straight fibres under compressive loads. Lopes et al. [14] studied the postbuckling progressive damage behavior and final structural failure for composite panels with curved fibres, and found that composite panels with curved fibres have higher strength than straight-fibre laminates and the damage initiation is postponed.

The above work indicates that using curved fibres can improve the structural performance of a composite, such as increasing the critical buckling load or fundamental natural frequency, and bringing a greater degree of flexibility in designing the structure. The most common way to analyze composite laminates with curved fibres is by using finite element methods, because the complicated geometries and loading of the curved fibres and the orthotropic material properties of composites make analytical solutions difficult to obtain. However, using finite element methods with curved fibres requires a fine mesh to achieve sufficient accuracy. This increases the computational cost. When a finite element-based optimization is performed, the computational expense will be additionally increased by the use of a fine mesh since the finite element system has to be solved in each iteration. To overcome this issue, one can use large elements to reduce the dimension of the global stiffness matrix, which reduces the computational time for solving the finite element system. Meanwhile, sufficient accuracy needs to be maintained when using larger elements. Therefore, a finite element formulation that enables the use of larger element size to improve computational efficiency while maintaining sufficient accuracy is very attractive.

1.2.2 Mesh Convergence for Composite Laminates with Curved Fibres

When applying the conventional finite element method on composite laminates with curved fibres, the continuous curved fibres are divided into finite elements with straight fibres. For the conventional finite element approach, the assumption is that the fibres in each element are approximately straight. As the fibre curvature increases, the elements need to become smaller for this approximation to be sufficiently accurate. As the number of elements increases, the finite element solution approaches a single solution; this is mesh convergence. The number of elements necessary to achieve convergence depends upon the magnitude of the curvature of the fibres: higher curvature requires more elements.

Generally, the relative error between the FE solution and the exact solution should decrease monotonically as the mesh becomes finer. However, the presence of curved fibres in a composite laminate causes the convergence behavior of a finite element solution often not to behave in this manner. In a conventional FE process, the curved fires are discretized into small elements with straight fibres and the angle in the centre is assigned as the orientation. The FE solution strongly depends on the meshing of the curved fibres as the assigned orientation angles together determine the overall structural stiffness. However, modeling curved fibres as straight is inaccurate for some mesh arrangements, because the implied orientation angles result in particularly inaccurate calculations of stiffness. This leads to an incorrect calculation for the element stiffness matrices, resulting in oscillation of the mesh convergence.

Fig. 1.2 shows a composite laminate consisting of curved fibres. The waviness follows a sine function $\theta(x) = \sin(4\pi x)$, which is used to calculate the orientation angle at any location. The plate is fixed on the left edge and loaded with a uniform distributed load, F=20000, as shown in Fig. 1.2(a). The displacement on the right edge of the plate is calculated using the conventional finite element method. This plate is discretized into different number of small square elements with locally straight fibres as shown in Fig. 1.2(b), and each element is assigned with an average fibre orientation angle. The short lines represent the fibre orientation in each element, which is the fibre angle between the tangent line at the centre point and the x-axis.

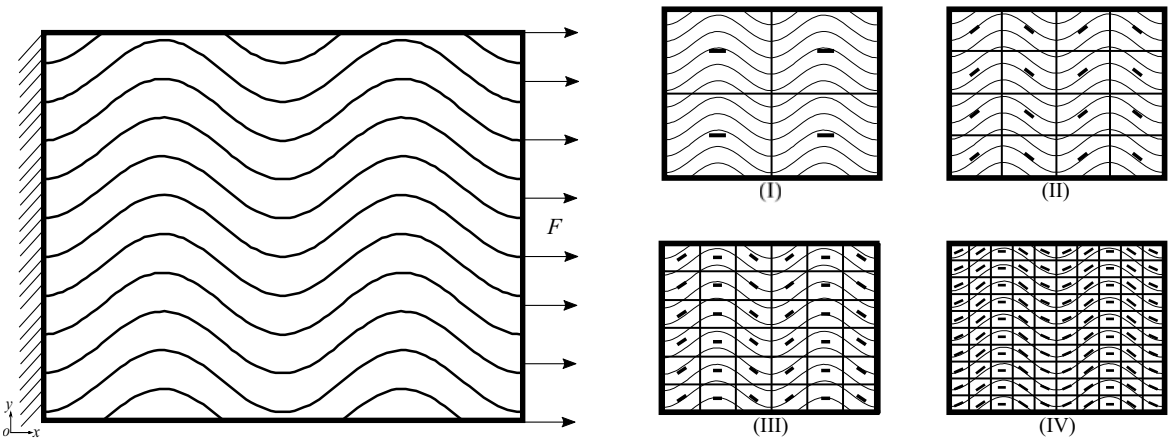

(a) A 1×1 single composite lamina with curved fibres. The wavy curves represent curved fibres. The waviness follows a sine function $\theta(x) = \sin(4\pi x)$. The plated is fixed on the left edge and loaded with a uniform distributed load, F=20000.

(b) The plate is meshed into different numbers of square elements: (I) 2 elements×2 elements; (II) 4 elements×4 elements; (III) 6 elements×6 elements; (IV) 10 elements×10 elements. The short lines represent the fibre orientation in the elements.

Figure 1.2: A 1×1 single composite lamina with sinusoidal curved fibres. The fibre angle in the element centre is assigned as the orientation. The orientations vary due to variations both in mesh size and in position. The conventional finite element method is used to calculate the displacement on the right edge of the plate.

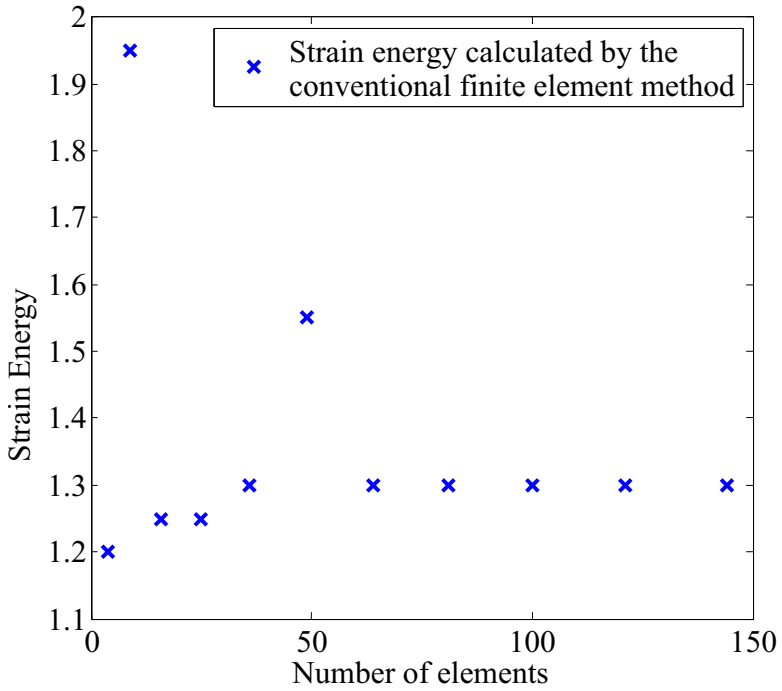

Figure 1.3: The strain energy of the plate with respect to the number of elements. The strain energy oscillates first as the number of elements increases, but eventually approaches convergence around 100 elements.

Fig. 1.3 shows the strain energy of the plate as a function of the number of elements. The conventional finite element method is used for the analysis. The strain energy is calculated,

$$U = \frac{1}{2} D^T K D, \tag{1.1}$$

where D and K are the global displacement vector and stiffness matrix obtained from the conventional finite element analysis, respectively. The data points denote the strain energy calculated for different mesh densities. In the typical finite element process, it is known that as the number of elements is increased, the strain energy of the domain will also increase and eventually approach an asymptote as mesh convergence is attained. However, for laminates with curved fibres, there are points of discontinuity whereby sudden increases in strain energy are seen at intermediate points along the path to mesh convergence. These are inconsistent with the mesh convergence paths of typical finite element methods that do not model curved fibre composites. The sudden increases are due to the selection of only uniform angles to model a curved fibre, resulting in inaccurate approximations. For certain element counts, this translates into markedly inaccurate calculation of the stiffness of the element. Increasing the number of elements mitigates this effect, as seen in Fig. 1.3, but increases computational cost substantially. When modeling composites with curved fibres, it is always possible to choose, inadvertently, element configurations that result in highly inaccurate modeling of the mechanics of the system. To avoid this issue, one option is to formulate a higher fidelity finite element that explicitly models the fibre curvature.

1.3 Parametrization of the Fibre Arrangement

The design of composite structures with curved fibres needs to have a spatial definition of the fibre arrangement in the representative domain. Generally a mathematical function is used to describe how the fibre orientation varies spatially throughout the structure. In order to express the curved shape of fibres, a reference path is defined and the orientation angle is calculated based on the position. The path is often defined by a polynomial function, and the coefficients of the polynomial are parameters that can be adjusted to achieve the desired

paths of the curved fibres.

Such parametrization of the fibre arrangement can reduce the number of design variables in the optimization for curved fibre composites [2]. Simple functions such as polynomial or trigonometric functions are often used for determining the curved shape, as they are easy to implement for calculating integrals and derivatives in the modeling. Gürdal and Olmedo [15] proposed a linear function to represent the reference path, which varies linearly from the angle at the plate centre to the angle at the plate edge. They used linear interpolation to express any angle on the path between the centre and edge. Lopes et al. [13] used this linear function to run a variable-stiffness simulation to improve the buckling and first-ply failure strength for composite panels with curved fibres. This linear function was also employed in the study of natural frequencies and vibrational mode shapes of variable stiffness composite laminates [12] and the effect of curved fibre paths on the in-plane flexibility and out-of-plane bending stiffness of morphing wing skin [16]. Blom et al. [17] defined a sinusoidal function for the fibre path in a laminate to study the influence of tow-drop areas on the stiffness and strength. The geometry was built based on the starting angle and the fibre angle at a prescribed distance. Nik and Fayazbakhsh [18] used a similar concept to build a cosine function as a reference path to optimize the stiffness and buckling load. Akbarzadeh et al. [19] analyzed the role of shear deformation on the plate responses with the same function, while Fayazbakhsh et al. [20] applied the same model to find the influence of gaps and overlaps in variable stiffness laminates. Luersen, Steeves, and Nair [21] optimized the fibre path in a laminated composite cylindrical shell using a Kriging-based approach. The fibre angle was assumed to follow a curvilinear path over eight segments of the circumference, then its variation in the circumferential direction was expressed in terms of the fibre orientation on the eight segments. Blom et al. [22] ran an optimization for a cylinder to maximize the buckling load under bending with a strength constraint. The cosine function was used to define the fibre path on the cylinder.

Another option is to employ higher order functions to describe the fibre reference path, but this approach requires more coefficients to define the function. Increasing the number of coefficients will increase the computational expense of the analysis. Parnas et al. [23] defined cubic Bezier curves and cubic polynomials for curved fibres to minimize the weight of the

composite laminate under stress constraints. Honda et al. [24] used a cubic polynomial function involving with both x and y-coordinates to maximize the mechanical properties, including fundamental frequencies or in-plane strengths, while minimizing the average curvatures of fibres. The curved shape was determined by the coefficients of the cubic polynomial. Honda and Narita [11] presented an analytical method for determining natural frequencies and vibration modes of laminated plates with curved fibres. Spline functions were employed to represent arbitrarily shaped fibres, while the function was represented as a linear combination of B-spines.

While basic functions can be easily implemented into the structure analysis and optimization, using higher order functions can give more accurate shapes, but requires more information for the curvilinear parameterization. Both schemes need proper selection of function coefficients, which affects the quality of the simulation. In addition, the optimization of a composite is critically dependent upon the parametrization chosen for the fibres. More general parameterizations require more parameters and greater computational expense. Using an insufficiently flexible parametrization results in being unable to represent accurately the actual optimal configuration. One can build an analytical expression of the fibre configuration based on its geometry due to the assumption of small fibre curvature. In this work, the analytical expression for fibre orientation angles at arbitrary locations in a square element is derived, assuming that the curved fibres are locally circular arcs.

1.4 Optimization of Composite Laminates with Curved Fibres

As AFP makes composite laminates with curved fibres easier to fabricate, it enables tailoring of the mechanical properties to improve the structural performance. To take advantage of this, it is desirable to find optimal fibre configurations that provide better mechanical performance such as maximum stiffness or vibrational frequency. Structure optimization has various forms such as topology optimization and fibre angle optimization.

1.4.1 Topology Optimization

Topology optimization distributes material within a given design space under specified loads and boundary conditions in order to improve structural performance. The design variable for topology optimization is usually the local material density, known as density-based topology optimization. This is described by the density of the material at each location. Typically it is used to determine the optimal material layout in a structure so that the mechanical properties of the structure are maximized while a constraint on mass is satisfied [25], but it can also be applied to wide variety of scenarios such as compliant mechanisms for multifunctional materials [26] and biomedical design [27].

The choice of design variables is the major difference between the topology optimization and fibre angle optimization. Topology optimization uses the material density of the elements, while fibre angle optimization uses the orientation of the principal material direction. Topology optimization is employed to optimize material layout within a given design space. Blasques and Stolpe [28] proposed simultaneous optimization of both the topology and laminate properties for laminated composite beam cross sections. The beam cross section was optimized using a density-based topology optimization. Minimum compliance multi-material topology optimization with weight constraints was also formulated simultaneously. The design variables represented the volume fractions of each of the candidate materials. The SIMP method was applied to optimize the cross section topology and material properties for square and L-shape beam sections. They also extended this work with eigenfrequency constraints [29]. Coelho et al. [30] proposed a multiscale topology optimization model to minimize compliance of composite laminates. The material model interpolated between two material constituents, strong fibre, and soft matrix phases. The fibre orientation angle was also introduced to find the optimal fibre configuration. Several finite elements were grouped as a design sub-domain. However, this research only focuses on taking advantage of fibre composites and AFP technology to propose optimal fibre arrangement design with the goal of maximizing structural performance. Therefore, only fibre orientation angle optimization is considered in this work.

1.4.2 Fibre Angle Optimization

1.4.2.1 Conventional Composite Laminates

For conventional composite laminates with single orientations per ply, the design variables are fibre orientations of individual layers and layer thickness. The typical optimization for conventional composite laminates is to find the optimal laminate layup or thickness in each layer given a set of pre-defined values of design variables. When the design space is enlarged, the computational efficiency will decrease as more design candidates need to be searched and tested. If the number of candidate orientation angles is limited by restricting the optimization to specific angles, issues associated with non-gradient-based optimization also arise.

Computational efficiency is a major issue for the optimization of conventional composite laminates, as it needs to search an optimal combination of design variables. Non-gradient-based optimizations such as stochastic algorithms are employed as they are capable of finding the global optimal solution for the optimization, but is less computationally efficient [31]. Walker and Smith [32] minimized the weighted sum of the mass and deflection of composite structures subjected to Tsai-Wu failure criterion using genetic algorithms with the finite element method. The design variables were the fibre orientation and the laminate thicknesses. Bagheri et al. [33] used the genetic algorithm for the optimization of maximum fundamental frequency and minimum structural weight of a ring-stiffened cylindrical shell subjected to constraints, including fundamental frequency, structural weight, axial buckling load, and radial buckling load. The design variables included shell thickness and the number of stiffeners, the width and height of stiffeners. Erdal and Sonmez [34] studied the maximization of the buckling load capacity for laminated composites subjected to in-plane static loads using direct simulated annealing, while later applying this optimization algorithm to the minimization of laminate thickness [35]. Omkar et al. [36] used the Vector Evaluated Artificial Bee Colony algorithm to solve the optimization of minimizing weight and the total cost of the composite component. The number of layers, the orientation of the layers and thickness of each layer were all design variables. Roque and Martins [37] optimized the stacking sequences for maximization of the natural frequency of symmetric and asymmetric 8-ply laminates using differential evolution optimization.

1.4.2.2 Composite Laminates with Curved Fibres

There is essentially an infinite number of design variables for composite laminates with curved fibres. Because of the large number of design variables, gradient-based approaches are most efficient for computational optimization of composite laminates with curved fibres. However, optimization requires repeated evaluations of the underlying mechanical models, in this case a finite element model of the composite. The conventional approach to finite element modeling of composites with curved fibres is the patch method, where the composite is divided into many small elements, in each of which the fibres are assumed to be effectively straight. As more curvature is introduced through AFP, the elements need to get smaller and smaller. More elements means a larger stiffness matrix to solve at each step of optimization, which is computationally expensive.

The efficiency of fibre angle optimization relies on the sensitivity analysis of the objective function with respect to the design variables. Lund and Stegmann [38] derived a theoretical expression for the gradient of stiffness and eigenvalues with respect to fibre angle. They proposed the discrete material optimization (DMO) approach that expresses the element stiffness as a weighted sum of a finite number of candidate materials. The design variables were the weights instead of fibre orientation angle. The effective stiffness matrices were calculated by driving one weight to 1, while the other weights must be equal to 0. This enables gradient-based optimization to perform more quickly, because only one candidate is chosen in each iteration and the effective stiffness is equal to the elastic stiffness of this candidate. They applied the DMO approach first on single-layer clamped composite plate [38] and then on a composite cantilever beam [39]. The DMO approach was employed to maximize the buckling load [40] and the eigenfrequency [41] of composite plates. Lund and his colleagues also studied the nonlinear fibre angle optimization of laminated composite shell structures such as square plates [42] and laminated composite U-profile beams [43]. The derivative of the stiffness matrix with respect to the design variable, fibre angle, was approximated semi-analytically at the element level by central finite differences. The optimization problems were solved using the method of moving asymptotes (MMA) [44]. Lund's work provided a detailed sensitivity analysis for the maximizing the stiffness and eigenfrequency. Although

they applied the DMO approach to various studies, they still did not remove the influence of a fine mesh on the computational efficiency of the optimization, as the FE equation needs to be solved in each iteration. The work in this thesis is to mitigate this issue by introducing larger elements with curved fibres.

As it is easy to fall into local minimum using gradient-based optimization, some researchers proposed different methodologies to apply gradient-based optimization to mitigate this issue. Güdal and his colleagues presented a generalized reciprocal approximation for maximizing the fundamental frequency [45] and the buckling load [46] of rectangular composite plates. The fibre orientation angles at each node were considered as design variables and the sensitivity analysis was performed using the adjoint method. The reciprocal approximation was used to update the fibre angles at each finite element node. Due to the difficulty of analytical sensitivity analysis, some researchers also apply gradient-based optimization using a commercial optimizer [47–49]. The gradient is the direction along which the objective function decreases the fastest. To avoid obtaining a local minimum, a stochastic algorithm is first employed to find a potential optimal point in the design space, which is set as the initial guess for the gradient-based optimization. Campen et al. [50] maximized the buckling load of a composite plate with curved fibres considering the constraint of realistic fibre angle curvature. A genetic algorithm was used to provide starting points for a gradient-based optimizer to avoid local minima. Montemurro and Catapano [51] proposed a multi-scale two-level optimization strategy for a composite laminate with curved fibres. This optimization first maximized the stiffness to obtain the optimal fibre configuration considering manufacturing constraints (macroscopic scale), and then optimized the fibre path in each layer to meet all the geometric, technical and mechanical requirements (mesoscopic scale). The genetic algorithm was first employed to provide a potential sub-optimal point in the design space, then a built-in MATLAB gradient-based function was used to find the global solution. Similarly, the present work also tries to find the starting points near the global optimum before performing gradient-based optimization. This is done by using the direction of maximum principal stresses as the initial fibre configurations.

1.5 Thesis Layout

This section summarizes the technical content of each chapter and the detailed structure of this work. Haystead [52] optimized the fibre orientations throughout a single layer composite laminate for the maximization of specific eigenfrequencies and eigenfrequency bandgaps. He used a brute force finite difference method to perform the sensitivity analysis, whereby the gradient is calculated by perturbing the design variable, the fibre orientation angle, and the value of the objective function is recalculated. As a result, the computational cost is very large. Also, the optimized fibre orientation angle remains discontinuous as the conventional finite element method is used. This thesis work aims to mitigate these two major issues, computational efficiency and fibre discontinuity.

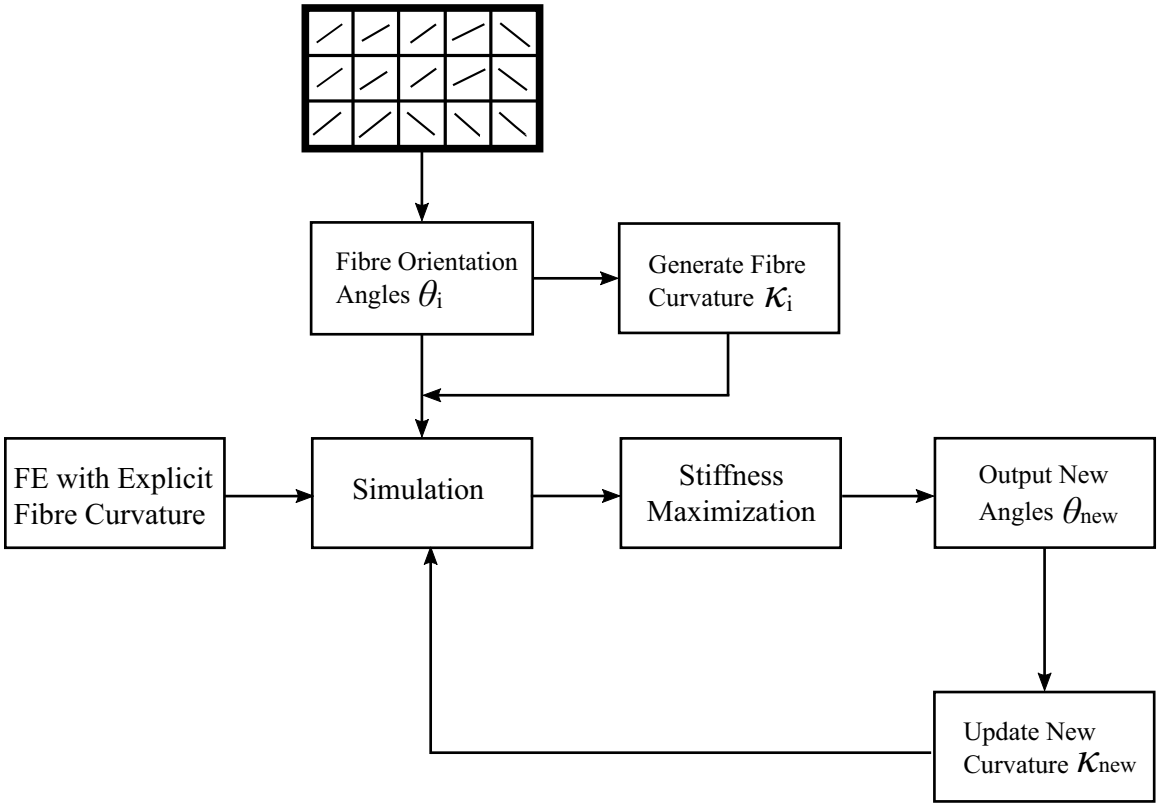

Figure 1.4: Flowchart of the gradient-based optimization for stiffness maximization of a thin single-layer composite lamina with curved fibres. Given an initial fibre configuration, the fibre curvature is generated by minimizing the discontinuity between elements. The finite element with explicit fibre curvature is formulated for the structure analysis and sensitivity analysis. Then the gradient of the objective function is calculated. The fibre orientation angles are updated and the values of objective function are recalculated until the convergence criterion is satisfied.

To increase the computational efficiency, a novel finite element method with explicit fibre

curvature is formulated, which allows the use of larger elements while attaining sufficient accuracy. Using larger elements violates the assumption that fibres are locally straight, so fibres in each element need to be curved. When calculating element stiffness matrices, the Gauss quadrature process is modified to capture stiffness changes due to fibre curvature, while the local stiffness is constant in the conventional finite element process. The results are verified for different composite structures through comparison with converged conventional finite element solutions. Both the computation time and accuracy are compared between this new method and the conventional FE process. In each element the fibre orientation is the design variable. The fibre curvature is calculated by minimizing the discontinuity between fibres in adjacent elements. This is done through minimizing the sum of the squares of the angle difference between adjacent elements, where the angle difference is the difference of fibre orientations on shared edges of adjacent elements. The normal equation is obtained by letting the derivative of the sum of square of the angle difference be zero. The curvatures are obtained by solving the normal equation, and compared to curvatures from the analytical solutions for different composite structures.

Combining these together, stiffness maximization for the single-layer thin composite lamina is performed using a gradient descent algorithm. The flowchart of the optimization is shown in Fig. 1.4. The finite elements with explicit curvature are used for the structural analysis. The sensitivity analysis is conducted analytically. The gradient of the objective function and constraints with respect to the fibre angles, considering the influence of curvature, is derived using the adjoint method. The initial fibre configuration in each element is orientated with the maximum principal stress for the relevant geometry with an isotropic material. The maximization of stiffness is performed on different structures using this new optimization scheme, while the efficiency and accuracy is studied and compared to the gradient descent optimization using conventional finite elements.

The detailed structure of this thesis is as follows:

• Chapter 1: The literature review gives motivation for this thesis work by introducing relevant work, explaining the problem origin and highlighting areas of novelty. The review is divided into three main areas: finite element formulation for composite laminates with curved fibres; parametrization of the fibre arrangement; and optimization of composite laminates

with curved fibres.

• Chapter 2: The study of deformation of curved elastic fibres shows that the influence of interlayer slip between fibres is marginal. The deformation of curved elastic fibres is modeled as a two-layer curved composite column composed of two elastically-connected sub-beams with initial curvature subjected to an axial load. The interlayer slip is assumed to obey a linear constitutive relation. The governing equation is obtained using a variational principle with a simply supported boundary condition. The results show that the assumption of perfect bonding between fibre tows is reasonable.

• Chapter 3: A finite element with explicit fibre curvature is developed, which improves the computational efficiency and maintains good accuracy. This method takes the fibre curvature into consideration, allowing the use of large element size to reduce the dimension of the global stiffness matrix. In the process of calculating the element stiffness, the Gauss quadrature is modified to collect information on stiffness changes caused by fibre curvature. An 8-node quadrilateral element with reduced integration is used to formulate finite elements with explicit fibre curvature. Various test cases with different fibre configuration and loading conditions are tested to verify this finite element. The comparison between the finite element with explicit fibre curvature and the conventional finite element method shows that the proposed method can greatly improve the computational efficiency with good accuracy, which is critical for the analysis of complicated composite structures.

• Chapter 4: While the design variables are the fibre orientations in each element, the implied curvatures must be determined by some other method. A novel curvature generation method is presented to reduce fibre discontinuity and enable the modeling of curved fibres in an element. An expression in terms of curvature is built to give fibre orientation on the element boundaries based on the geometry of curved fibres. It is assumed that fibres in the element are circular arcs with constant small curvature. The difference in the angles between each adjacent element can be obtained. The minimization of the sum of the angle difference can generate curvature for each element, which is considered as a least square minimization problem and solved through its normal equation. Several test cases, including square plates with multiple curved fibres shapes and an L-shaped structure, are presented to verify this method. The results from the curvature generation method show good agreement with the

analytical solution, which indicates that it is an efficient way to generate the curvature.

• Chapter 5: The stiffness maximization for a thin single-layer composite lamina is performed using a new optimization scheme to improve the efficiency. A gradient descent algorithm and the finite element formulation with explicit fibre curvature are used. With the curvature considered in the sensitivity analysis, the objective function with respect to the fibre orientation angles is derived analytically using the adjoint method. The test case using a square region shows that this new optimization method is efficient for reaching the exact solution. Finally, the maximum stiffness gradient-based optimization with explicit fibre curvature is performed on an L- and a T-shaped structure with different loading conditions. The direction of the maximum principal stress for the relevant geometry with an isotropic material is set as the initial fibre orientation in each element. The results are compared to gradient-based optimization using the conventional finite elements.

Chapter 2

Interlayer Slip between Curved Fibres

2.1 Introduction

Advanced composite manufacturing methods make curved fibres in composite structures possible. The local stiffness of the composite varies due to fibre curvature and many small elements need to be employed in a finite element simulation in order to get good accuracy of the structural analysis. In addition, curved fibres experience transverse deflections when subjected to axial loads. As a consequence, a model of composites with curved fibres is necessary to account for this.

One key issue in the development of such a model is the scale at which the fibres must be modeled. When modeling composites with straight fibres, it is assumed that the fibres remain effectively straight and that any slip of adjacent fibres is captured in the homogenized shear modulus of a lamina. When modeling curved fibres, fibre tows are typically exposed to tensile or compressive loads that, respectively, tend to straighten or bend the fibres. During this elongation or contraction, the fibres may slip relative to adjacent fibres because of the lower shear modulus of the inter fibre matrix material. This is similar to a sheaf of paper that is easily bent if the individual leaves are allowed to slide, but is very stiff if the leaves are bonded. The magnitude of this effect determines how the fibre tows must be modeled, or

if they can be modeled as bundles at all.

This chapter contains a verification study of the effective stiffness of elastic fibres with initial curvature subjected to an axial load, analyzing the influence of interlayer slip in a two-layered curved composite beam. The governing equation was derived by Challamel [53] using a variational principle with a simply supported boundary condition. The interlayer slip obeys a linear constitutive relation. The Euler elastica theory is employed to account for large curvature. The shape of the curved beam is assumed to be a circular arc before and after deformation as only the linear elastic case is considered. The axial displacement of the curved beams is obtained by solving the governing equation and the effective stiffness is approximated linearly as the ratio of the load to the displacement.

To verify the analytical solution, the effective stiffness of the composite beam with initial curvature is also computed using finite element methods. The analytical predictions agree with the computational results for relevant combinations of material and geometric parameters, and the effect of interlayer shear slip on the effective stiffness is discussed in detail. The results indicate that interlayer slip does not have a significant impact on the elastic properties of a composite, either for individual fibres slipping, or for adjacent fibre tows slipping. This knowledge is helpful to formulate finite elements with curved fibres modeled explicitly.

2.2 Effective Axial Stiffness of A Two-layered Curved Beam

2.2.1 Interlayer Slip

The problem of interlayer slip in a two-layered beam has been studied multiple times due to the widespread applications of composite steel-concrete beams in the field of civil engineering. The interlayer slip is the relative displacement between two imperfectly bonded beams along the interface. The bending of the beam causes interlayer slip between the steel and concrete components. Typically the relationship between the interlayer shear load f and interlayer slip displacement Δu is non-linear, but frequently approximated as a linear relationship by using a constant slip modulus k [54]. The slip can affect the mechanical behavior of the

composite, such as buckling [55] and vibrations [56]. With a typical linear relation for the slip in the composite beam, the governing equation is derived based on one of a variety of possible beam theories. Xu and Chen [57] studied the principle of virtual work of partial-interaction composite beam based on both Timoshenko beam theory and Euler-Bernoulli beam theory. The principle of minimum potential energy, the variational formulae for the frequency of free vibration and the critical load of buckling were derived. Approximate solutions for bending, vibration, and buckling were obtained by using variational principles. Girhammar and Pan [58] developed the closed-form solutions for the displacement for a composite beam with partial interaction subjected to a uniform transverse load. A sixth order governing differential equation in terms of displacement was developed and solved using the Laplace transformation.

Curved fibres are similar to curved beams. The mechanical properties of curved fibres can be obtained by modeling the behavior of curved beams. For the interlayer slip of a curved beam expressed in terms of the in-plane rotation of the cross-section $\theta(s)$, Challamel [53] gives an expression for the slip,

$$u(s) = \frac{h_1}{2}\theta_1(s) + \frac{h_2}{2}\theta_2(s), \tag{2.1}$$

where s, $\theta_i(s)$ and h_i are the curvilinear abscissa, the in-plane cross-section rotation and the depth of each layer, respectively.

Generally, it is convenient to treat interlayer slip as a linear relation between force and displacement [57, 59–61]. The relation between the interlayer shear force per unit length $f(s)$ and the slip $u(s)$ is,

$$f\left(s\right) = ku\left(s\right) = \frac{k}{2}\left(h_1\theta_1\left(s\right) + h_2\theta_2\left(s\right)\right), \tag{2.2}$$

where k is the constant slip modulus. Challamel [53] assumes that each layer in the two-layered beam has the same geometry and experiences the same deformations, $h_1 = h_2 = h$, $\theta_1 = \theta_2 = \theta$, Eq. (2.2) becomes:

$$f(s) = kh\theta(s). \tag{2.3}$$

2.2.2 Derivation of the Effective Axial Stiffness

To simplify the analysis of the elastic fibres with initial curvature subjected to axial load, the shape of the curved fibre is assumed to be a circular arc. This has the eventual advantage of enabling parametrization of the fibre configuration in a region by two variables: average orientation and curvature. A two-layered curved composite beam composed of two identical sub-beams is used to study the effective stiffness of the curved beam, as shown in Fig. 2.1. The two-layered curved beam is pinned at point A and point B is subjected to an axial load, P. The two points A and B are located on a horizontal line. The solid and dashed line represent the beam before and after deformation, respectively.

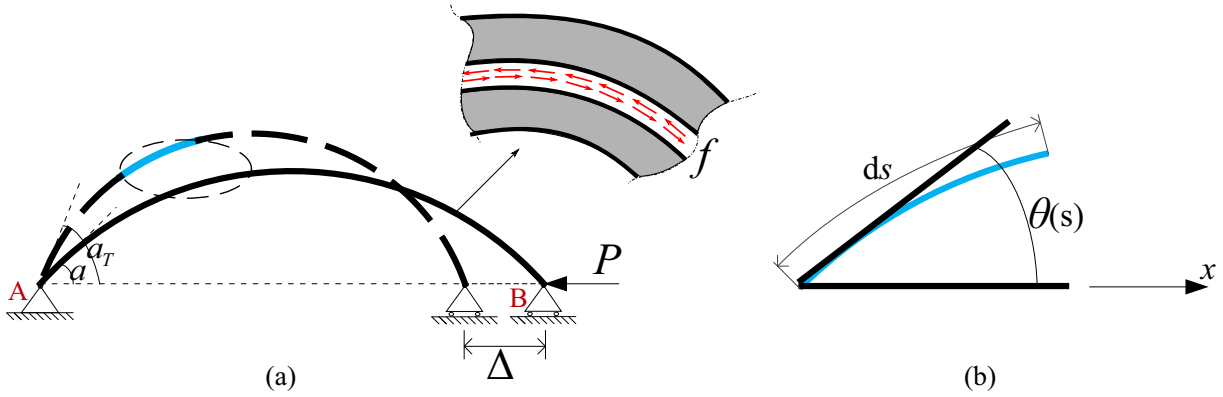

Figure 2.1: An initially curved beam as a circular arc: (a) geometry and coordinate system and (b) an infinitesimal element. The curved beam is fixed at two horizontal points A and B. Point A is constrained by a pinned boundary condition and point B is subjected to an axial load, P, while its vertical displacement is zero. The solid and dashed line represent the beam before and after deformation, respectively. f is the shear force between two beams. a and a_T are tangent angles at point A before and after deformation, respectively.

The elastica theory developed by Euler is applied to the curved beam. Euler and Jakob Bernoulli developed the theory for elastic lines yielding the solution known as the elastica curve and employed it to study buckling [62]. This theory allows very large elastic deflections of structures, which is suitable for solving large deflection problems of beams [63–66]. In the elastica theory, the shape of an elastic curve is expressed in the exact differential equation, while the second derivative of deflection is used to approximate the curvature in Euler-Bernoulli beam theory. The state of the curved beam is specified by the in-plane rotation of the cross-section $\theta(s)$, where s is the curvilinear abscissa. The exact expression of the curvature, κ, is:

$$\kappa = \frac{d\theta(s)}{ds}. \tag{2.4}$$

Challamel [53] gives the governing equations of the deformation of a two-layered composite beam subjected to an axial load with interlayer slip. The governing equation for this system is,

$$EI_0\theta'' - k{h_0}^2\theta + P\sin\theta = 0, \tag{2.5}$$

with the boundary conditions:

$$[EI_0\theta'\delta\theta]_0^L = 0, \tag{2.6}$$

where θ'' is the second derivative of θ with respect to s, $EI_0 = EI_1 + EI_2$ and $h_0 = (h_1 + h_2)/2$. Both layers have the same Young's modulus, and I_i is the second moment of area of each layer. The bending stiffness EI_i in each layer is identical, therefore, $EI_1 = EI_2$. For the simply supported case, the beam is free to rotate and does not experience any torque at the boundaries. Therefore, the boundary conditions are,

$$\theta'(0) = \theta'(L) = 0. \tag{2.7}$$

The dimensionless form of the equation is,

$$\frac{d^2\theta}{d\bar{s}^2} - \bar{c}\theta + \bar{b}\sin\theta = 0, \tag{2.8}$$

where the dimensionless parameters are

$$\bar{s} = \frac{s}{L}, \quad \bar{b} = \frac{PL^2}{EI_0}, \quad \bar{c} = \frac{k{h_0}^2 L}{EI_0}, \tag{2.9}$$

with the boundary conditions

$$\frac{d\theta}{d\bar{s}}(\bar{s} = 0) = 0, \ \frac{d\theta}{d\bar{s}}(\bar{s} = 1) = 0. \tag{2.10}$$

In the governing equation, both θ and $\bar{b}$ are unknown. Given a small value for P to determine $\bar{b}$, there is a corresponding solution for θ. Challamel [53] solved this governing equation as a non-linear boundary value problem and studied the post-buckling behavior of the composite beam. To find the displacement at point B as shown in Fig. 2.1, the tangent

angle a_T at point A after the deformation is calculated. Since only the small linear elastic case is considered, it is convenient to treat the curved beam as a circular arc before and after the deformation. Therefore, the displacement at the right end is obtained:

$$\Delta = \frac{L}{a}\sin(a) - \frac{L}{a_T}\sin(a_T), \tag{2.11}$$

where a is the initial tangent angle at point A before the deformation.

Given P, there is a corresponding displacement Δ. The relation between P and Δ is approximated as linear, giving the effective stiffness of the two-layered curved beam, S_k:

$$S_k = \frac{P}{\Delta}. \tag{2.12}$$

For beams that are initially straight or nearly straight, the elastic stretching of the beam is also a significant contribution to the beam stiffness. The axial elongation caused by normal stresses is considered for the extensible case, therefore $1/E$ is introduced by modifying Eq. (2.12). The displacement and effective stiffness obtained from Eq. (2.11) and (2.12) are caused by bending only. Therefore, this solution will be incorrect for the case of small curvature as the bending has little influence. Then Δ will approach zero causing S_k to be infinity. Including the term $1/E$ mitigates this problem since it will dominate compared to $1/S_k$ for small curvature. Therefore, the linear solution can be modified by introducing $1/E$,

$$E_{eff} = \frac{1}{\dfrac{1}{S_k} + \dfrac{L}{EA}}, \tag{2.13}$$

where A is the cross-section area of the beam.

2.3 Analytical Solution and Finite Element Verification

In order to verify the analytical solution using Challamel's method [53] to calculate the effective stiffness of a two-layered curved beam, an FE model of a three-layer curved beam,

consisting of two beam columns as the fibres or fibre tows and one thin layer as the resin, was constructed. The commercial finite element software ABAQUS 6.12 was used to conduct the finite element verification. Fig. 2.2 shows the finite element model. Both slip between two fibres and slip between two fibre tows is of interest. The model can be used for both situations by varying the geometric parameters.

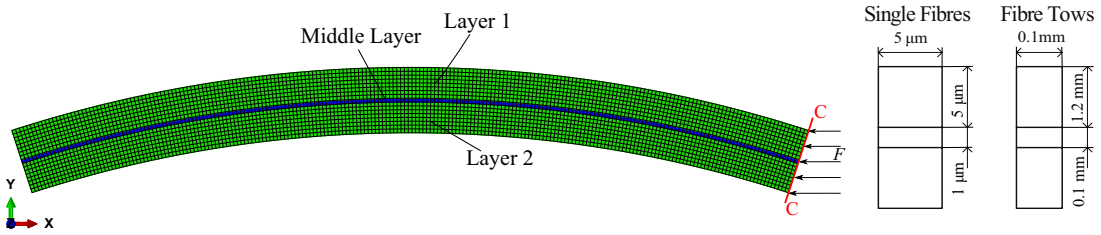

Figure 2.2: The finite element model of a three-layer simply supported curved beam. Layer 1 and 2 represent the single fibres or the fibre tows, and the thin layer between them is the resin. Both the geometric size of single fibres and fibre tows are tested in this FE model.

The material properties of AS4 carbon fibre tow (3K) produced by Hexcel [67] was used, of which the Young's modulus is 231 GPa and Poisson's ratio is 0.26. For the resin layer, the Young's modulus is 3.5 GPa and Poisson's ratio is 0.35, respectively [68]. All three layers are perfectly bonded.

The beams were meshed with 4-node bilinear plane stress elements (CPS4). The simply supported boundary condition was set at the left end, while section C-C was loaded with axial force, 10 N, as shown in Fig. 2.2. The interlayer slip is modeled as the relative movement between layers enabled by the high shear compliance of the resin. There is relative slip between layer 1 and 2 because their shear moduli are different from the middle thin resin layer. To calculate the effective stiffness from the simulation, a C-C section is defined as the cross section of the right end. The axial displacement Δ from the finite element model is obtained by calculating the average value of the horizontal displacements of all nodes on C-C section. The effective stiffness of the curved beam from the finite element model is calculated using Eq. (2.12) as well. The slip modulus is calculated according to the definition of shear,

$$k = G\frac{h}{t}, \tag{2.14}$$

where G and t is the shear modulus and thickness of the middle layer, respectively. The slip

modulus is determined by the material properties and geometry of the middle layer.

The fibre curvature reduces the effective stiffness of curved beams. The effective stiffness as a function of the initial curvature determined by the analytical solution and the finite element method for single fibres and fibre tows are shown in Fig. 2.3(a) and 2.3(b), respectively. It can be seen that the effective stiffness of the two-layered curved beam system decreases as the initial curvature increases, and approaches zero quickly.

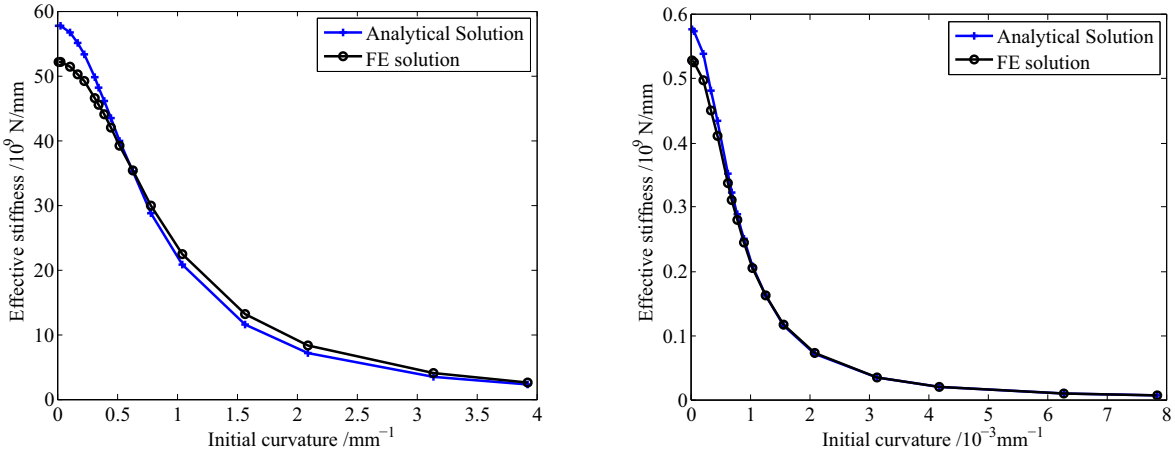

(a) Effective stiffness as a function of the initial curvature for single fibres.

(b) Effective stiffness as a function of the initial curvature for fibre tows.

Figure 2.3: Analytical and FE solution for the stiffness of pairs of fibres or pairs of fibre tows as a function of the initial curvature. The effective stiffness of the three-layer curved beam system decreases as the initial curvature increases. The curvature greatly influences the compliance of the beam system.

Fig. 2.4(a) and 2.4(b) present the effective stiffness as a function of interlayer slip determined by the analytical solution and the FE method for single fibres and fibre tows, respectively. In the analytical solution, the axial displacement is calculated under the assumption of linear elasticity, where the stress states do not produce yielding. As the slip modulus increases, the effective stiffness is unbounded due to the approximation of this analytical solution, represented by the blue line. The red dashed line is the limit of the effective stiffness that all layers are treated as a monolithic beam. In the FE solution it can been seen that the effective stiffness is not sensitive to increase of the slip modulus at higher values of the slip modulus. When the material properties of the middle layer approach those of layers 1 and 2, the effect of the interlayer slip will disappear and all layers will behave as a monolithic beam. The cross markers in Fig. 2.4(a) and 2.4(b) show the actual estimated slip

modulus of the resin based upon the shear modulus of the matrix material and the geometry of the matrix layer. The thickness and width of the matrix layer are estimated from their micrographs [69, 70]. The slip modulus between single fibres and fibre tows are 6.48 GPa and 1.29 GPa, respectively. They are not identical because the single fibres and fibre tows have different interlayer spacing. At the value of the actual slip modulus of the resin, the FE solutions are close to the analytical solutions that assume all layers act as a monolithic beam, and the effective stiffness is not sensitive to the change of slip modulus at higher values. This indicates that interlayer slip between either single fibres, or fibre tows, has little effect on the effective stiffness of the curved beam system. As a result, the mechanical properties of curved composite fibres are only affected by fibre curvature, and the effect of interlayer slip between fibres can be neglected in the structural analysis.

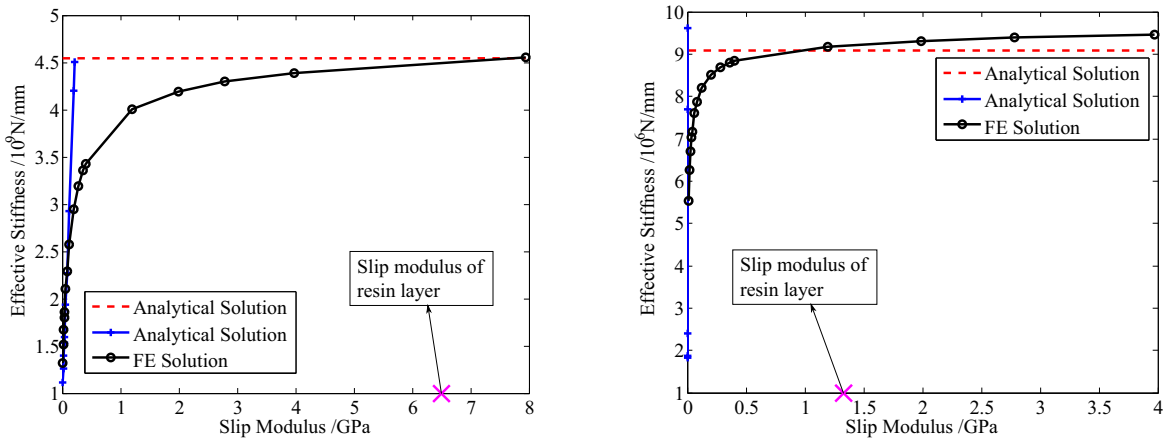

(a) Effective stiffness as a function of slip modulus for single fibres.

(b) Effective stiffness as a function of slip modulus for fibre tows.

Figure 2.4: Analytical and FE solution for the effective stiffness as a function of the slip modulus. The interlayer slip between fibre has little influence on the effective stiffness of two-layered curved beam.

2.4 Concluding Remarks

The deformation of bonded, curved elastic fibres with initial curvature subjected to axial load is studied considering the influence of interlayer slip. The interlayer slip is assumed to be linear. The Euler elastica theory and variational principle are used to find the analytical solution of the effective stiffness. FE analysis is also conducted for verifying the single curved beam, interlayer slip between to single fibres and fibre tows. The analytical solution agrees

well in the region of large slip modulus, and the actual material properties of the slip layer are correspond to these values. This indicates that the curvature has a large impact on the effective stiffness, while the slip effects between either individual fibres or adjacent fibre tows has little impact on the mechanical properties of curved fibres. As a result, perfect bonding between fibres is a reasonable assumption in composite structural analysis. This work will help formulate the curved finite element for solving complicated composite structures.

Chapter 3

Finite Element with Curved Fibres

3.1 Introduction

For composite structures with curved fibres, using conventional finite element methods requires discretization of the complex structure into many small elements, assuming the fibres in each element are straight, and assigning a unique orientation angle to each element. The conventional method requires fine meshes to attain high accuracy, as fine meshes enable a series of locally straight fibre to provide a close approximation to the curved fibre path. However, fine meshes entail a large stiffness matrix. In each iteration of a structural optimization process, one linear system equation involving the stiffness matrix must be solved. This has high computational expense, and this drawback increases when optimization is performed since the finite element system has to be solved in each iteration. Reducing the dimension of the stiffness matrix can greatly improve computational efficiency. To reduce matrix size and hence computation time, it is necessary to use larger elements to reduce the dimension of the global stiffness matrix. However, larger elements violate the approximation that fibres are locally straight. Retaining relatively large elements may be enabled by modeling the fibre curvature explicitly in order to capture the changes in stiffness. Such an approach is explored in this chapter.

In this work, two finite element formulations with curved fibres are proposed. The first one is the averaged compliance method (ACM) [71]. This method approximates the stiffness

by calculating the mean of compliance over the element domain. A reference fibre path is defined for curved fibres and the fibre orientation along the path is expressed as a linear function with respect to the location of the element. The compliance, determined by the fibre orientation, can be obtained as a function of the location as well. The mean of compliance is calculated over the element domain. The effective element stiffness is the reciprocal of the averaged compliance. The method is used to solve the problem of a rectangular plate with curved fibres subjected to an uniform distributed axial load. It is found that this method improves the computational efficiency since it has good accuracy with fewer elements than the conventional finite element method, but the improvement is marginal.

The other method is the finite element with explicit fibre curvature. This models the fibre curvature explicitly to capture the changes in stiffness. In an element with curved fibres, the orientation varies at different locations due to the fibre curvature. As a result, the local stiffness is not constant. In the finite element with explicit fibre curvature, the orientation angles at each sample point in the element are picked, and then the corresponding local stiffness is calculated at each point. During the Gauss quadrature process, the integral of the element stiffness matrix is approximated as a weighted sum of these local stiffnesses at specified sample points within the domain of the integral. By considering the stiffness change due to the fibre curvature, it collects more information from the curved fibre. This is in contrast with the assumption that the fibres are locally straight as in conventional FE methods. This method uses varying local stiffness to approximate the integral, while ACM has a constant stiffness over the element domain obtained by averaging the compliance.

An 8-node quadrilateral element with reduced integration is used to formulate the finite element with explicit fibre curvature. The approach used here is to assume that both the fibre orientation angle and the curvature are known for each element. In practice, this will involve treating the fibre orientation angle as the primary design variable and generating a set of curvatures that minimizes the overall fibre discontinuity. Various test cases with different fibre configurations and loading conditions are used to verify this proposed method to show that it provides higher accuracy and efficiency compared to the conventional FE approach. In one verification case, the curved finite element uses 96 nodes (0.1s) to have an average relative error of 0.23%, while the conventional finite element needs 676 nodes (0.42s).

The comparison between the finite element with explicit fibre curvature and the conventional FE shows that the proposed method can greatly improve the computational efficiency with good accuracy, which is critical for the analysis of complicated composite structures.

3.2 Averaged Compliance Method

To formulate the curved fibre finite element, the first requirement is to calculate the stiffness matrix of an element with curved fibres. When large elements with curved fibres are used in a simulation, the assumption of straight fibres cannot accurately describe the stiffness of the elements. Therefore, it is necessary to find the effective stiffness of curved fibres considering the fibre curvature and the slip betweens fibres. In Chapter 2, it was shown that modeling many curved beams bonded together approximates the properties of curved fibres. The solution of effective stiffness for multiple curved beams indicates that the interlayer slip has little influence on the overall stiffness of the structure. As a result, the influence of fibre slip can be neglected when modeling a laminate with curved fibres. Fibre curvature is the only factor that affects the stiffness of the structure. The effective stiffness of the curved fibres can be calculated by averaging the local stiffness over the element domain.

To calculate the effective stiffness of curved fibres, the fibre orientation angles must be known as they determine the stiffness. The orientation can be calculated from a predefined fibre path, which serves as the basis for creating other fibre paths that together form a single ply [12]. The fibre path is made to vary only along one of the coordinates for the convenience of calculation. A fibre path with linear variation of the orientation along the x-coordinate [15][72] is defined by,

$$\theta(x) = \frac{\theta_1 - \theta_0}{a} x, \tag{3.1}$$

where θ_0 and θ_1 are the orientation angle at the left and right edge of the square element, as shown in Fig. 3.1.

With a defined fibre path, one can calculate the average stiffness over the element domain. For an orthotropic material in the 2-D state of stress, the stress-strain relationship is given by [73],

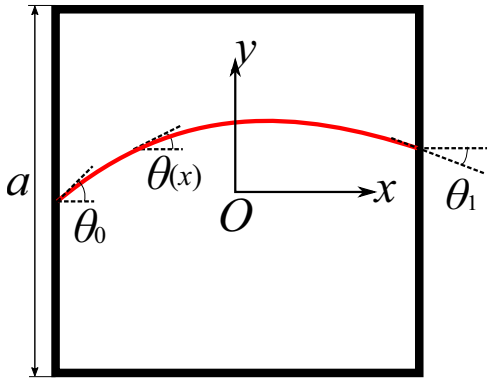

Figure 3.1: A reference fibre path in a square element with curved fibres. The curve is the reference fibre path, which starts from the left edge and ends at the right edge. θ_0 and θ_1 are the orientation angle on the left and right edge, respectively. The orientation angle $\theta(x)$ is the angle between the x-axis and the tangent line to an arbitrary point on the path.

$$\begin{Bmatrix} \varepsilon_{11} \\ \varepsilon_{22} \\ \varepsilon_{33} \\ \gamma_{23} \\ \gamma_{13} \\ \gamma_{12} \end{Bmatrix} = \begin{bmatrix} S_{11} & S_{12} & S_{13} & 0 & 0 & 0 \\ S_{12} & S_{22} & S_{23} & 0 & 0 & 0 \\ S_{13} & S_{23} & S_{33} & 0 & 0 & 0 \\ 0 & 0 & 0 & S_{44} & 0 & 0 \\ 0 & 0 & 0 & 0 & S_{55} & 0 \\ 0 & 0 & 0 & 0 & 0 & S_{66} \end{bmatrix} \begin{Bmatrix} \sigma_{11} \\ \sigma_{22} \\ \sigma_{33} \\ \tau_{23} \\ \tau_{13} \\ \tau_{12} \end{Bmatrix}, \tag{3.2}$$

where S_{ij} are the material compliances. They are determined by the longitudinal and transverse modulus of elasticity, E_1 and E_2, shear modulus, G_{12}, and Poisson's ratio, v_{12}. Laminated composite plates are thin and therefore a plane stress condition is assumed. The strains resulting from a state of plane stress ($\sigma_{33} = \tau_{23} = \tau_{13} = 0$) are,

$$\begin{Bmatrix} \varepsilon_{11} \\ \varepsilon_{22} \\ \gamma_{12} \end{Bmatrix} = \begin{bmatrix} S_{11} & S_{12} & 0 \\ S_{21} & S_{22} & 0 \\ 0 & 0 & S_{33} \end{bmatrix} \begin{Bmatrix} \sigma_{11} \\ \sigma_{22} \\ \tau_{12} \end{Bmatrix}, \tag{3.3}$$

where

$$S_{11} = \frac{1}{E_1}, \quad S_{22} = \frac{1}{E_2}, \quad S_{33} = \frac{1}{G_{12}},$$
$$S_{12} = -\frac{v_{12}}{E_1} = -\frac{v_{21}}{E_2} = S_{21},$$
$$S_{13} = S_{23} = S_{31} = S_{32} = 0.$$

The transformed relation between strain and stress in the global rectangular Cartesian coordinate system for transversely isotropic materials is,

$$\begin{Bmatrix} \varepsilon_x \\ \varepsilon_y \\ \gamma_{xy} \end{Bmatrix} = [T]^T [S] [T] \begin{Bmatrix} \sigma_x \\ \sigma_y \\ \sigma_{xy} \end{Bmatrix} = \begin{Bmatrix} \bar{S}_{11} & \bar{S}_{12} & \bar{S}_{13} \\ \bar{S}_{12} & \bar{S}_{22} & \bar{S}_{23} \\ \bar{S}_{13} & \bar{S}_{23} & \bar{S}_{33} \end{Bmatrix} \begin{Bmatrix} \sigma_x \\ \sigma_y \\ \sigma_{xy} \end{Bmatrix}, \tag{3.4}$$

where

$$\begin{aligned}
\bar{S}_{11} &= S_{11}\cos^4\theta + (2S_{12} + S_{33})\sin^2\theta\cos^2\theta + S_{22}\sin^4\theta, \\
\bar{S}_{12} &= (S_{11} + S_{12} - S_{33})\sin^2\theta\cos^2\theta + S_{22}\sin^4\theta, \\
\bar{S}_{13} &= (2S_{11} - 2S_{12} - S_{33})\sin\theta\cos^3\theta + (2S_{12} - 2S_{22} + S_{33})\sin^3\theta\cos\theta, \\
\bar{S}_{22} &= S_{11}\sin^4\theta + (2S_{12} + S_{33})\sin^2\theta\cos^2\theta + S_{22}\cos^4\theta, \\
\bar{S}_{23} &= (2S_{11} - 2S_{12} - S_{33})\sin^3\theta\cos\theta + (2S_{12} - 2S_{22} + S_{33})\sin\theta\cos^3\theta, \\
\bar{S}_{33} &= 2(2S_{11} + 2S_{22} - 4S_{12} - S_{33})\sin^2\theta\cos^2\theta + S_{33}\left(\sin^4\theta + \cos^4\theta\right).
\end{aligned}$$

Since all elements in the compliance matrix are a function of the fibre orientation angle and the orientation only varies in the x-direction, the averaged compliance matrix [71] can be obtained:

$$S_{av} = \frac{1}{a}\int_{-\frac{a}{2}}^{\frac{a}{2}} \bar{S} dx. \tag{3.5}$$

Since Eq. (3.1) and Eq. (3.4) are explicit, the integration of Eq. (3.5) is straightforward. The effective elastic matrix D_e of the curved finite element can be obtained by calculating the inverse of the averaged compliance matrix,

$$D_e = {S_{av}}^{-1}. \tag{3.6}$$

The element stiffness matrix K^e can be calculated,

$$K^e = \int_{\Omega^e} B^T D_e B d\Omega, \tag{3.7}$$

where B and D_e are the strain-displacement matrix and elastic matrix, respectively. The

strain-displacement matrix is for a 4-node quadrilateral element is,

$$B = [B_1 \;\; B_2 \;\; B_3 \;\; B_4 \;\;], \qquad B_i = \begin{bmatrix} \frac{\partial N_i}{\partial x} & 0 \\ 0 & \frac{\partial N_i}{\partial y} \\ \frac{\partial N_i}{\partial y} & \frac{\partial N_i}{\partial x} \end{bmatrix}. \tag{3.8}$$

In the strain-displacement matrix B, the shape functions N_i are:

$$\begin{aligned} N_1(\xi,\eta) &= \frac{1}{4}(1-\xi)(1-\eta), \quad N_2(\xi,\eta) = \frac{1}{4}(1+\xi)(1-\eta), \\ N_3(\xi,\eta) &= \frac{1}{4}(1+\xi)(1+\eta), \quad N_4(\xi,\eta) = \frac{1}{4}(1-\xi)(1+\eta), \end{aligned} \tag{3.9}$$

where ξ and η are parent coordinates. The shape function derivatives used in Eq. (3.8) are calculated as follows:

$$\begin{bmatrix} \frac{\partial N_i}{\partial x} \\ \frac{\partial N_i}{\partial y} \end{bmatrix} = [J]^{-1} \begin{bmatrix} \frac{\partial N_i}{\partial \xi} \\ \frac{\partial N_i}{\partial \eta} \end{bmatrix}, \tag{3.10}$$

and the Jacobian matrix, J, is

$$J = \begin{bmatrix} \frac{\partial x}{\partial \xi} & \frac{\partial y}{\partial \xi} \\ \frac{\partial x}{\partial \eta} & \frac{\partial y}{\partial \eta} \end{bmatrix}, \tag{3.11}$$

where the partial derivatives of x and y are calculated by,

$$\begin{aligned} \frac{\partial x}{\partial \xi} &= \sum_{i=1}^{4} \frac{\partial N_i}{\partial \xi} X_i, \;\; \frac{\partial x}{\partial \eta} = \sum_{i=1}^{4} \frac{\partial N_i}{\partial \eta} X_i, \\ \frac{\partial y}{\partial \xi} &= \sum_{i=1}^{4} \frac{\partial N_i}{\partial \xi} Y_i, \;\; \frac{\partial y}{\partial \eta} = \sum_{i=1}^{4} \frac{\partial N_i}{\partial \eta} Y_i, \end{aligned}$$

where X_i and Y_i are the coordinates of node i.

3.2.1 Element Verification

To verify the efficiency and accuracy of ACM, regions containing fibres with paths defined by a linear equation will be used, as shown in Fig. 3.2. The displacement on the right edge will be calculated using both the finite element incorporating the ACM and the conventional finite element approach. The conventional FE assumes fibres in each element are locally

straight. The results of the two methods will be compared.

A rectangular plate containing curved fibres is used. Its length and width is 10 and 4, respectively. The lamina properties are set as $E_1 = 127$, $E_2 = 10$, $G_{12} = G_{13} = 4$, $G_{23} = 1.8$, $\nu_{12} = 0.27$, and the thickness is 0.001. To simplify the calculation, the curved fibres are assumed to be circular arcs and the fibre orientation only varies linearly along the x-axis. The fibre orientation on the left and right edge are $\frac{\pi}{10}$ and $-\frac{\pi}{10}$, respectively. The origin of the coordinate is in the centre of the plate. Therefore, the fibre path is,

$$\theta(x) = -\frac{\pi}{50}x, \tag{3.12}$$

where x is the x-coordinate in each element. The left edge is fixed, and the right edge is subjected to a uniform distributed load, 50000. Path A-B is defined as the right edge of the plate. First, the convergence study is done using Abaqus with increasing mesh density. It is found that the Abaqus solution converges as the number of elements increases. Given that the finite element method is a convergent method and will eventually converge to the exact solution, the converged Abaqus solutions are considered to be good representation for the exact solution. After getting the exact solution, the average compliance method can be verified to see if it converges to the exact solution with fewer elements than the conventional finite element method.

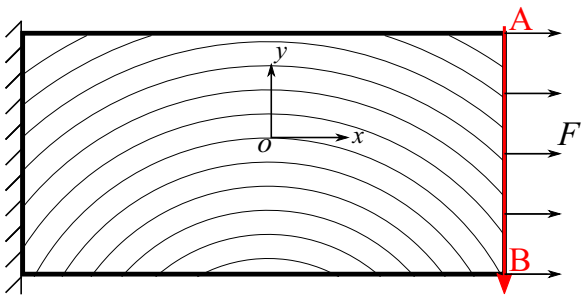

Figure 3.2: Geometric model of a curved fibre plate. The left edge of the plate is fixed, and the right edge is subjected to a uniform tensile distributed load, F=50000. The orientation angles at the left and right edges are $\frac{\pi}{10}$ and $-\frac{\pi}{10}$. Path A-B is the right edge of the plate.

An FE model of the rectangle plate subjected to an uniformly distributed axial load was constructed. The plate was meshed with 4-node doubly curved thin shell elements (S4R). The orientations in the elements can be calculated from Eq. (3.12) based on the element

location. Fig. 3.3 shows the horizontal displacement contour from the Abaqus simulation. The convergence study of the Abaqus simulation is conducted on path A-B, as shown in Fig. 3.4. As the number of elements increases, both the horizontal and vertical displacement on path A-B will approach convergence at the mesh of 2560 (80×32) elements, as the difference between the results of using 640 and 2560 elements is close to zero. Therefore, the Abaqus simulation with 2560 elements can be considered as the exact solution.

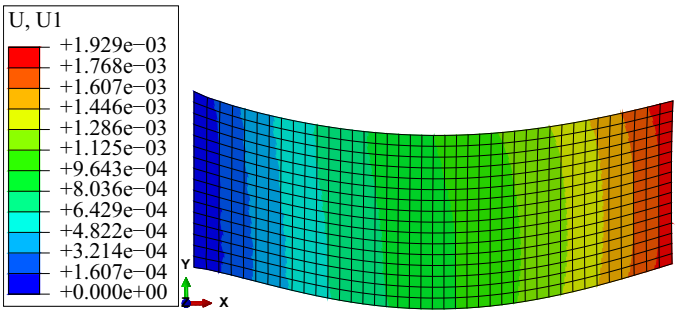

Figure 3.3: Contour of the horizontal displacement from the Abaqus simulation. The blue and red color represents the minimum and maximum horizontal displacement on this plate.

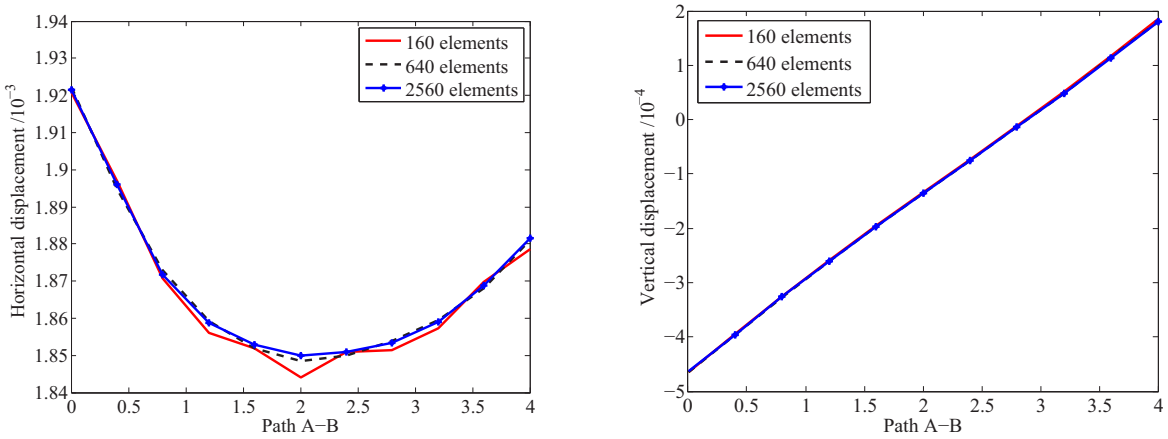

(a) Convergence of the Abaqus simulation for the horizontal displacement of path A-B.

(b) Convergence of the Abaqus simulation for the vertical displacement on path A-B.

Figure 3.4: Convergence of the Abaqus simulation for the displacement on path A-B. Three meshes, 160 (20×8), 640 (40×16) and 2560 (80×32) elements are used. The displacement on path A-B approaches convergence at the mesh of 2560 elements, which can be considered as the exact solution.

Based on the exact solution, the results from the ACM and the conventional FE approach will be compared. In the conventional FE method, the plate is meshed into 4-node quadrilateral elements. Each element is assigned with one orientation angle since fibres are assumed to be straight in these elements. Fig. 3.5 shows the comparison between the average compliance

method and the conventional FE method. Different symbols represent the Abaqus solution, average compliance method (ACM) with 40 elements, and the conventional FE method with 40 and 160 elements, respectively. The maximum relative error is defined as,

$$\epsilon_m = \max\left(\frac{\mid d_A^i - d_{FE}^i \mid}{d_A^i}\right), \tag{3.13}$$

where d_{FE} is the nodal displacement on path A-B calculated using the finite element method, and d_A^i is the displacement at the same nodal position from the exact Abaqus calculation.

The maximum relative error of the horizontal displacement between ACM with 40 elements and the exact solution is 0.7%, and 1.3% for the conventional FE with same mesh. With 160 elements used in the conventional FE element, the results agree well with the Abaqus solution with the maximum relative error less 0.1%. The vertical displacement obtained by ACM and conventional FE method can both agree well with the Abaqus solution with 40 elements, with a maximum error less than 0.2%. This indicates that ACM has good accuracy with 40 elements, as the relative error is less than 0.7%. Also, ACM is a better approximation than the conventional FE method for the same mesh. Therefore, the ACM improves the computational efficiency since it allows the use of fewer elements. However, this improvement is not large enough because the relative error of conventional FE method is only 0.6% more than ACM, which is also an acceptable approximation in this simulation.

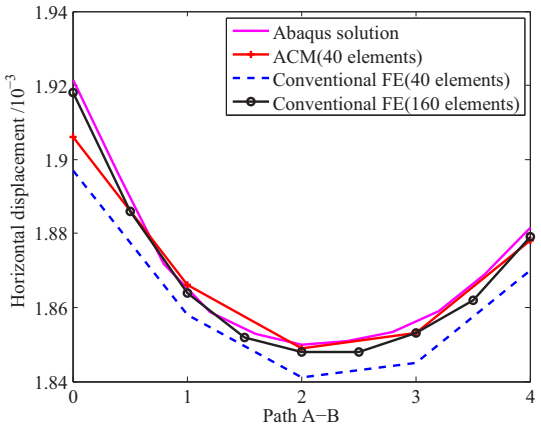

(a) Comparison of horizontal displacement on path A-B. The maximum relative error of the horizontal displacement between ACM (40 elements) and the exact solution is 0.7%, and 1.3% for the conventional FE with same mesh. Therefore, the average compliance method shows better accuracy than the conventional FE method.

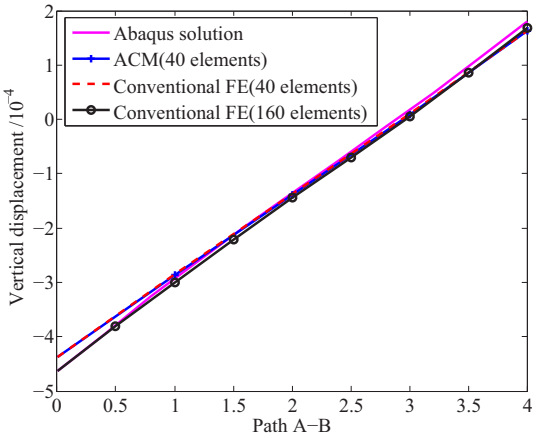

(b) Comparison of vertical displacement on path A-B. The vertical displacement obtained by average compliance method and conventional FE method can both agree well with the Abaqus solution using 40 elements, with relative error less than 0.2%.

Figure 3.5: Comparison of displacement on path A-B of the exact solution, ACM (40 elements), conventional FE (40 and 160 elements).

3.3 Finite Element with Explicit Fibre Curvature

The ACM makes an average of compliance along the reference fibre path, and uses the averaged value to approximate its stiffness. Therefore, the effective stiffness of any curved shape is equivalent to the stiffness of a unidirectional laminate with a constant fibre orientation, but their stress state are not identical. The ACM works well on the verification study because the shear strain is not dominant in the case of uniform loading. If the average fibre direction is off-axis from the loading direction, the lamina will develop shear strain as the fibres try to orient along the loading direction. Therefore, the ACM is not a good method to model the coupling between the normal stress and shear strain. When it comes to a highly curved shape or more complicated loading condition, the averaging method will not be a good approximation of the deformation since it cannot reflect the influence of curvature changes on the local stiffness exactly.

Therefore, a finite element with explicit curvature is developed to approximate structures with arbitrary fibre configuration and various loading condition considering the influence

of fibre curvature on the local stiffness. It is able to model the fibre curvature explicitly to capture the changes in stiffness for an element with curved fibres.

In the conventional FE process, the element stiffness matrix K^e is given as,

$$K^e = \int_{\Omega^e} B^T \bar{D} B d\Omega, \tag{3.14}$$

where B and $\bar{D}$ are the strain-displacement matrix and elastic matrix, respectively. The elastic matrix $\bar{D}$ is given as,

$$\begin{aligned}
\bar{D}_{11} &= D_{11}\cos^4\theta + (2S_{12} + D_{33})\sin^2\theta\cos^2\theta + D_{22}\sin^4\theta, \\
\bar{D}_{12} &= (D_{11} + D_{12} - D_{33})\sin^2\theta\cos^2\theta + D_{22}\sin^4\theta, \\
\bar{D}_{13} &= (2D_{11} - 2D_{12} - D_{33})\sin\theta\cos^3\theta + (2D_{12} - 2D_{22} + D_{33})\sin^3\theta\cos\theta, \\
\bar{D}_{22} &= D_{11}\sin^4\theta + (2D_{12} + D_{33})\sin^2\theta\cos^2\theta + D_{22}\cos^4\theta, \\
\bar{D}_{23} &= (2D_{11} - 2D_{12} - D_{33})\sin^3\theta\cos\theta + (2D_{12} - 2D_{22} + D_{33})\sin\theta\cos^3\theta, \\
\bar{D}_{33} &= 2\left(2D_{11} + 2D_{22} - 4D_{12} - D_{33}\right)\sin^2\theta\cos^2\theta + D_{33}\left(\sin^4\theta + \cos^4\theta\right).
\end{aligned}$$

where

$$\begin{aligned}
&D_{11} = \frac{E_1}{1 - \nu_{12}\nu_{21}}, \quad D_{22} = \frac{E_2}{1 - \nu_{21}\nu_{12}}, \quad D_{33} = G_{12}, \\
&D_{12} = \frac{v_{12}E_2}{1 - \nu_{12}\nu_{21}}, \quad D_{21} = \frac{v_{21}E_1}{1 - \nu_{12}\nu_{21}}, \\
&D_{13} = D_{23} = D_{31} = D_{32} = 0.
\end{aligned}$$

To handle the complex deformations as a result of curved fibres, 8-node quadrilateral elements are used because the second-order interpolation polynomials are used for displacements and rotations, as shown in Fig. 3.6(a). The strain-displacement matrix is,

$$\begin{aligned}
B &= [B_1 \;\; B_2 \;\; \cdots \;\; B_8], \\
B_i &= \begin{bmatrix} \frac{\partial N_i}{\partial x} & 0 \\ 0 & \frac{\partial N_i}{\partial y} \\ \frac{\partial N_i}{\partial y} & \frac{\partial N_i}{\partial x} \end{bmatrix}.
\end{aligned} \tag{3.15}$$

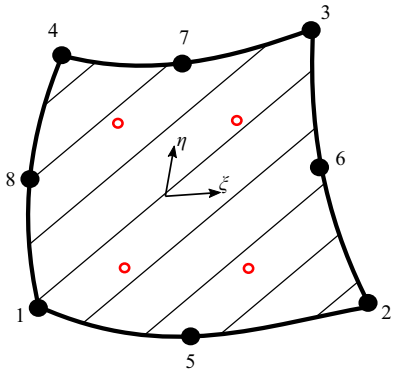

(a) 8-node quadrilateral element with straight fibres.

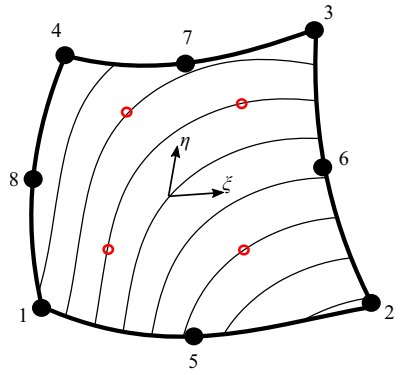

(b) 8-node quadrilateral element with curved fibres.

Figure 3.6: A typical 8-node quadrilateral element in the natural coordinate system (ξ, η). The vector of element degrees of freedom is $d = (u_1, w_1, u_2, w_2, \cdots, u_8, w_8)^T$. The shape function N_1, N_2, $\cdots$, N_8 for this element in natural coordinates are given in Eq. (3.16). The red circles in the element are Gauss points.

In the strain-displacement matrix B, the shape functions N_i are:

$$\begin{aligned}
N_1(\xi,\eta) &= -\frac{1}{4}(1-\xi)(1-\eta)(1+\xi+\eta), \quad N_2(\xi,\eta) = \frac{1}{2}(1-\xi)(1+\xi)(1-\eta), \\
N_3(\xi,\eta) &= -\frac{1}{4}(1+\xi)(1-\eta)(1-\xi+\eta), \quad N_4(\xi,\eta) = \frac{1}{2}(1+\xi)(1+\eta)(1-\eta), \\
N_5(\xi,\eta) &= -\frac{1}{4}(1+\xi)(1+\eta)(1-\xi-\eta), \quad N_6(\xi,\eta) = \frac{1}{2}(1-\xi)(1+\xi)(1+\eta), \\
N_7(\xi,\eta) &= -\frac{1}{4}(1-\xi)(1+\eta)(1+\xi-\eta), \quad N_8(\xi,\eta) = \frac{1}{2}(1-\xi)(1+\eta)(1-\eta).
\end{aligned} \tag{3.16}$$

Integration for the stiffness matrix in Eq. (3.7) cannot be performed analytically for general cases of isoparametric elements. Instead, the stiffness matrix is evaluated numerically using Gauss quadrature over quadrilateral regions. The Gauss quadrature formula for the integral in the two-dimensional case is:

$$K^e = h\sum_{i=1}^{n}\sum_{j=1}^{n} w_i w_j B(\xi_i,\eta_j)^T \bar{D} B(\xi_i,\eta_j)\,|J|, \tag{3.17}$$

where h, n, and w are the thickness of plate, number of integration points, and weights, respectively.

Gauss quadrature approximates the definite integral as a weighted sum of function values at prescribed sample points within the domain of integration. A minimal number of Gauss points is used to achieve a desired level of accuracy and efficiency. For each of these points,

the matrix product in Eq. (3.17), $B^T\bar{D}B$, is calculated, multiplied by a weight function and added together to evaluate the integral in Eq. (3.14).

According to Eq. (3.15-3.17), the matrix product $B^T\bar{D}B$ in Eq. (3.17) is determined by the orientation angle θ in each element and the local coordinates. In conventional finite element theory, the fibre orientation angle in each element is constant as fibres are assumed to be straight. As the orientation angle determines the matrix $\bar{D}$ in the product product $B^T\bar{D}B$, this matrix $\bar{D}$ is constant at all sample points.

However, in an element containing curved fibres, different orientation angles are present at different Gauss points due to fibre curvature as shown in Fig. 3.6(b). Hence, the matrix $\bar{D}$ varies between Gauss points. Instead of using one orientation angle, the local orientation at each sample point is picked and the local matrix product $B^T\bar{D}B$ is calculated for the Gauss quadrature. Eq. (3.17) should be modified as:

$$K^e = h\sum_{i=1}^{n}\sum_{j=1}^{n} w_i w_j B(\xi_i,\eta_j)^T D(\xi_i,\eta_j)B(\xi_i,\eta_j)\left|J(\xi_i,\eta_j)\right|, \tag{3.18}$$

where the elastic matrix $\bar{D}$ is a function of the location of the sample points.

Reduced integration is also applied to entail the use of fewer integration points to evaluate the integral than the full integration. It takes less time to form an element stiffness matrix due to the reduction in the number of Gauss points. Also, displacement-based finite element formulations overestimate the element stiffness, and reduced integration balances this by artificially reducing the element stiffness [74]. Therefore, in some cases the use of reduced integration can increase the accuracy of the results. Reduced integration can also avoid shear-locking during bending of a Timoshenko beam [75]. On the other hand, the use of too few Gauss points cause issues such as instability, spurious singular modes or hourglass modes. As a result, four Gauss points is recommended for an 8-node quadrilateral element [76].

3.3.1 Element Verification

To verify this finite element, regions containing different curved fibre configurations will be used. The deformation on a predefined path is calculated using three finite elements: the eight-node quadrilateral elements with curved fibres described above (S8 CFE), of which the

value of $B^T \bar{D} B$ at each sample point is determined by the local orientation; conventional 8-node finite elements (S8) and conventional 4-node finite elements (S4). Both S8 and S4 assume the fibres in each element to be straight, and assign a single fibre orientation angle. The results of the three methods will be compared. The S8 CFE should approximate the analytical solution closely, and be more efficient than the other two conventional FE methods.

A 1×1 square region containing fibres with paths defined by simple trigonometric equations is used, as shown in Fig. 3.7, 3.8 and 3.9. The orientation of curved fibres is determined by the coordinates

$$\theta(x) = \sin(n\pi x), \tag{3.19}$$

where $n = 1$, 2 and 4, and x is the x-coordinate in the plate. The left edge of the plate is fixed and the right edge is subjected to a uniform distributed load, F=20000, as shown in Fig. 3.7(a), 3.8(a) and 3.9(a). The fibre orientation at different sample points and the element centre can be calculated by Eq. (3.19). The path A-B is the right edge of the region and the horizontal displacement on it is computed. An Abaqus simulation is performed for this square region. A mesh convergence is studied to find the mesh size that gives a desired level of accuracy for the analysis. The result from a converged mesh is considered to be the exact solution for the displacement on path A-B. The same region is then meshed with 5×5 elements of the three types to be compared, and the simulation is rerun for each element type.

The horizontal displacement from the Abaqus simulation, S8 CFE, S8 and S4 are marked with different symbols in Fig. 3.7(b), 3.8(b) and 3.9(b). The maximum relative error of the horizontal displacement between the three FE methods and the exact solution is calculated using Eq. (3.20) and listed in Table 3.1.

	S8 CFE	S8	S4
$\theta(x) = \sin \pi x$	0.4%	1.8%	3.8%
$\theta(x) = \sin 2\pi x$	1.6%	6.8%	6.7%
$\theta(x) = \sin 4\pi x$	0.8%	6.9%	6.8%

Table 3.1: The maximum relative error of the horizontal displacement on path A-B for the square region containing sinusoidal fibres between the three FE methods and the exact solution

Table 3.1 shows that the relative error of the horizontal displacement on path A-B between

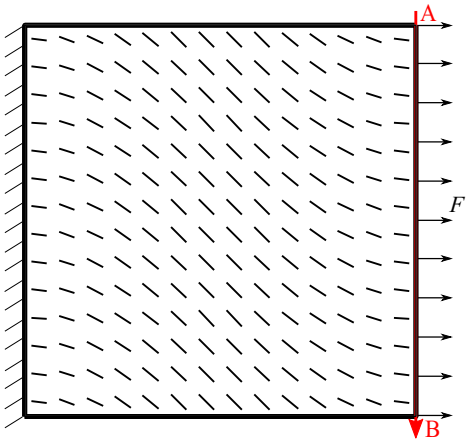

(a) 1×1 square plate containing fibres with paths defined by Eq. (3.19) with $n = 1$. The short lines represent the fibre orientation in each element. The left edge is fixed, and the right edge is subjected to a uniform distributed load, F=20000. Path A-B is the right edge.

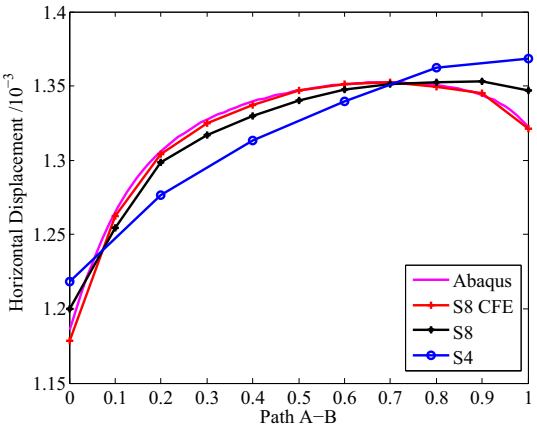

(b) Horizontal displacement of path A-B from the Abaqus calculation, 8-node curved finite element (S8 CFE), conventional 8-node finite element (S8) and conventional 4-node finite element (S4).

Figure 3.7: 1×1 square plate containing fibre with path defined by the sinusoidal curve $\theta = \sin(\pi x)$ and comparison of horizontal displacement from the Abaqus simulation, S8 CFE with 5 elements×5 elements, S8 with 5 elements×5 elements and S4 with 5 elements×5 elements on path A-B. The horizontal displacement obtained the S8 CFE is closest to the Abaqus calculation since the maximum relative error between the three finite element methods and Abaqus result are 0.4%, 1.8% and 3.8%, respectively.

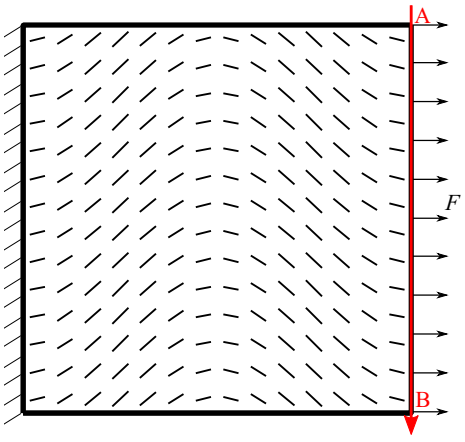

(a) 1×1 square plate with sinusoidal curve $\theta = \sin(2\pi x)$. The short lines represent the fibre orientation in each element obtained by Eq. (3.19). The left edge is fixed, and the right edge is subjected to a uniform distributed load, F=20000.

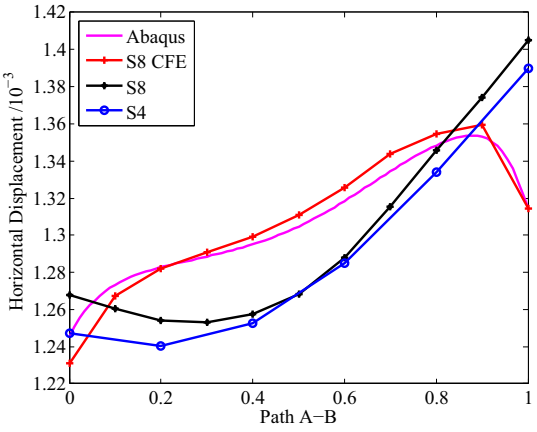

(b) Horizontal displacement of path A-B from the convergent Abaqus solution, 8-node curved finite element (S8 CFE), conventional 8-node finite element (S8) and conventional 4-node finite element (S4).

Figure 3.8: 1×1 square plate with sinusoidal curve $\theta = \sin(2\pi x)$ and comparison of horizontal displacement from the Abaqus simulation, S8 CFE with 5 elements×5 elements, S8 with 5 elements×5 elements and S4 with 5 elements×5 elements on path A-B. The horizontal displacement from S8 CFE is closest to the Abaqus convergent results since the maximum relative error between the three finite element methods and Abaqus result are 1.6%, 6.8% and 6.7%, respectively.

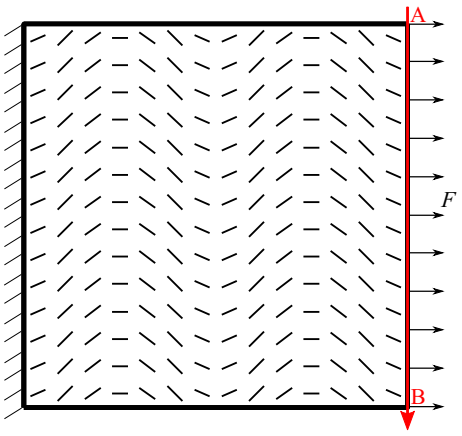

(a) 1×1 square plate with sinusoidal curve $\theta = \sin(4\pi x)$. The short lines represent the fibre orientation in each element obtained by Eq. (3.19). The left edge is fixed, and the right edge is subjected to a uniform distributed load, F=20000.

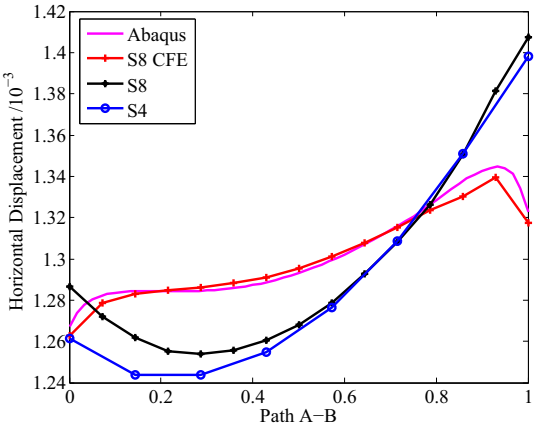

(b) Horizontal displacement of path A-B from the convergent Abaqus simulation, 8-node curved finite element (S8 CFE), conventional 8-node finite element (S8) and conventional 4-node finite element (S4).

Figure 3.9: 1×1 square plate with sinusoidal curve $\theta = \sin(4\pi x)$ and comparison of horizontal displacement from the Abaqus simulation, S8 CFE with 7 elements×7 elements, S8 with 7 elements×7 elements and S4 with 7 elements×7 elements on path A-B. More elements are used here as the fibre configuration is more complex. The horizontal displacement from S8 CFE is closest to the Abaqus convergent simulation since the maximum relative error between the three finite element method and Abaqus result are 0.8%, 6.9% and 6.8%, respectively.

S8 CFE and the exact solution is less than the other two conventional FE methods for the same mesh. As a consequence, using S8 CFE enables the use of larger elements on complicated curved shapes, while the conventional finite element method requires a finer mesh to attain equally accurate results. A larger element size enables the use of fewer elements, reducing computation time.

Computational efficiency is an important factor for the finite element method and is the main reason for developing this new element. Therefore, it is necessary to investigate its efficiency and compare it with conventional finite element methods. Fig. 3.10, Fig. 3.11 and Fig. 3.12 shows the running time as a function of the average relative error for three finite element methods. The line with different symbols represent S8 CFE, S8 and S4, respectively. The numbers on the markers are the number of nodes. The running time includes the process of calculating the element stiffness matrix, assembling the global stiffness matrix and solving

the FE equations. The average relative error is defined as,

$$\epsilon = \frac{\sum_{i=1}^{k} \frac{|d_A^i - d_{FE}^i|}{d_A^i}}{k}. \tag{3.20}$$

where k is the number of nodes on path A-B.

The comparison in all three cases indicates that the 8-node curved finite element (S8 CFE) is more accurate for the same computation time, and is faster for the same error. For example, Fig. 3.10(a) shows that S8 CFE only uses 96 nodes (0.1s) to have an average relative error of 0.23%, while S8 and S4 need 408 nodes (0.34s) and 676 nodes (0.42s). Fewer nodes means a reduced dimension of the global stiffness matrix, implying less computation time. Also, the figure shows that S8 CFE has the smallest error for the same running time. When the computation time is around 0.1s in the simulations using these three methods, the average relative errors of S8 CFE, S8 and S4 are 0.23%, 0.74% and 0.62%. Therefore, S8 CFE has better accuracy and efficiency than the other two conventional finite element methods on the three fibre laminates with sinusoidal curved shape.

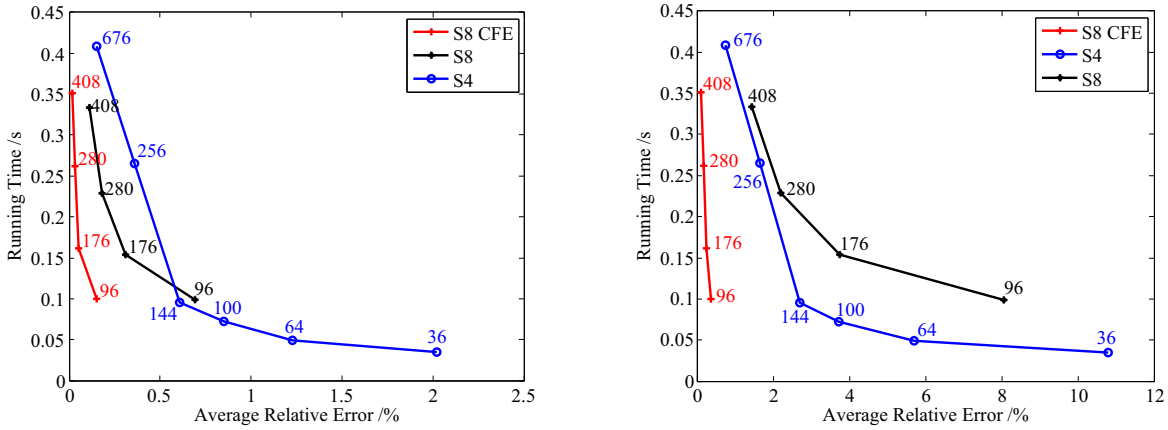

(a) Running time vs. relative error of horizontal displacement for 1×1 square plate with sinusoidal curve $\theta = \sin(\pi x)$.

(b) Running time vs. relative error of vertical displacement for 1×1 square plate with sinusoidal curve $\theta = \sin(\pi x)$.

Figure 3.10: Running time vs. relative error of displacement for 1×1 square plate with sinusoidal curve $\theta = \sin(\pi x)$ for three finite element method: S8 CFE, S8 and S4. The running time is the processing time of formulating the element stiffness matrix, assembling the global stiffness matrix and solving the FE equations. The numbers on each data points are the number of nodes used during the finite element process. The average relative errors are calculated based on Abaqus convergent solution using Eq. (3.20). S8 CFE is more efficient and accurate than the other two methods.

To assess this new FE method on a different curved shape, consider a 1×1 square region

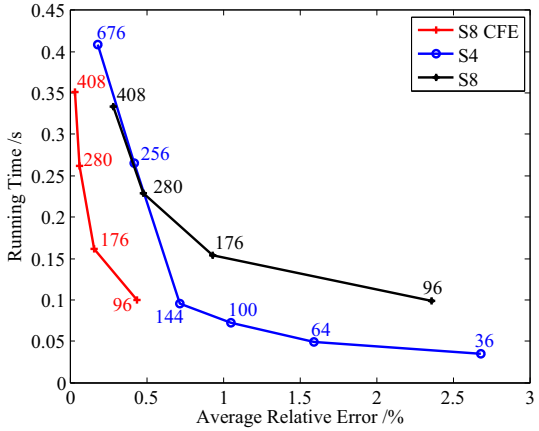

(a) Running time vs. relative error of horizontal displacement for 1×1 square plate with sinusoidal curve $\theta = \sin(2\pi x)$.

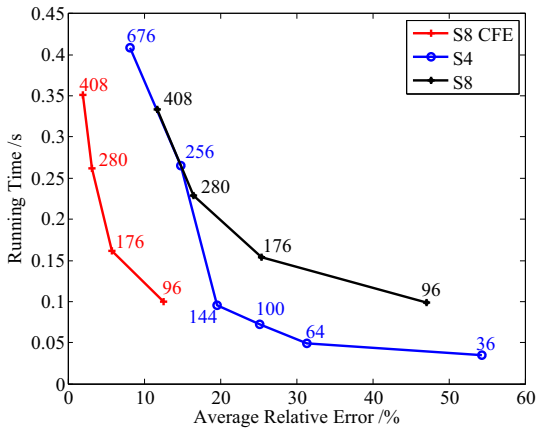

(b) Running time vs. relative error of vertical displacement for 1×1 square plate with sinusoidal curve $\theta = \sin(2\pi x)$.

Figure 3.11: Running time vs. relative error of displacement of the right edge for 1×1 square plate with sinusoidal curve $\theta = \sin(2\pi x)$.

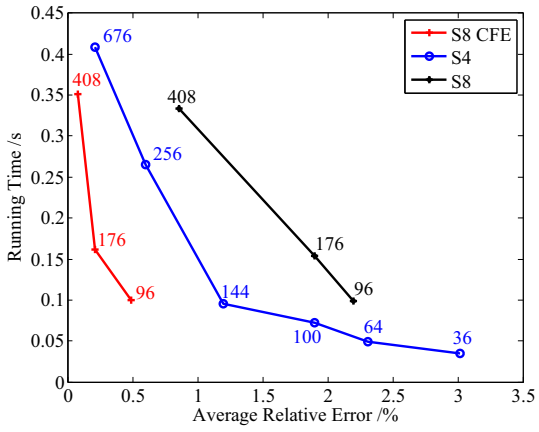

(a) Running time vs. relative error of horizontal displacement for 1×1 square plate with sinusoidal curve $\theta = \sin(4\pi x)$.

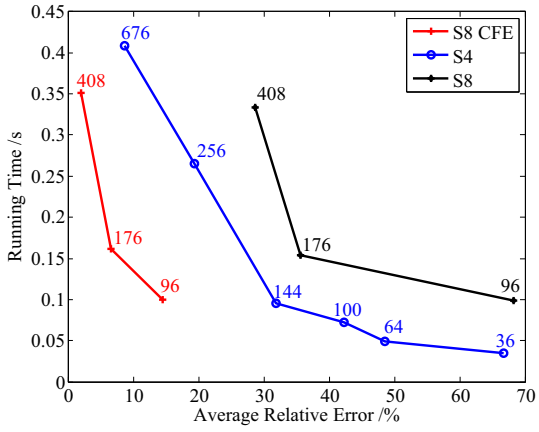

(b) Running time vs. relative error of vertical displacement for 1×1 square plate with sinusoidal curve $\theta = \sin(4\pi x)$.

Figure 3.12: Running time vs. relative error of displacement of the right edge for 1×1 square plate with sinusoidal curve $\theta = \sin(4\pi x)$.

containing fibres with paths defined as a set of concentric arcs in the second quadrant, so that the fibre orientation as a function of location is

$$\theta = \arctan \frac{\mid x \mid}{y}, \tag{3.21}$$

where x and y are the physical coordinates. Fig. 3.13 shows the curved fibre shape and the comparison of the horizontal displacement on Path A-B. An Abaqus simulation is conducted first, and the converged result is considered to be the exact solution. The maximum relative error of the horizontal displacement on path A-B between the three finite element methods (S8 CFE, S8 and S4) and the exact solution are 0.1%, 0.3% and 10.5%, respectively. This indicates that the S8 CFE works better than the other conventional finite element methods on this fibre configuration.

Fig. 3.14 shows the running time as a function of the average relative errors for three finite element methods. Both Fig. 3.14(a) and 3.14(b) indicate that S8 CFE uses fewer nodes and less time to run the simulation with same relative error. Also, the figure indicates that S8 CFE has the smallest error with the same running time. Therefore, S8 CFE has better accuracy and efficiency than the two conventional finite elements on this curved shape.

The above cases are all a square plate. In order to test a somewhat more practical and realistic case, an L-shaped plate with a loaded hole shown in Fig. 3.15(a) is used to access the accuracy and efficiency of the 8-node curved finite element. The hole is square because only structured meshes are currently considered. The top edge is fixed, and a point load is applied in the middle of the right side of the hole. The fibre orientations are determined by Eq. (3.19) with $n = 2$. The deformation on the right edge, path A-B, is calculated using three finite elements: S8 CFE, S8 and S4. Their results will be compared.

An Abaqus simulation is conducted for this L-shaped structure to obtain the exact displacement on path A-B. Fig. 3.15(b) shows the horizontal displacement from the Abaqus simulation. The horizontal and vertical displacements on path A-B are studied to show the convergence of the Abaqus simulation employing meshes of 92, 368, 1472, 5888 and 9200 elements, as shown in Fig. 3.16. It shows that the displacement approaches convergence as the number of elements increases. The mesh of 9200 elements in the Abaqus simulation will

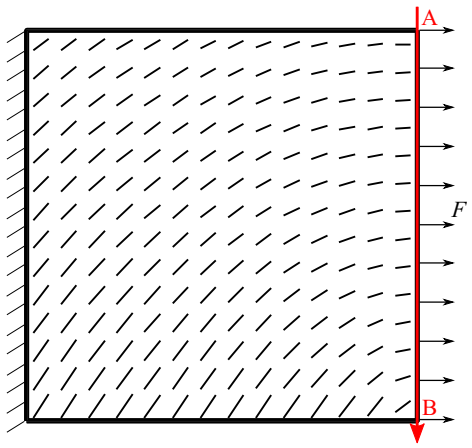

(a) 1×1 square plate with a set of concentric circular arc. The short lines represent the fibre orientation in each element obtained by Eq. (3.21). The left edge is fixed, and the right edge is subjected to a uniform distributed load, F=20000.

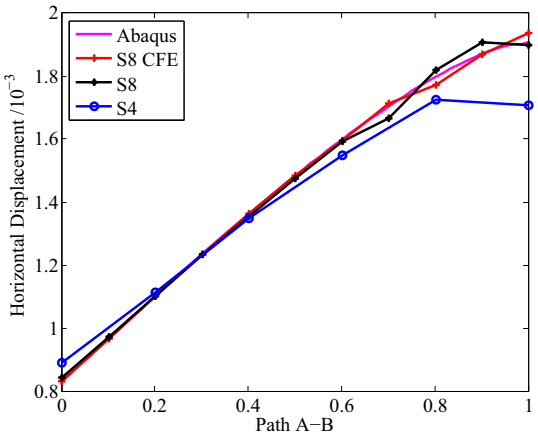

(b) Horizontal displacement of path A-B from the Abaqus calculation, 8-node curved finite element (S8 CFE), conventional 8-node finite element (S8) and conventional 4-node finite element (S4).

Figure 3.13: 1×1 square plate with a set of circular concentric arcs and comparison of horizontal displacement from the Abaqus simulation, S8 CFE with 5 elements×5 elements, S8 with 5 elements×5 elements and S4 with 5 elements×5 elements on path A-B. The horizontal displacement from S8 CFE is closest to the Abaqus calculation since the maximum relative error between the three finite element method and Abaqus result are 0.1%, 0.3% and 10.5%, respectively.

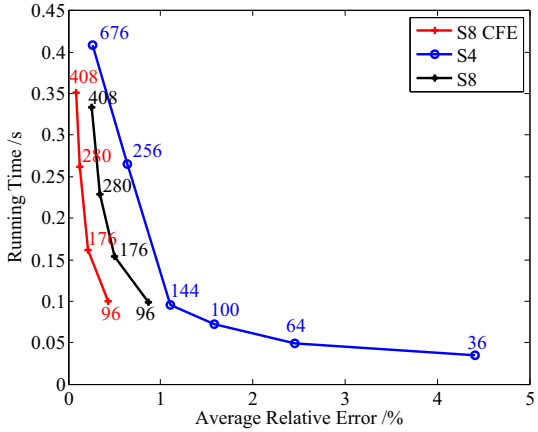

(a) Running time vs. relative error of horizontal displacement for 1×1 square plate with a set of concentric arcs.

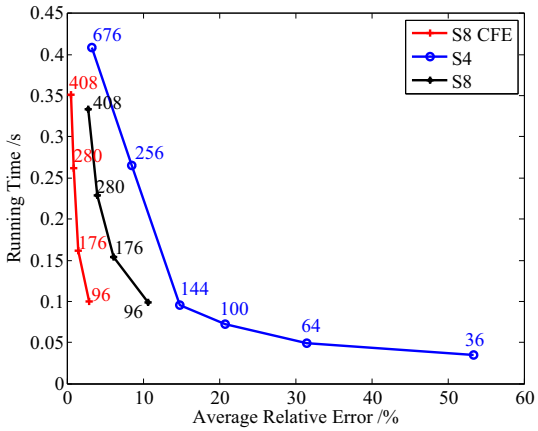

(b) Running time vs. relative error of vertical displacement for 1×1 square plate with a set of concentric arcs.

Figure 3.14: Running time vs. relative error of displacement for 1×1 square plate with a set of concentric arcs. The running time is the processing time of formulating the element stiffness matrix, assembling global stiffness matrix and solving FE equations. The numbers on each data points are the number of nodes used during the finite element process. The average relative errors are calculated based on Abaqus convergent solution using Eq. (3.20).

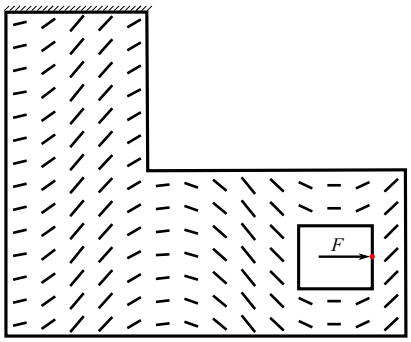

(a) An L-shaped structure with top edge fixed. The point load, F=10000, is applied in the middle of the right edge of the square hole. The fibre layout is determined by Eq. (3.19).

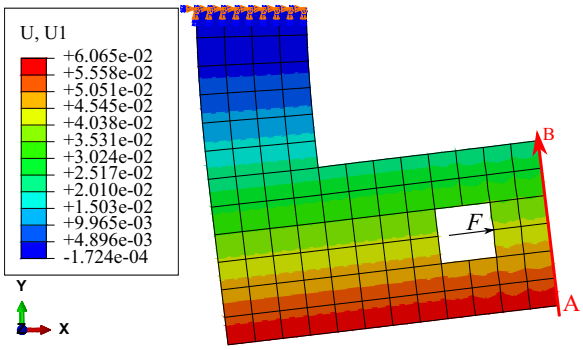

(b) Abaqus contour of the horizontal displacement of path A-B. The path is on the right edge from the point A to B.

Figure 3.15: An L-shaped structure with top edge fixed and a point load in the middle of the right of the square hole. The contour of the horizontal displacement in Abaqus solution is in the right figure.

be considered to provide the exact displacement of path A-B.

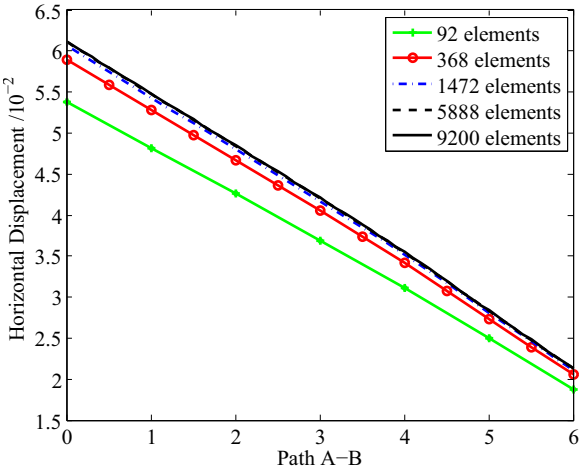

(a) Convergence of the Abaqus simulation for the horizontal displacement on path A-B.

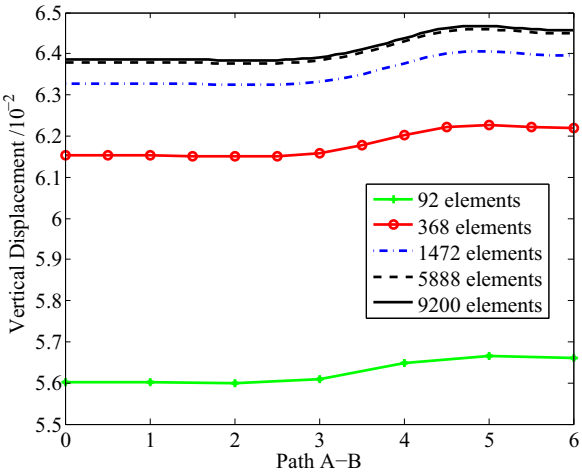

(b) Convergence of Abaqus simulation for the vertical displacement on path A-B.

Figure 3.16: Convergence of Abaqus simulation for the displacement on path A-B. The Abaqus simulation with a mesh of 92, 368, 1472, 5888 and 9200 elements are performed, respectively. As the number of elements increases, the displacement on path A-B approaches convergence at the mesh of 9200 elements, which can be considered as the exact solution.

After obtaining the exact solution, the comparison between S8 CFE, S8 and S4 is also conducted by showing the running time of the FE process as a function of the average relative error. The running time of the FE process includes calculating the element stiffness matrix, assembling the global stiffness matrix and solving the FE equations. The average relative error of the three FE methods and the exact solution is calculated from Eq. (3.20). Fig. 3.17

shows the running time of the FE process as a function of the average relative error compared to the Abaqus simulation. It can be seen that using 603 nodes (0.58s) with S8 CFE has good agreement with the Abaqus solution, for which the average relative error is around 1% for both horizontal and vertical displacement, while using 1584 nodes (1.16s) and the S4 can result in an average relative error of 3%. Again, the S8 CFE element improves the computation efficiency and maintains accuracy.

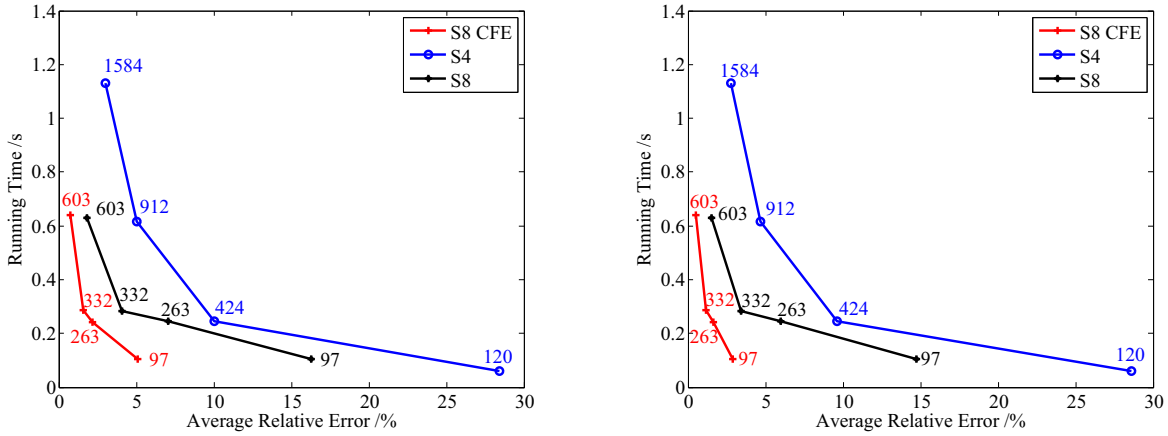

(a) Running time vs. relative error of horizontal displacement for the L-shaped structure.

(b) Running time vs. relative error of vertical displacement for the L-shaped structure.

Figure 3.17: Running time vs error of displacement for an L-shaped structure with square hole. The running time is the processing time of formulating the element stiffness matrix, assembling global stiffness matrix and solving FE equations. The numbers on each data points are the number of nodes used during the FE process. The average relative errors are calculated based on Abaqus convergent solution using Eq. (3.20).

3.4 Concluding Remarks

Two new methods are studied to formulate the finite element with curved fibres. The averaged compliance method is first used to formulate curved finite element to solve the problem of a rectangular plate with curved fibres subjected to an uniform distributed axial load. The results show that the ACM has acceptable accuracy when using large elements. However, the improvement is not large enough because the accuracy of the conventional FE method is also acceptable with the same mesh. The relative error of the horizontal displacement for conventional FE is only 0.6% more than ACM. The ACM approximates the stiffness of composite laminates with curved fibres to be equivalent to a unidirectional laminate with a

constant orientation. This is not effective when it comes to highly curved fibres or complex loading conditions because it fails to capture the influence of curvature changes on the local stiffness. Therefore, a better approach is necessary to account for this.

The second method is the finite element with explicit fibre curvature. It is developed for arbitrary fibre configurations and various loading conditions. The fibre curvature leads to different orientation angles at different Gauss points in an element containing curved fibres. As a result, the elastic matrix $\bar{D}$ in the product, $B^T \bar{D} B$, is not constant. When using Gauss quadrature to evaluate the integral for the element stiffness, this matrix product at each Gauss point is calculated based on the local orientation. This method reflects the influence of curvature changes on local stiffness, as it collects more local information in the element. As a consequence, this method enables enlargement of the element size and reduction of the dimension of the global stiffness matrix. The computational efficiency is improved. The results of finite element calculation using elements with explicit fibre curvature are compared with the conventional FE analysis. In the cases of a plate with sinusoidal and circular arc fibres, and an L-shaped structure with a loaded hole, the finite element with explicit fibre curvature has better agreement with the exact solution and is faster than the other conventional FE methods. Therefore, using curved finite elements can greatly improve the computation efficiency while maintaining a desired level of accuracy.

Chapter 4

Curvature Generation

4.1 Introduction

The finite element method is applied to analyze tailored fibre composite structures with curved fibres [8, 77, 78, 24]. The finite element method approximates continuous curved fibres as locally straight, and assigns an orientation angle to each element. Typically, if the fibre curvature is significant, the finite element mesh must be very fine to achieve sufficient accuracy.

However, computational time will significantly increase with a large number of elements. There is a trade-off between computational time and accuracy: increasing the number of elements to achieve the desired accuracy may require prohibitive calculation time. This is particularly pressing in an optimization setting, where the underlying analysis has to be performed repeatedly. To reduce the computational cost, it is necessary to use larger element size, but accuracy is sacrificed if the fibres are assumed to be locally straight. Difficulty arises because larger elements are not consistent with the approximation that the fibres are locally straight within an element: it is necessary to consider the fibre curvature as another important parameter. With two parameters for each element, curvature and orientation angle, it is possible to formulate finite elements that explicitly account for curved fibres. This enables larger element sizes, improving computational efficiency while maintaining accuracy However, continuous fibre angle optimization employing elements with straight fibres often

results in fibres on element boundaries that cannot be reconnected smoothly [38, 79, 80, 50]. The approach used here is to treat the fibre orientation angle within an element as the primary design variable, and to select a curvature for each element that minimizes the fibre discontinuity at the element boundaries.

In order to use large elements with curved fibres, it is necessary to know both the fibre orientation and curvature. A novel method to calculate the curvature is presented in this chapter. The approach is to employ the fibre orientation in each element as the primary design variable. The curvatures implied by the requirement that fibres are continuous are then generated for each element. The combination of the orientation angle and the curvature is then used to calculate element stiffness matrices. In an optimization scenario, the fibre orientation angles are updated at every optimization step, and the implied curvatures are then generated. The goal of this method is to enable the use of larger element sizes to reduce the computational cost of the calculation. Small fibre curvature is assumed in this work, because the maximum allowed curvature for fibres is 1.57 m^{-1} [81]. Highly curved fibres are physically unrealistic, as there will be defects such as local buckling and wrinkles on the fibre tows [50]. Meanwhile, elements that are significantly larger than conventional finite elements are used, but these elements are still small so that fibre angles are not varying dramatically. As a result, it is convenient to assume that fibres in a single element are circular arcs with constant curvature, which simplifies the modeling.

First the fibre orientation on the element boundaries is expressed with respect to the unknown curvature based on the geometry of curved fibres. The fibre angles at the middle of element edges, θ_t, θ_b, θ_l and θ_r, as shown in Fig. 4.1, are employed to represent the fibre orientation on the element edges. They are calculated by substituting the midpoint coordinates of each edge into the fibre angle expression, which is a function of the fibre orientation and (unknown) curvature for each element. The angle difference between each adjacent element edge is obtained. Finally the minimization of the sum of the angle differences generates curvature for each element, which is treated as a least squares minimization problem and solved through its normal equation. Several test cases, including a square plate with multiple curved fibres and an L-shaped structure, are presented to verify this method. The results from the curvature generation method show good agreement with analytical solutions

for the curvature of different continuous fibres, which indicates that it is an efficient way to generate distributions of curvature.

4.2 Analytical Expression for Fibre Angles in an Element

The curvature of a plane curve at any point is the change of angle of an infinitesimal segment of the curve. A curved fibre in a lamina can be treated as a plane curve. In order to obtain the curvature of a curved fibre, it is necessary to know the fibre orientations at arbitrary locations on this fibre. The fibre orientations are calculated by defining a reference path that approximates the curvilinear shapes of the fibres. The reference path employs basic functions such as linear functions [13, 16, 12, 21], or trigonometric functions [18, 19, 17, 20, 22]. Other researchers use higher order functions such as cubic Bezier curves [23], cubic polynomials [24] and spline functions [11]. Both basic and higher order functions require selection of function coefficients, but it is difficult to find the appropriate coefficients to model a composite structure with curved fibres.

Another option to obtain the fibre orientations at arbitrary locations is to specify the fibre orientation angle at discrete points and then build an analytical expression of the fibre configuration based on the geometry of curved fibres. This is the approach taken here, where the fibre orientation angle is specified at the centre of each element in a finite element mesh and the fibre orientations throughout the remainder of the element are calculated assuming a single constant curvature throughout the element. The geometric model of a square element with curved fibres is shown in Fig. 4.1. The element has side length $2a$, and the circular arcs represent fibres. Note that the circular arcs are not concentric. The angle θ_0 in the centre is the fibre orientation of the element, which is the angle between the x-axis and tangent line passing through the centre point O. The angle at an arbitrary location, M, in this element is the smallest angle between x-axis and the tangent line of the fibre passing through the point. In Fig. 4.1, the fibre orientation at point M is θ. The orientation angle is between -90° and 90° .

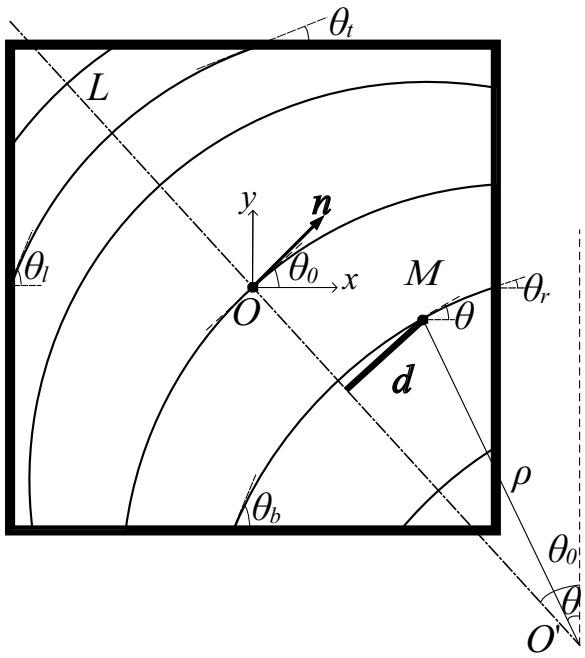

Figure 4.1: A geometric model of an element with curved fibres. The circular arcs represent the curved fibres and and centres of all the curved fibres are on the line L. Point O is the element centre with coordinate (0, 0) and M is an arbitrary point with coordinate (x,y). The normal vector $\boldsymbol{n}$ of line L starts at point O. The angles θ_0 and θ are between the x-axis and the tangent line of the fibre passing through the point O and M respectively. The orientation angle is between -90° and 90° . The radius of curvature is ρ and d is the distance from point M to line L.

In this work, each element has finite size, but is larger than the conventional finite element size. Assuming small fibre curvature, all fibres in one element are treated as a set of circular arcs with the same curvature, with the centres of all the arcs on a straight line L, as shown in Fig. 4.1. Point O is the element centre with coordinate (0, 0). $M(x, y)$ is an arbitrary point above line L and $\overrightarrow{OM} = (x, y)$. The normal vector $\boldsymbol{n}$ of line L has direction $(1/\tan\theta_0, 1)$. The normal vector is also the tangent line of the arc passing through the centre point. The distance d from point M to line L is equal to the length of the orthogonal projection of $\overrightarrow{OM}$ on $\boldsymbol{n}$. The length of this projection is given by:

$$d = \frac{\overrightarrow{OM} \cdot \boldsymbol{n}}{\|\boldsymbol{n}\|} = \frac{\frac{1}{\tan\theta_0}x + y}{\sqrt{1/\tan^2\theta + 1}} = x\cos\theta_0 + y\sin\theta_0. \tag{4.1}$$

The distance d can also be obtained using the radius of curvature ρ

$$d = \rho\sin(\theta_0 - \theta) = x\cos\theta_0 + y\sin\theta_0, \tag{4.2}$$

which can be transformed to:

$$\sin(\theta_0 - \theta) = \kappa x \cos\theta_0 + \kappa y \sin\theta_0, \tag{4.3}$$

where $\kappa = \rho^{-1}$ is the fibre curvature.

Similarly, for an arbitrary point below line L, the direction of vector $\boldsymbol{n}$ is $(-1/\tan\theta_0\ ,-1)$. The relation corresponding to Eq. (4.3) is

$$d = \rho \sin(\theta - \theta_0) = -x\cos\theta_0 - y\sin\theta_0. \tag{4.4}$$

This can be simplified to Eq. (4.3). Therefore, Eq. (4.3) can be used to obtain angles at any location in the element. The signs of κ and θ_0 indicate the concavity of fibre curves. Due to the assumption of small curvature, the angle change, $\theta_0 - \theta$, from the centre to any arbitrary point is approximately equal to $\sin(\theta_0 - \theta)$. Therefore, the left side of Eq. (4.3) can be approximated as $\theta_0 - \theta$ with acceptable accuracy. Then the angle at arbitrary position (x,y) is given by:

$$\theta = \theta_0 - \kappa x \cos\theta_0 - \kappa y \sin\theta_0. \tag{4.5}$$

It can be seen that θ is a function of θ_0, κ and position within the element. No other parameters are needed.

4.3 Calculation of Curvatures

With Eq. (4.5) it is possible to calculate the fibre orientation angle at an arbitrary location in an element. If a continuous fibre passes through a shared boundary of two adjacent elements, the orientation angles at the two element edges on the shared boundary should be identical. In a conventional finite element model, the orientation angles of fibres in any two adjacent elements on the shared boundary are different as the continuous curved fibres are discretized into locally straight segments. Thus, there is an angle difference at each boundary. Since every element shares boundaries with others, there is an angle difference on every shared boundary due to different θ_0. In a real composite, the fibres must curve so that there are

no discontinuities. In this discretized representation of a fibre composite, curvature in each element can be calculated by minimizing the overall discontinuity.

One option is to calculate angles on element edges and minimize the sum of the angle difference between each adjacent elements. The orientations also vary along the element edges. A convenient approach is to pick a value at the mid-point of an edge to represent boundary angles along that edge because it is an average of all angles on that edge. In Fig. 4.1, let (0, a), (0, $-a$), ($-a$, 0) and (a, 0) be the coordinates of middle point of the top, bottom, left and right side of the element, where a is the half-length of the element. Then those mid points fibre orientation angles are given from Eq. (4.5):

$$\begin{aligned} \theta_t &= \theta_0 - a\kappa \sin\theta_0, \\ \theta_b &= \theta_0 + a\kappa \sin\theta_0, \\ \theta_l &= \theta_0 + a\kappa \cos\theta_0, \\ \theta_r &= \theta_0 - a\kappa \cos\theta_0, \end{aligned} \tag{4.6}$$

where θ_t, θ_b, θ_l and θ_r are the top, bottom, left and right middle point angles, respectively.

After determining the fibre angles on element edges using Eq. (4.6), the sum of angle differences can be calculated. The larger the angle difference, the more discontinuous are the fibres. Therefore, the sum of the angle differences indicates the discontinuity of the fibre distribution. In order to make fibres as continuous as possible, it is reasonable to minimize the sum of angle difference between any adjacent elements to reduce the discontinuity. By selecting values of κ that minimize the sum of the angle differences, the curvatures that entail the minimum discontinuity can be calculated.

4.3.1 Steepest Descent Method

The goal is minimize the sum of the squares of the angle difference between each pair of adjacent elements. For a 2 element by 2 element square region, there are 4 shared boundaries as shown in Fig. 4.2. The sum of the squares of the differences in angles is,

$$f = (\theta_{1r} - \theta_{2l})^2 + (\theta_{3r} - \theta_{4l})^2 + (\theta_{1b} - \theta_{3t})^2 + (\theta_{2b} - \theta_{4t})^2, \tag{4.7}$$

where the first subscript letter is the element number, and the second subscript is the position of boundary angle.

Let a be unit length and substitute Eq. (4.6) into the above equation:

$$\begin{aligned} f =&(\theta_1 - \theta_2 - \kappa_1 \cos\theta_1 - \kappa_2 \cos\theta_2)^2 + (\theta_3 - \theta_4 - \kappa_3 \cos\theta_3 - \kappa_4 \cos\theta_4)^2 \\ &(\theta_1 - \theta_3 + \kappa_1 \sin\theta_1 + \kappa_3 \sin\theta_3)^2 + (\theta_2 - \theta_4 + \kappa_2 \sin\theta_2 + \kappa_4 \sin\theta_4)^2, \end{aligned} \tag{4.8}$$

where κ_1, κ_2, κ_3 and κ_4 are the curvatures that must be selected. The minimization of the objective function is,

$$\min_{\kappa} : f(\kappa). \tag{4.9}$$

The steepest descent method is chosen for its simplicity and ease of implementation.

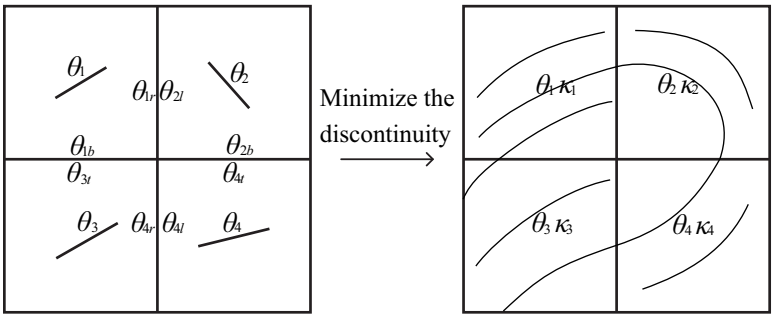

Figure 4.2: Orientation angles and shared boundaries for a square region of 2 element by 2 element. The curvatures that entail the minimum discontinuity are obtained by the selection of the value of κ that minimize the angle difference between adjacent elements. It is noticed that this 2×2 region is the only case where its objective function will go to zero because the number of boundaries is same as the number of parameters.

The convergence criterion used determines convergence based on the magnitude of successive changes in the objective function falling under a user defined limit:

$$\|\nabla f(\kappa)\| \leq \varepsilon, \tag{4.10}$$

where ε is the tolerance. If this criterion is satisfied, the optimization process has converged and the iterative loop will end.

Fig. 4.3 shows the convergence of curvature optimization for a 2 elements $\times$ 2 elements region with orientation angles 30°, 36°, 45° and 36°, respectively. It can be seen that the optimization is convergent after 115 iteration steps with the objective function less than 10^{-6},

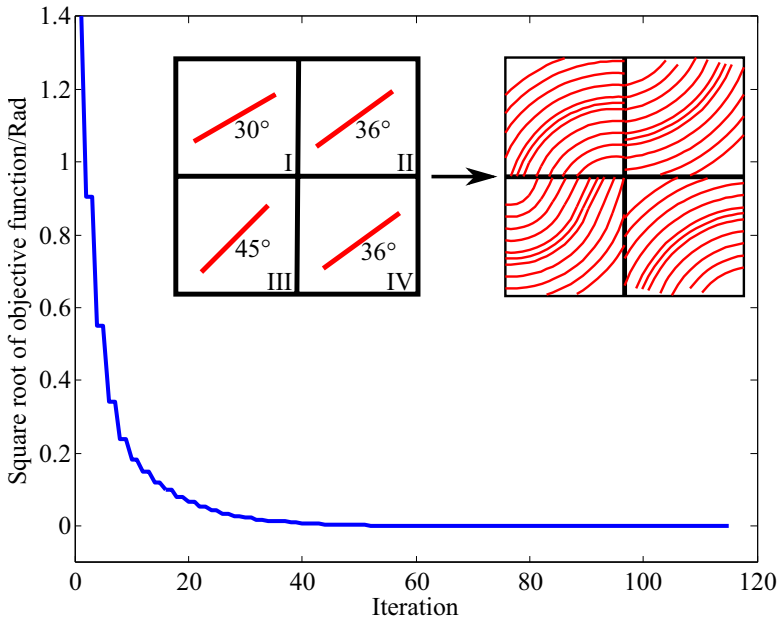

Figure 4.3: Convergence for the objective function for a 2 element by 2 element region with different orientation angles. The orientation angles in element I–IV are 30°, 36°, 45° and 36°, respectively.

which makes fibres in the elements continuous. The corresponding curvatures in elements I–IV are -0.5722, 0.4831, 0.7748 and -0.4831, respectively. However, the objective function will only go to zero for a 2 element by 2 element region since the number of boundaries is same as the number of parameters. In all other cases, it is likely that the final value of the objective function will be non-zero, implying some fibre discontinuity.

4.3.2 The Normal Equation

The number of elements will greatly influence the computation efficiency of the steepest descent method, because the number of design variables is same as the number of elements for using the steepest descent method to generate the curvature. It is necessary to find a more efficient way to obtain curvatures.

The objective function is a homogeneous quadratic polynomial in 4 variables in Eq. (4.8), so it can be written as a sum of squares and expanded to n elements with m shared boundaries,

$$f = \sum_{i=1}^{m} \frac{1}{2}\left(c^T \kappa^{(i)} - y^{(i)}\right)^2, \tag{4.11}$$

where c is a coefficient vector for curvature vector κ, and y is the corresponding constant vector

in the objective function. This is a least squares minimization problem. The minimization can be performed explicitly by taking derivatives of Eq. (4.11) with respect to the κ_i, and setting them to zero.

The derivative of the objective function is,

$$\nabla_\kappa f = A^T A\kappa + A^T b, \tag{4.12}$$

where $\kappa = [\kappa_1\ \kappa_2\ ...\ \kappa_n]^T$ is the vector of curvatures for each element, A is a symmetric matrix and b is a column vector involving θ_i. For example, the corresponding A and b for a 2 element by 2 element region is,

$$A = \begin{bmatrix} 1 & \cos\theta_1\cos\theta_2 & \sin\theta_1\sin\theta_3 & 0 \\ \cos\theta_1\cos\theta_2 & 1 & 0 & \sin\theta_2\sin\theta_4 \\ \sin\theta_1\sin\theta_3 & 0 & 1 & \cos\theta_3\cos\theta_4 \\ 0 & \sin\theta_2\sin\theta_4 & \cos\theta_3\cos\theta_4 & 1 \end{bmatrix},$$

$$b = \begin{bmatrix} -(\theta_1-\theta_2)\cos\theta_1 + (\theta_1-\theta_3)\sin\theta_1 \\ -(\theta_1-\theta_2)\cos\theta_2 + (\theta_2-\theta_4)\sin\theta_2 \\ -(\theta_3-\theta_4)\cos\theta_3 + (\theta_1-\theta_3)\sin\theta_3 \\ -(\theta_3-\theta_4)\cos\theta_4 + (\theta_2-\theta_4)\sin\theta_4 \end{bmatrix}.$$

First order optimality requires that the gradient be zero to find a local minimum of a function. Similarly, we can set the gradient to zero, and obtain its normal equation [82],

$$A^T A\kappa + A^T b = 0. \tag{4.13}$$

Then the curvature that minimizes the discontinuity can also be obtained by solving the linear system. Thus, the value of κ that minimizes f is given by,

$$\kappa = -(A^T A)^{-1} A^T b. \tag{4.14}$$

If matrix A is of full rank, then $A^T A$ is symmetric positive definite. This linear system

has a solution. It is difficult to determine whether matrix A is of full rank from the objective function. If A is close to singular, the vector κ that solves the system may not exist, or if one does exist, it may not be unique. In addition, the condition number of the normal equation is the square of the condition number of A, and the solution will deteriorate if A is ill-conditioned [83]. However, one can calculate its pseudoinverse instead of inverse to get more stable solution. The pseudoinverse constructs the solution of minimum Euclidean norm $\|A\kappa + b\|_2$ among all solutions [84]. When A is non-singular, it gives the actual inverse of A. Matlab, the C++ package LAPACK and the Python package NumPy all provide a pseudoinverse calculation. In addition, it is necessary to specify a value for the singular value tolerance [85], because the calculation of pseudoinverse treats singular values of A that are smaller than the tolerance as zero. How to choose this value will be discussed in detail.

4.3.3 Physical Interpretation of The Tolerance in The Pseudoinverse Calculation

The selection of tolerance in the pseudoinverse calculation influences the value of generated curvatures. If A does not have full rank, the least squares problem still has a solution, but it is no longer unique. The optimal solution is the vector κ that minimizes $\|A\kappa + b\|$. This solution is κ^+ and the matrix that produces κ^+ from b is the pseudoinverse of A, called A^+,

$$\kappa^+ = A^+ b. \tag{4.15}$$

The pseudoinverse A^+ is obtained from a singular-value decomposition (SVD) [86]. The SVD of matrix A is,

$$A = U\Sigma V^*, \tag{4.16}$$

where U is an $n \times n$ unitary matrix whose columns form an orthonormal basis, Σ is a diagonal $n \times n$ matrix with the singular values of A, σ_1, σ_2,..., σ_r, (r is the number of singular values) on the diagonal, and V^* is the conjugate transpose of the $n \times n$ unitary matrix V. The

pseudoinverse matrix can be represented as,

$$A^{+} = V^{T}\Sigma^{+}U^{T}, \tag{4.17}$$

where Σ^{+} is an $n \times n$ diagonal matrix with the reciprocals of the singular values, $\frac{1}{\sigma_1}$, $\frac{1}{\sigma_2}$, ..., $\frac{1}{\sigma_r}$, on the diagonal. Substituting this equation into Eq. (4.15), the solution that minimizes $\|Ax + b\|$ is:

$$\kappa^{+} = V^{T}\Sigma^{+}U^{T}b. \tag{4.18}$$

When some singular values of A are close to zero, the values on the diagonal entries of Σ^{+} approach infinity. This solution will have components of entries x^{+} that are extremely large. To avoid that, a tolerance is selected to treat singular values smaller than the tolerance as zero. Then entries in Σ^{+} at the same location as these singular values in A are also zero. For example, if the Σ is truncated at the third singular value of A, $r = 3$, then all singular values of A less than or equal to σ_3 will be treated as zero. Eq. (4.18) becomes,

$$\kappa^{+} = \begin{bmatrix} v_{11} & v_{12} & \cdots & v_{1n} \\ v_{21} & v_{22} & \dots & v_{2n} \\ \vdots & \vdots & \ddots & \vdots \\ v_{n1} & v_{n2} & \cdots & v_{nn} \end{bmatrix} \begin{bmatrix} 1/\sigma_1 & & & & \\ & 1/\sigma_2 & & & \\ & & 0 & & \\ & & & \ddots & \\ & & & & 0 \end{bmatrix} \begin{bmatrix} u_{11} & u_{12} & \cdots & u_{1n} \\ u_{21} & u_{22} & \dots & u_{2n} \\ \vdots & \vdots & \ddots & \vdots \\ u_{n1} & u_{n2} & \cdots & u_{nn} \end{bmatrix} \begin{bmatrix} b_1 \\ b_2 \\ \vdots \\ b_n \end{bmatrix}. \tag{4.19}$$

The matrix product result is:

$$\kappa^{+} = \begin{bmatrix} \frac{v_{11}(u_{11}b_1+u_{12}b_2+\ldots+u_{1n}b_n)}{\sigma_1} + \frac{v_{12}(u_{21}b_1+u_{22}b_2+\ldots+u_{2n}b_n)}{\sigma_2} \\ \frac{v_{21}(u_{11}b_1+u_{12}b_2+\ldots+u_{1n}b_n)}{\sigma_1} + \frac{v_{22}(u_{21}b_1+u_{22}b_2+\ldots+u_{2n}b_n)}{\sigma_2} \\ \vdots \\ \frac{v_{n1}(u_{11}b_1+u_{12}b_2+\ldots+u_{1n}b_n)}{\sigma_1} + \frac{v_{n2}(u_{21}b_1+u_{22}b_2+\ldots+u_{2n}b_n)}{\sigma_2} \end{bmatrix}. \tag{4.20}$$

The entries of U and V are all less than one because they are unitary matrices, and the upper

bound for the solution is:

$$\kappa_i^+ \leq (\frac{1}{\sigma_1} + \frac{1}{\sigma_2}) \sum_{i=1}^{n} b_i \leq (\frac{2}{\sigma_2}) \sum_{i=1}^{n} b_i. \tag{4.21}$$

Similarly, the upper bound of the solution at any truncated point $r = k$ is:

$$\kappa_i^+ \leq \left(\frac{1}{\sigma_1} + \frac{1}{\sigma_2} + \cdots + \frac{1}{\sigma_{k-1}}\right) \sum_{j=1}^{n} b_j \leq \left(\frac{k-1}{\sigma_{k-1}}\right) \sum_{j=1}^{n} b_j, \tag{4.22}$$

where σ_k is the largest singular value less than the tolerance, and all singular values less than or equal to the tolerance will be treated as zero. The upper bound of the curvature, κ_u, based on selected tolerance is:

$$\kappa_u = \begin{cases} 0, & \text{tol} \geq \sigma_1 \\ \left(\dfrac{k-1}{\sigma_{k-1}}\right) \sum\limits_{j=1}^{n} b_j, & \text{tol} = \sigma_k \, (1 < k \leq n) \, . \end{cases} \tag{4.23}$$

The upper bound of the generated curvature depends on the reciprocals of the singular values. Singular values that are close to zero can result in the curvature approaching infinity, which is physically unrealistic. Thus, it is necessary to truncate these singular values to avoid highly curved fibres. A physically reasonable value for the tolerance will be discussed later.

4.4 Verification of The Calculation of Curvature

To verify this approach, regions discretized into finite elements containing fibres with paths defined by simple trigonometric or polynomial equations will be used. The goal is to show that the calculation of curvatures using the normal equation and the pseudoinverse approaches the analytical values of curvature for fields of curved fibres with known fibre paths. The curvature in every element can be calculated in two ways: analytically based on the equation for the fibre paths or numerically through the application of the normal equation. The results of the two methods will be compared. The numerical approach should very closely approximate the analysis if the normal equation is to provide a satisfactory distribution of fibre curvatures.

First the curvature distribution obtained by the normal equation is compared to the

steepest descent method. A square region containing fibres with path defined as a set of concentric arcs is used, as shown in Fig. 4.4. The circular arcs are in the second quadrant and the circular arc centre is at the origin, then the fibre orientation θ in each element can be obtained by,

$$\theta(x) = \arctan \frac{\mid x \mid}{y}, \tag{4.24}$$

where x and y are the x and y-coordinate of the centre point in each element.

Fig. 4.4 compares the distribution of generated curvatures obtained by the steepest descent method and the normal equation in a 10×10 square region. This region contains fibres with paths defined as a set of concentric arcs. The square is meshed into 10 elements $\times$ 10 elements and the curved fibres are discretized into straight segments. The short lines represent the fibre orientations. The steepest descent method and the normal equation are both applied to compute the curvatures. The curvature distributions obtained from these two methods are identical. The normal equation is much faster than the steepest descent method since the gradient-based method will usually approach the optimal solution asymptotically. The following analytical curvature distribution will be only compared to the numerical solution found through the application of the normal equation, and the steepest descent method will be no longer considered.

Two additional cases are presented to verify this method for the calculation of curvature through the application of the normal equation. They are a square region containing fibres with paths defined by simple trigonometric or polynomial equations. The trigonometric equation that determines the fibre path is:

$$t(x) = \sin \frac{2x}{\pi}, \tag{4.25}$$

where x is the x-coordinate. The curvature is:

$$\kappa(x) = \left| \frac{t''(x)}{(1 + t'(x))^{3/2}} \right| = \left| \frac{4 \sin \frac{2x}{\pi}}{\pi^2 \left(1 + \frac{4 \cos^2 \frac{2x}{\pi}}{\pi^2}\right)^{1.5}} \right|. \tag{4.26}$$

The curvature obtained numerically through the application of the normal equation is

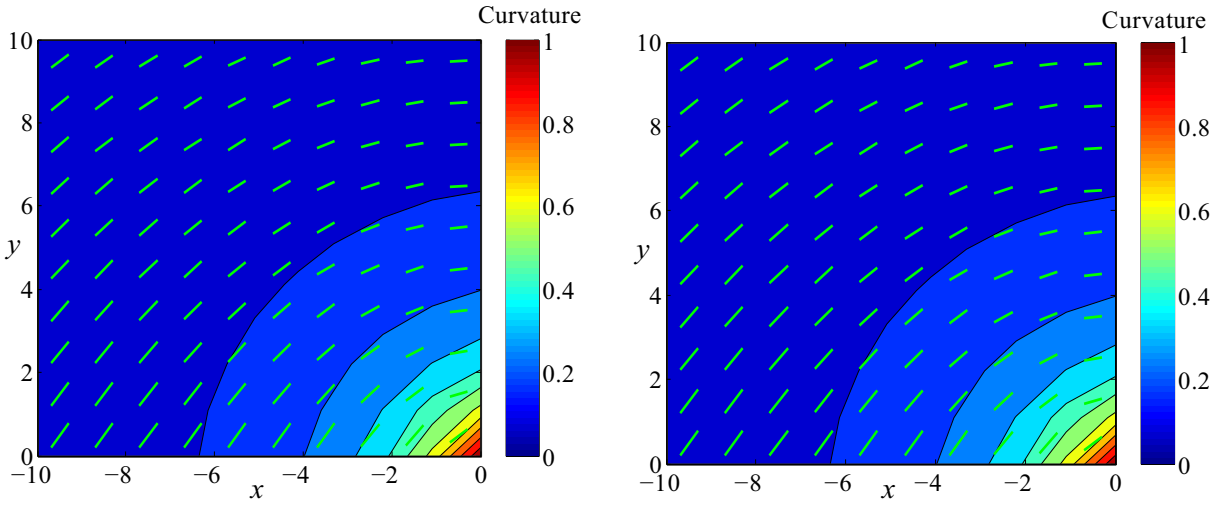

(a) Contour of curvature obtained by the application of steepest descent method.

(b) Contour of curvature obtained by the application of the normal equation.

Figure 4.4: Contours of the curvature distribution obtained by the steepest descent method and the normal equation for a 10 × 10 square region. This region contains fibre with path defined as a set of concentric arcs. The square is meshed into 10 elements × 10 elements with straight fibres. The fibre orientations are represented as short lines.

compared to the analytical result for curvature in this square region calculated using Eq. (4.26) in Fig. 4.5. The 10 × 10 square region contains fibres with paths defined by the trigonometric function. The region is meshed into 80 elements × 80 elements. Fig. 4.5(a) is the analytical solution of the curvature distribution obtained by Eq. (4.26). The continuous sinusoidal curves represent curved fibres. The numerical solution of curvature through the application of the normal equation is shown in Fig. 4.5(b). At the centre of each element, the fibre orientation is calculated using Eq. (4.25). This distribution of fibre orientations is then used with the normal equation to calculate the implied curvature in each element.

Since the sinusoidal curves describe a smooth repetitive oscillation, the corresponding curvature also varies with location as shown in Fig. 4.5(a). After applying the normal equation to calculate curvature, Fig. 4.5(b) shows that the numerical solution gives close approximation to the analytical curvature distribution. The average relative error between the numerical and analytical solution is defined as:

$$e = \frac{\sum_{i=1}^{n} \frac{\kappa_n^i - \kappa_a^i}{\kappa_a^i}}{n}, \tag{4.27}$$

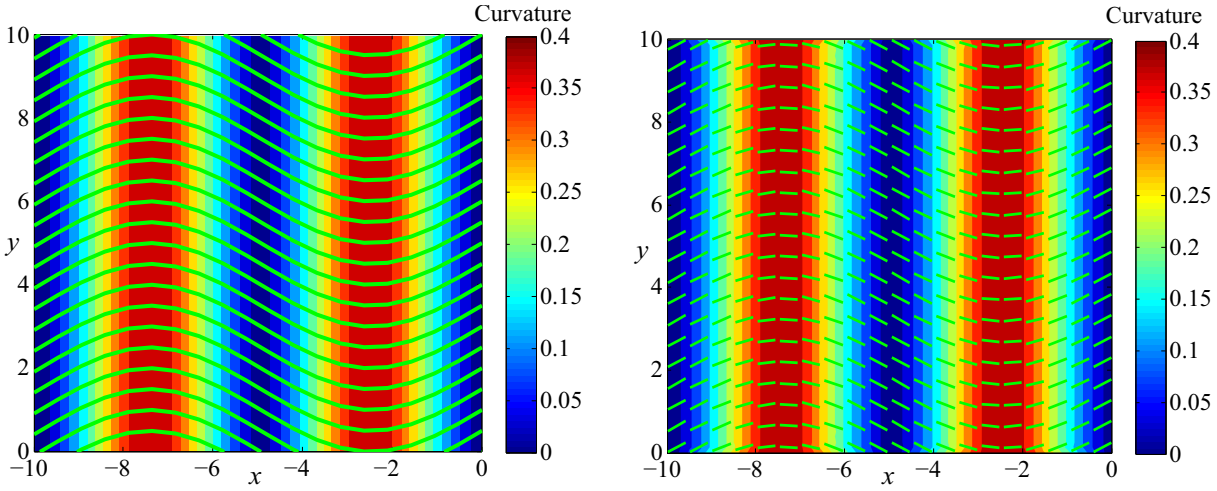

(a) Analytical contour of curvature for a square containing fibres with paths defined by Eq. (4.25). One sinusoidal curve is created based on Eq. (4.25) first, then it is shifted to generate a set of parallel curves in the square region.

(b) Numerical contour of curvature obtained by using the normal equation. The square region is meshed into 80 elements × 80 elements with straight fibres. The short lines represent the fibre orientation.

Figure 4.5: Contours of curvature distribution from the analytical solution based on the trigonometric equation for the fibre paths and the numerical solution through the application of the normal equation. The square region contains fibres with paths defined by a sinusoidal function.

where κ_n^i and κ_a^i are the numerical and analytical curvature in ith element. The average relative error between the numerical and analytical solution for this sinusoidal curved shape is 1.05%. The difference between the numerical and analytical curvature is primarily near the top and bottom boundaries, but this area is small. Thus, the normal equation provides an accurate distribution of fibre curvatures.

The sinusoidal equation that defines the fibre paths may be also replaced with a quadratic equation:

$$t(x) = \frac{x^2}{2\pi} + 2x. \tag{4.28}$$

The analytical curvature can be calculated as:

$$\kappa(x) = \left| \frac{t''(x)}{(1 + t'(x)^2)^{3/2}} \right| = \left| \frac{1}{\pi(1 + \left(2 + \frac{x}{\pi}\right)^2)^{1.5}} \right|. \tag{4.29}$$

Fig. 4.6 shows the distribution of curvatures from the analytical solution based on the quadratic equation for the fibre paths and the numerical solution through the application of the normal equation. The 10 × 10 square region contains fibres with paths defined the quadratic

function. The region is discretized into 80 elements × 80 elements. Fig. 4.6(a) is the analytical solution of the curvature distribution obtained by Eq. (4.29). The continuous quadratic curves are curved fibres. The numerical solution of curvature through the application of the normal equation is shown in Fig. 4.6(b). The curved fibres are discretized into straight segments. The fibre orientations are represented as short lines in Fig. 4.6(b). The average relative error between the numerical and analytical solution for this sinusoidal curved shape is 0.97%.

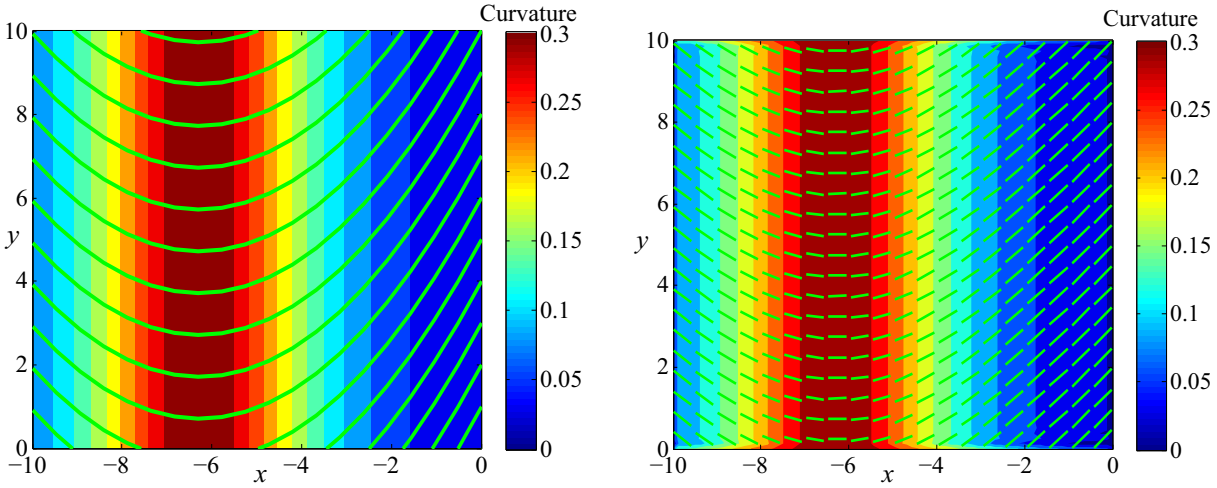

(a) Analytical contour of curvature for a square containing fibres with paths defined by Eq. (4.28). One sinusoidal curve is created based on Eq. (4.28) first, then it is shifted to generate a set of parallel curves.

(b) Numerical contour of curvature obtained by using the normal equation. The square region is discretized into 80 elements × 80 elements with straight fibres. The short lines represent the fibre orientation.

Figure 4.6: Contours of curvature distribution from analytical solution based on the quadratic equation for the fibre paths and the numerical solution through the application of the normal equation. The square region contains fibres with paths defined by a quadratic function.

The comparisons of different curved shapes show that this method for curvature generation agrees well with the analytical solutions for various fibre configuration, but both cases involve a square region containing fibres with paths defined by simple functions. It is necessary to verify this application of the normal equation on a region with discretized fibre orientation as well.

Fig. 4.7 presents contours of curvatures calculated using the normal equation for a discretized 24 × 8 plate section meshed into 192 (24×8) elements. The short lines represent the direction of the discrete fibre orientation that originated from an optimization [52]. The contour of the distribution of generated curvatures shows greater changes at areas with large

discontinuity.

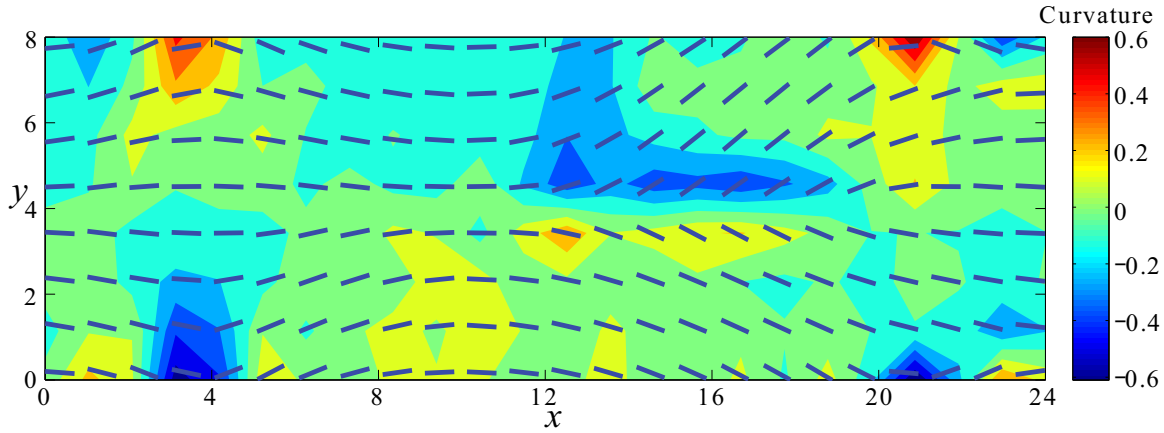

Figure 4.7: Contour of curvature for a discretized 24 × 8 plate section meshed into 192(24 × 8) elements. The short lines represent the fibre orientation from an optimization of eigenfrequency.

To verify this method for the calculation of curvature in a more realistic case, an L-shaped single layer thin composite lamina with a loaded hole is used. It is fixed on the top edge and subjected to a point load, F=10000, at the middle of the right side of the square hole as shown Fig. 4.8(a). The fibre configuration in each element is orientated with the maximum principal stress for the relevant geometry with an isotropic material. The orientation of maximum principal stress is determined by an Abaqus simulation, represented as arrows in each element in Fig. 4.8(b).

The curvature is calculated numerically through the application of the normal equation. Fig. 4.9(a) shows the contours of curvature by setting the orientation of maximum principal stress as the fibre orientation angle in each element. The contour shows areas with large discontinuity, resulting a great change of curvature. As an aside, it is worth noting that this result indicates that, at least for this case, simply selecting the fibre angles as the orientations of the largest principal stress for the isotropic case will result in fibre discontinuities that make the composite effectively unmanufacturable.

Fig. 4.9(b) shows curved fibre orientations based on solutions for curvatures obtained from the normal equation. As the fibres are assumed to be circular arcs, their centres are determined by the fibre orientation angle and the concavity. Circles are plotted based on this centre and the radius of curvature. The more highly curved fibre shapes indicates areas with larger curvature.

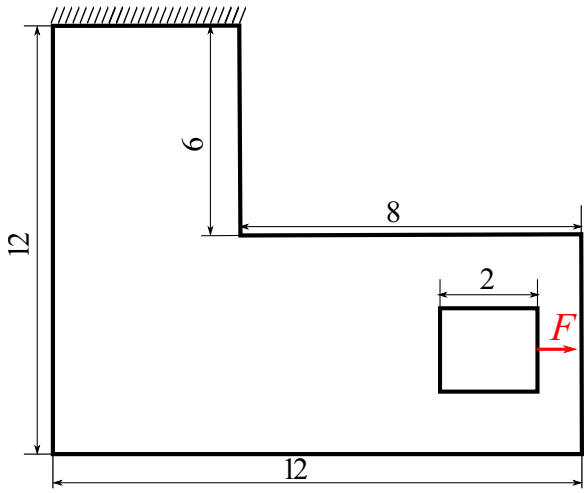

(a) Geometric model of an L-shaped structure with a square hole. The top edge is fixed and a point load, F=10000, is applied in the middle of the right side of the square hole.

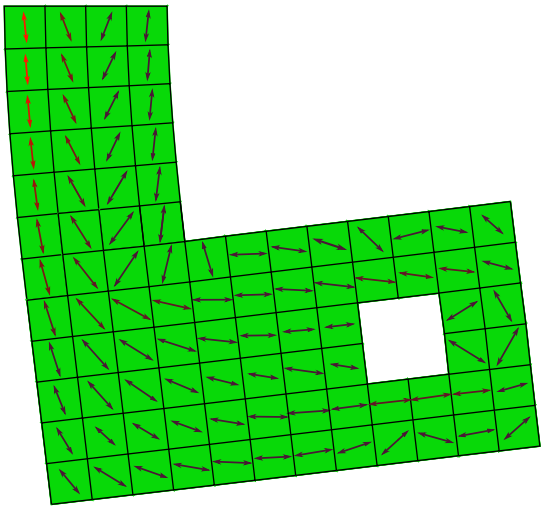

(b) Maximum principal stress direction for the same L-shaped structure with an isotropic material, represented as lines with arrow. The length of lines indicates the magnitude of the maximum principal stress.

Figure 4.8: Geometric model of the L-shaped single-layer composite lamina. The fibre orientation in each element is same as the maximum principal stress for the relevant geometry with an isotropic material.

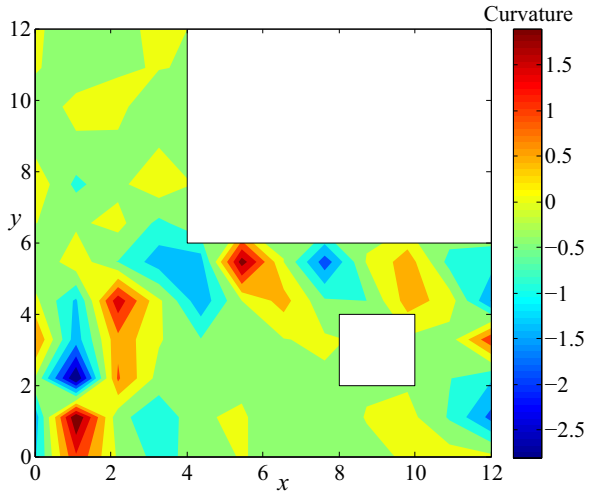

(a) Contour of curvature for the L-shaped composite lamina. The fibre configuration in each element is oriented with the maximum principal stress for an isotropic material with the same geometry and loading conditions.

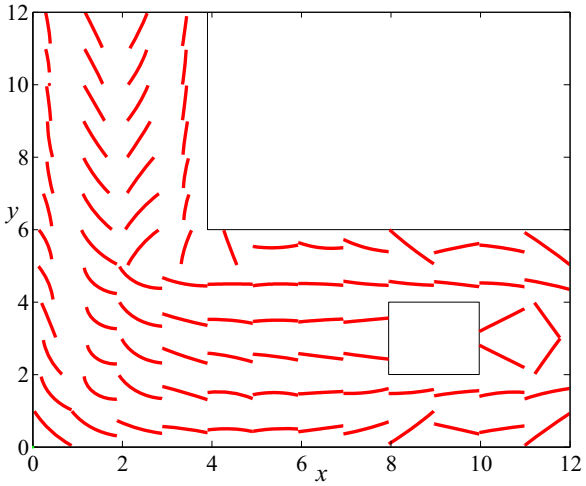

(b) Curved fibre orientations based on solution for curvatures obtained from the normal equation in the L-shaped domain. The tolerance is 0.7 when calculating the pseudoinverse to generate the curvature.

Figure 4.9: Contour of curvature and curved fibre orientations for the L-shaped structure.

When calculating the curvature, selecting the value of tolerance during the computation of the pseudoinverse is critical to the magnitude of the curvature, thereby influencing the curved fibre orientations. This is because the pseudoinverse is computed through SVD. The entries of the diagonal matrix from SVD are known as the singular values of the matrix A. During the computation of the pseudoinverse, the inverse of this diagonal matrix is needed. If the singular values of A contain numbers close to zero, their reciprocal will be several orders of magnitude larger than the reciprocal of other singular values, sometimes approaching infinity. Those reciprocals form the inverse of the diagonal matrix, which causes a pseudoinverse matrix with entries that can be close to infinity. This will lead to large values of curvature as well, resulting in highly curved fibres. The large curvature are physically unrealistic. Therefore, it is necessary to eliminate the singular values that are close to zero to prevent large values of the reciprocals. This can be avoided by choosing a value of tolerance so that the computation treats singular values of the matrix A that are smaller than the tolerance as zero.

The value of tolerance will influence the curved fibre orientation. If the tolerance is too large, singular values that are much larger than zero are also treated as zero. The resulting curvatures are close to zero, so that the fibres will be nearly straight as shown in Fig. 4.10(a), and the simulation will be equivalent to the conventional finite element with straight fibres. On the other hand, small values of tolerance will lead to extremely large curvature in some elements as shown in the highlighted areas in Fig. 4.10(b), making the laminates impossible to manufacture. The selection of tolerance depends on manufacturing constraints as the magnitude of curvatures are limited [50].

With the generated curvatures, it is possible to plot an intuitive image of how curved fibres are spatially varying in the laminate domain. Fig. 4.11 shows the spatially varying fibres in each element for the L-shaped structure. They are created by shifting the curved fibre equidistantly in each element domain. Different tolerances are selected to show the influence of tolerance on the curved fibre orientation. It can be seen that in Fig. 4.11(a) there are full circles in the highlighted areas with tolerance of 0.5, and the highly curved fibres are physically unrealistic. As small curvature is assumed in this work, the resulting fibres should be slightly curved. Fig. 4.11(b) shows a good example of fibres that are not

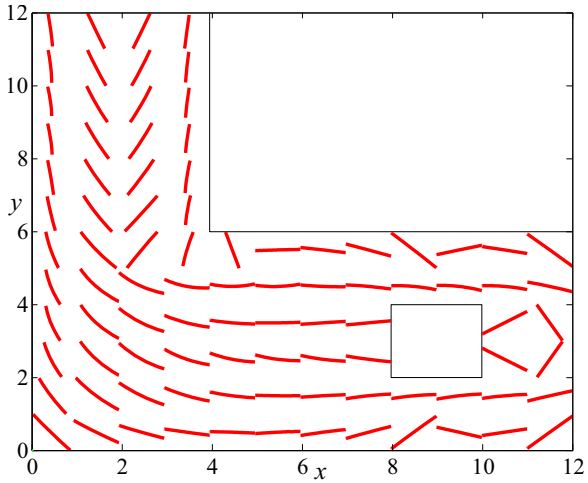

(a) Curved fibre orientations based on solution for curvatures obtained from the normal equation in the L-shaped domain. The tolerance is 0.9 when calculating the pseudoinverse to generate the curvature. Fibres are close to straight.

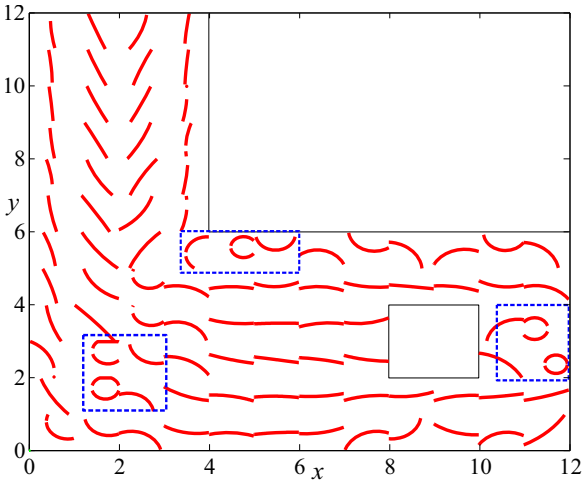

(b) Curved fibre orientations based on solution for curvatures obtained from the normal equation in the L-shaped domain. The tolerance is 0.1 when calculating the pseudoinverse to generate the curvature. Highlighted area are unrealistic fibre layout.

Figure 4.10: Curved fibre orientations in the L-shaped domain using different tolerance.

over curved or straight with tolerance of 0.7. However, there is still fibre discontinuity among some elements. Further work will be penalizing the continuity to get more continuous fibres, or even an explicit mathematical model of discontinuity.

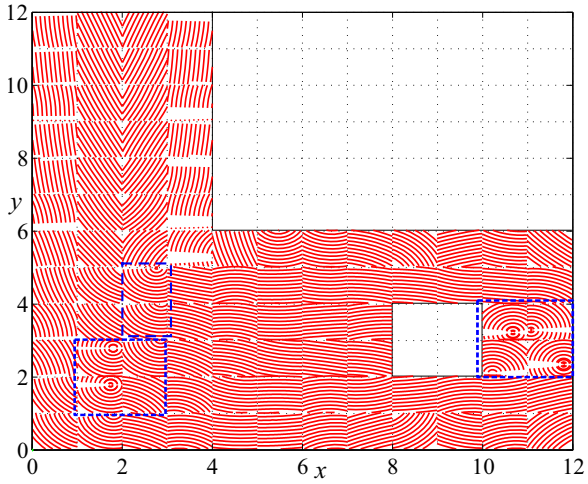

(a) Plot of spatially varying curved fibres in each element, and the tolerance is 0.5 when calculating the pseudoinverse to generate curvatures. Highlighted area shows unrealistic fibre layout.

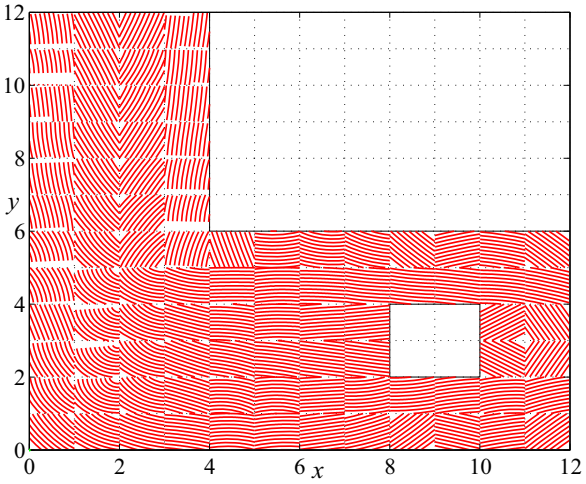

(b) Plot of spatially varying curved fibres in each element, and the tolerance is 0.7 when calculating the pseudoinverse to generate curvatures.

Figure 4.11: Plots of spatially varying curved fibres for the L-shaped structure.

Selecting tolerance controls the magnitude of the calculated curvatures. Eq. (4.23) gives the theoretical upper bound of the minimum norm solution of Eq. (4.13) using the normal equation. It shows that the upper bound of the minimum norm solution is a reciprocal function with respect to the tolerance. As the tolerance increases, the values of entries in the pseudoinverse of matrix A should decrease as more singular values of A are treated as zero. Fig. 4.12 shows a semi-log plot of the theoretical upper bound of curvatures using Eq. (4.23) and the actual maximum curvatures calculated using different tolerance for the L-shaped structure. It can be seen that the actual curvatures are far below the theoretical upper bound. Therefore, the tolerance prevents the generated curvature from being extremely large.

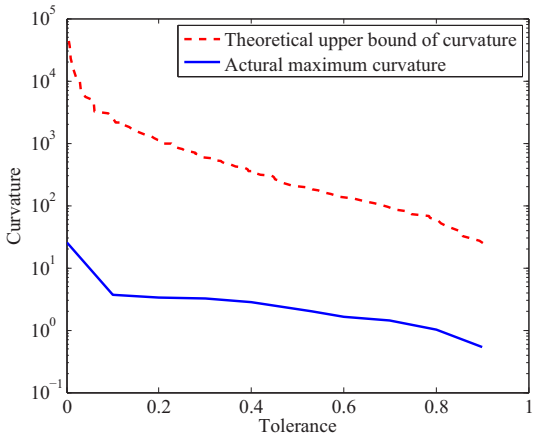

Figure 4.12: The theoretical upper bound of curvatures generated and the actual maximum curvatures (semi-log scale) as a function of the tolerance for the L-shaped structure.

4.5 Concluding Remarks

By varying the fibre orientations across a composite lamina it is possible to tailor the composite structure spatially to have optimal mechanical properties. One of the issues with optimizing composites modeled in this way is that the computational efficiency is greatly affected by using the conventional finite element method with a fine mesh. Therefore, it is necessary to use large element sizes to improve efficiency, but assuming fibres are locally straight is not sufficiently accurate in a finite element simulation with larger elements. Since larger elements violate the approximation that the fibres are locally straight, the fibre model must explicitly account for curvature. By modeling the curvature explicitly, it is possible to

formulate finite elements with curved fibres, which allows using larger elements to improve the computational efficiency and maintain the accuracy. As a result, fibre curvature has to be calculated. Also, adjusting the value of fibre curvature in each element can reduce the degree of spatial discontinuity of the fibre orientations achieved in the optimization. The calculation of curvature was done first by deriving a concise analytical expression of fibre angles at arbitrary locations in the elements based on the geometry of curved fibres, and then using it to get boundary angles of each element. The sum of the square of the angle difference between shared element boundaries is calculated and minimized in order to calculate the curvature that entails the minimum discontinuity. This is considered as a least square minimization problem. It was found that using the steepest descent method is slower than solving the normal equation. The normal equation uses pseudoinverse to find the minimum Euclidean norm solution to a system of linear equations with multiple solutions, as the matrix A is not always positive definite. The selection of tolerance during the computation of pseudoinverse influences the magnitude of curvature. Small tolerance will results highly curved fibres that are physically unrealistic, while large tolerance will lead to nearly straight fibres, making the use of larger element size impossible. The calculation of curvature is verified on several test cases, including a square plate containing curved fibres and an L-shaped thin single-layer composite lamina. The results of the calculation of curvature from the application of the normal equation show good agreement with analytical solutions. With the curvatures, it is possible to show an intuitive image of the spatially varying curved fibres in each element domain. More importantly, it enables the formulation of larger size finite element with curved fibres, while still accurately modeling the physics of the composite.

Chapter 5

Stiffness Optimization

5.1 Introduction

The use of advanced composite manufacturing methods enables tailoring of the mechanical properties of composite structures to improve their structural performance. To take advantage of such methods, it is desirable to find optimal fibre configurations that provide better mechanical performance. The optimization problem consists of an objective function, which may, as examples, be maximum stiffness or lowest eigenfrequency, combined with any necessary constraints. The optimization procedure for composite laminates includes discretizing the whole structure into a number of small elements, then assigning a fibre orientation angle in each element. The derivative of the objective function and the constraints with respect to the design variable, orientation angle, will be calculated. The fibre orientations and the value of objective function are recalculated and updated in each iteration until the maximum structural performance is achieved. This chapter will develop a method to optimize the fibre orientations throughout thin composite lamina structures for maximum structural stiffness. Because it is necessary to evaluate the objective function at each optimization step, an efficient method for doing so is necessary. This motivates the creation and application of a finite element that models fibre curvature explicitly, as developed in Chapter 3, and a method for calculating curvature, as explained in Chapter 4. Both of these will be applied in the optimization procedure described here.

Highly tailored fibre composite structures contain curved fibres, which change the local stiffness of the composite. The conventional strategy for modeling curved fibres with finite elements in fibre angle optimization is to employ many small elements, within each of which the fibres are assumed to be effectively straight. The disadvantage of this approach is that the fine mesh affects the computational efficiency since the finite element equation must be solved in each iteration. To overcome this efficiency issue, the finite element formulation with explicit fibre curvature developed in Chapter 3 is employed in the stiffness maximization for a single-layer composite lamina, which is performed using a gradient descent algorithm. This finite element method allows the use of larger elements with curved fibres. Fewer elements results in a smaller global stiffness matrix, and require less time to solve the finite element equation in each iteration. Fibre curvature becomes an intermediate variable to the objective function. The total derivatives of the objective function with respect to fibre orientation are augmented by adding a continuity constraint in terms of curvature, and calculated analytically using the adjoint method. In the optimization, the curvature for each element is calculated by minimizing the fibre discontinuity between adjacent elements given their average fibre orientation, and the finite element with explicit fibre curvature is used for the analysis in each iteration.

Three composites structures are used to verify the gradient-based fibre angle optimization integrated with finite element with explicit fibre curvature, including a square thin composite plate with randomly generated fibre configuration, and L- and T-shaped thin composite plates with a point load and square holes on them. In each case, two gradient-based fibre angle optimizations for maximum stiffness using different finite element approaches are performed. One uses the conventional finite element method for the structural analysis, assuming fibres are locally straight in each element. The objective function, minimizing strain energy, is subjected to an equilibrium constraint. The other approach applies the finite element with explicit fibre curvature for the analysis, using larger element with curved fibres. The objective function, minimizing strain energy, is subjected to equilibrium and continuity constraints.

The square plate case is first used to verify the two gradient-based fibre angle optimization methods because its theoretical solution is known to have all fibres aligned. Then the two gradient-based fibre angle optimizations are performed on the L- and T-shaped thin composite

lamina for maximum stiffness. The initial fibre configuration in each element is orientated with the maximum principal stress for the relevant geometry with an isotropic material. The results show that gradient-based fibre angle optimization with explicit fibre curvature is more efficient than the conventional gradient-based optimization, and that it reduces the fibre discontinuity for the composite structure.

5.2 Maximum Stiffness Design

The optimization problem in this chapter is the maximization of the stiffness in thin composite plates with curved fibres. The design variable is the fibre orientation angle. By adjusting the fibre orientations, it is possible to maximize the stiffness of a composite structure. Maximizing the stiffness of a composite structure is equivalent to the minimization of the compliance. The minimum compliance design problem can be treated as minimizing the total elastic strain energy U with equilibrium constraint $R_1 : KD - F = 0$ [38],

$$\begin{aligned} &\min_{\theta_i} : U(D), \\ &\text{s.t.} : KD - F = 0, \end{aligned} \tag{5.1}$$

where K, D and F are the global stiffness matrix, vector of global displacements and vector of applied loads. The total elastic strain energy for a discretized system can be computed as [38],

$$U = \frac{1}{2} D^T K D = \sum_{i=1}^{n} \frac{1}{2} {d_i}^T {K_i}^e d_i, \tag{5.2}$$

where the global stiffness matrix is assembled by the n element stiffness K^e. The element displacement vector is d_i.

The method of Lagrange multipliers is applied [87], and the augmented objective function can be written as,

$$L(\theta, \lambda_1) = U + \lambda_1 R_1, \tag{5.3}$$

where λ_1 is a Lagrange multiplier. This λ_1 can have any value because the equilibrium constraint is an equality.

In order to perform gradient-based optimization, it is necessary to analyze the sensitivity

of the objective function to the design variables by evaluating the gradient. The derivative of the augmented objective function, Eq. (5.3), to the design variable θ_i is:

$$\frac{\partial L}{\partial \theta_i} = \frac{\partial U}{\partial \theta_i} + \lambda_1 \frac{\partial R_1}{\partial \theta_i}. \tag{5.4}$$

The first-order sensitivity of the total elastic strain energy and constraint to the design variables can be obtained by differentiating the strain energy and the equilibrium equation with respect to the fibre orientation θ_i,

$$\frac{\partial U}{\partial \theta_i} = \frac{1}{2} D^T \frac{\partial K}{\partial \theta_i} D + \frac{1}{2} \frac{\partial D^T}{\partial \theta_i} K D + \frac{1}{2} D^T K \frac{\partial D}{\partial \theta_i}. \tag{5.5}$$

Since the global stiffness matrix K is symmetric, the last two terms in Eq. (5.5) are equal. Hence Eq. (5.5) can be rewritten as

$$\frac{\partial U}{\partial \theta_i} = \frac{1}{2} D^T \frac{\partial K}{\partial \theta_i} D + D^T K \frac{\partial D}{\partial \theta_i}. \tag{5.6}$$

The partial derivative of the constraint with respect to the design variable θ_i is

$$\frac{\partial R_1}{\partial \theta_i} = \frac{\partial K}{\partial \theta_i} D + K \frac{\partial D}{\partial \theta_i} = 0. \tag{5.7}$$

The vector of applied loads is independent of the design variable.

Substituting the derivative of the strain energy Eq. (5.6) and constraint Eq. (5.7) into Eq. (5.4) and collecting terms,

$$\begin{aligned} \frac{\partial L}{\partial \theta_i} =& \frac{1}{2} D^T \frac{\partial K}{\partial \theta_i} D + D^T K \frac{\partial D}{\partial \theta_i} + \lambda_1 \left(\frac{\partial K}{\partial \theta_i} D + K \frac{\partial D}{\partial \theta_i} \right) \\ =& \left(\frac{1}{2} D^T + \lambda_1 \right) \frac{\partial K}{\partial \theta_i} D + \left(D^T + \lambda_1 \right) \frac{\partial D}{\partial \theta_i}. \end{aligned} \tag{5.8}$$

The derivative of the displacement with respect to the fibre orientation, $\frac{\partial D}{\partial \theta_i}$, is difficult to compute, because the displacement with respect to the fibre orientation is implicit. As the constraint R_1 is zero everywhere, the Lagrange multiplier λ_1 can be chosen freely. In order

to eliminate $\frac{\partial D}{\partial \theta_i}$, let $D^T + \lambda_1 = 0$, hence $\lambda_1 = -D^T$ and substitute back:

$$\frac{\partial L}{\partial \theta_i} = -\frac{1}{2} D^T \frac{\partial K}{\partial \theta_i} D. \tag{5.9}$$

This is the analytical derivative of the strain energy, which is applied in the conventional gradient-based fibre angle optimization of composite structures.

During the optimization process, the finite element equation must be solved at each iteration to calculate the objective function and its derivative. The disadvantage of the conventional finite element method is the need for a fine mesh to reach a desired level of accuracy. This causes the global stiffness matrix to have a large dimension, and the computational efficiency of the optimization will be greatly degraded.

Using larger elements is an economic way to circumvent this efficiency issue. Larger elements means a smaller dimension of the global stiffness matrix, requiring less computation time when solving the finite element equation in each iteration. The finite element formulation with explicit fibre curvature developed in Chapter 3 is developed for this. Using larger elements involves explicitly modeling the fibre curvature. Because fibre curvature is a function of the fibre orientations, the curvature itself is not a design variable, but instead is an intermediate variable to the objective function. To find the total derivative of the objective function with respect to fibre orientation, it is also necessary to calculate the derivative of objective function with respect to curvature and the derivative of curvature with respect to fibre orientations. The curvatures themselves are included by adding a second constraint, $R_2 : A\kappa + b = 0$, to the optimization problem:

$$\begin{aligned} \min_{\theta_i} &: U(D) \\ \text{s.t.} &: KD - F = 0 \\ &: A\kappa + b = 0, \end{aligned} \tag{5.10}$$

where κ is an $n \times 1$ curvature vector. In this formulation, A is an $n \times n$ matrix and b is an $n \times 1$ vector from the normal equation. They are formed based on the average fibre orientations of each element. This constraint is explained in Chapter 4, and arises due to the calculation of the curvature through the application of the normal equation. The fibre discontinuity among adjacent elements is minimized by setting the gradient of the sum of the

square of the angle difference, $A\kappa + b$, to be zero.

The augmented objective function with equilibrium and continuity constraints becomes,

$$L(\theta, \kappa, \lambda_1, \lambda_2) = U + \lambda_1 R_1 + \lambda_2 R_2, \tag{5.11}$$

where λ_2 is the Lagrange multiplier for the continuity constraint. The total derivative of this objective function with respect fibre orientation θ_i is:

$$\frac{\mathrm{d}L}{\mathrm{d}\theta_i} = \frac{\mathrm{d}U}{\mathrm{d}\theta_i} + \lambda_1 \frac{\mathrm{d}R_1}{\mathrm{d}\theta_i} + \lambda_2 \frac{\mathrm{d}R_2}{\mathrm{d}\theta_i}. \tag{5.12}$$

The total derivative of the strain energy U with respect to θ_i is:

$$\frac{\mathrm{d}U}{\mathrm{d}\theta_i} = \frac{\partial U}{\partial \kappa}\frac{\partial \kappa}{\partial \theta_i} + \frac{\partial U}{\partial \theta_i} = \left(\frac{1}{2}D^T \frac{\partial K}{\partial \kappa} D + D^T K \frac{\partial D}{\partial \kappa}\right)\frac{\partial \kappa}{\partial \theta_i} + \frac{1}{2}D^T \frac{\partial K}{\partial \theta_i} D + D^T K \frac{\partial D}{\partial \theta_i}, \tag{5.13}$$

and the total derivatives of constraints R_1 and R_2 with respect to θ_i are:

$$\frac{\mathrm{d}R_1}{\mathrm{d}\theta_i} = \frac{\partial R_1}{\partial \kappa}\frac{\partial \kappa}{\partial \theta_i} + \frac{\partial R_1}{\partial \theta_i} = \left(\frac{\partial K}{\partial \kappa} D + K \frac{\partial D}{\partial \kappa}\right)\frac{\partial \kappa}{\partial \theta_i} + \frac{\partial K}{\partial \theta_i} D + K \frac{\partial D}{\partial \theta_i}, \tag{5.14}$$

$$\frac{\mathrm{d}R_2}{\mathrm{d}\theta_i} = \frac{\partial R_2}{\partial \kappa}\frac{\partial \kappa}{\partial \theta_i} + \frac{\partial R_2}{\partial \theta_i} = A\frac{\partial \kappa}{\partial \theta_i} + \frac{\partial A}{\partial \theta_i}\kappa + A\frac{\partial \kappa}{\partial \theta_i} + \frac{\partial b}{\partial \theta_i}. \tag{5.15}$$

Substituting Eq. (5.13), (5.14) and (5.15) back into Eq. (5.12) and collecting terms gives:

$$\begin{aligned}\frac{\mathrm{d}L}{\mathrm{d}\theta_i} = &\left(\frac{1}{2}D^T \frac{\partial K}{\partial \kappa} D + D^T K \frac{\partial D}{\partial \kappa} + \lambda_1 \left(\frac{\partial K}{\partial \kappa} D + K \frac{\partial D}{\partial \kappa}\right) + 2\lambda_2 A\right)\frac{\partial \kappa}{\partial \theta_i} \\ &+ \left(\frac{1}{2}D^T \frac{\partial K}{\partial \theta_i} D + D^T K \frac{\partial D}{\partial \theta_i} + \lambda_1 \left(\frac{\partial K}{\partial \theta_i} D + K \frac{\partial D}{\partial \theta_i}\right)\right) \\ &+ \lambda_2 \left(\frac{\partial A}{\partial \theta_i}\kappa + \frac{\partial b}{\partial \theta_i}\right).\end{aligned} \tag{5.16}$$

The derivative of the displacement D with respect to θ_i is difficult to calculate. Therefore one can use λ_1 and λ_2, the adjoint variables, to eliminate it. Let $D^T + \lambda_1 = 0$, hence $\lambda_1 = -D^T$ and substitute back:

$$\frac{\mathrm{d}L}{\mathrm{d}\theta_i} = -\frac{1}{2}D^T \frac{\partial K}{\partial \theta_i} D + \left(-\frac{1}{2}D^T \frac{\partial K}{\partial \kappa} D + 2\lambda_2 A\right)\frac{\partial \kappa}{\partial \theta_i} + \lambda_2 \left(\frac{\partial A}{\partial \theta_i}\kappa + \frac{\partial b}{\partial \theta_i}\right). \tag{5.17}$$

A second term, $\frac{\partial \kappa}{\partial \theta_i}$, is also difficult to express explicitly. For a given element, the derivative of curvature with respect to θ_i is influenced not only by the orientation angle in that element, but also by the orientation angles in nearby elements. Therefore, the coefficient of the second term needs be set to zero to avoid calculating the derivative of curvature. This avoids evaluating the derivative, $\frac{\partial \kappa}{\partial \theta_i}$, numerically with high computation expense. Finally, the total derivative is simplified as

$$\frac{\mathrm{d}L}{\mathrm{d}\theta_i} = -\frac{1}{2} D^T \frac{\partial K}{\partial \theta_i} D + \lambda_2 \left(\frac{\partial A}{\partial \theta_i} \kappa + \frac{\partial b}{\partial \theta_i} \right), \tag{5.18}$$

where λ_2 is found from:

$$\lambda_2 A = \frac{1}{4} D^T \frac{\partial K}{\partial \kappa} D. \tag{5.19}$$

The value of λ_2 can be found by solving this linear system, since $\frac{\partial K}{\partial \kappa}$ is easy to evaluate analytically. Fig. 5.1 shows the flowchart of the optimization process. Given an initial fibre configuration, the fibre curvature is calculated using the method developed in Chapter 4. The finite element with explicit fibre curvature is applied to calculate the strain energy and the gradient of the strain energy. The fibre orientation angles are updated and the values of objective function are recalculated until the convergence criterion is satisfied.

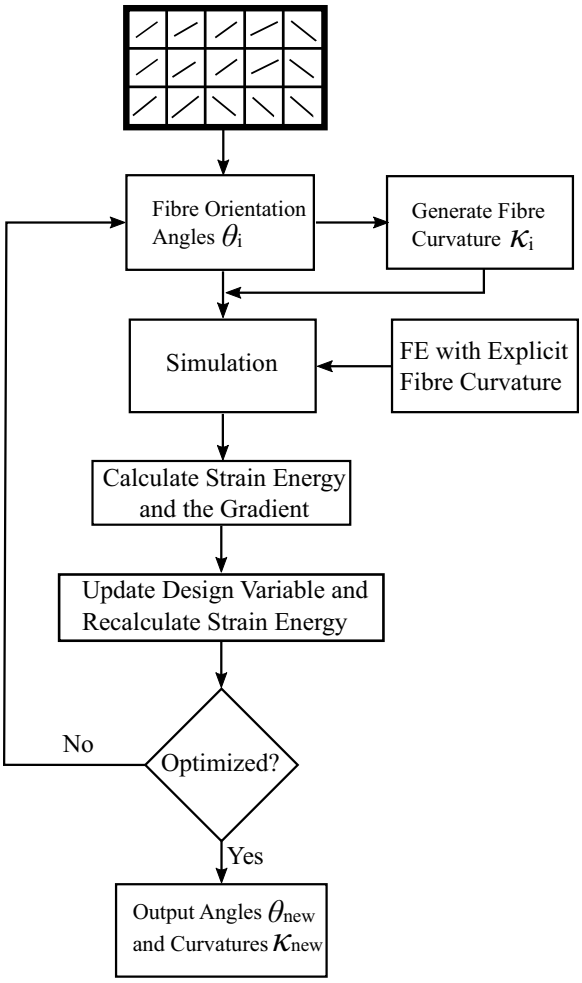

Figure 5.1: Flowchart of the fibre angle optimization for stiffness maximization of a thin single-layer composite lamina with curved fibres.

5.3 Results

Gradient-based minimization of compliance will be demonstrated on a square region. The fibre orientation angle is the design variable. By adjusting the fibre orientation in each element, the stiffness of the composite laminate will be maximized. Two gradient-based fibre angle optimizations for maximum stiffness of the square region using different finite element approach are performed, labeled as optimization A and B.

Optimization A is a conventional gradient-based fibre angle optimization, which uses the conventional finite element, where the fibres are assumed to be straight in each element for the structural analysis in each iteration. The gradient of the objective function is calculated

from Eq. (5.9). Optimization B applies the finite element with explicit fibre curvature for the analysis, using larger elements with curved fibres. The curvature in each element will be calculated through the application of the normal equation to minimize the fibre discontinuity. The curved fibres in each element are assumed to be circular arcs and the fibre orientation angle at an arbitrary location can be obtained based on that geometry. The finite element with explicit curvature uses the fibre angle at each Gauss integration point to form stiffness matrix. The finite element equation is then solved. The derivative of the objective function is calculated by Eq. (5.18).

A square composite lamina discretized into elements with arbitrary fibre configuration is used. The lamina properties are set as $E_1 = 127$, $E_2 = 10$, $G_{12} = G_{13} = 4$, $G_{23} = 1.8$, $\nu_{12} = 0.27$, and the thickness is 0.001. The initial fibre orientation in each element is randomly generated, ranging from $-30°$ to $30°$. The plate is fixed on the left edge and subjected to a uniformly distributed axial load on the right edge, as shown in Fig. 5.2(a). With this loading condition, the theoretical solution for this maximum stiffness optimization is known to be uniform horizontal fibre orientation. Fig. 5.2(b) shows the contour of the axial displacement for the square plate with horizontal fibre orientations from an Abaqus simulation. A convergence study shows that the strain energy of the square plate with horizontally aligned fibres is 0.1575. Therefore, it is convenient to verify the two gradient-based optimizations using this square composite laminate to see if they approach the known theoretical solution. Also, their efficiency is compared. The gradient-based fibre angle optimization using the finite element with explicit curvature is hypothesized to be faster than the conventional approach as larger elements are used.

It has been shown in Chapter 3 that using finite elements with explicit fibre curvature is more efficient than the conventional finite element formulation, which assumes fibres in each element are straight. According to the result from Chapter 3, applying 7×7 finite elements with explicit fibre curvature achieves the same accuracy as using 25×25 conventional finite elements.

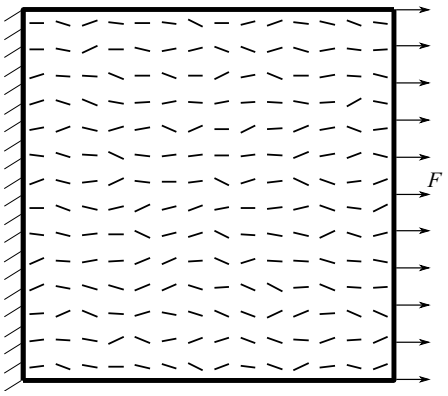

(a) A square composite laminate with random fibre configuration. The structure is fixed on the left edge and subjected an uniformly distributed axial load on the right edge, F=20000. The fibre orientations are generated randomly ranging from $-30°$ to $30°$.

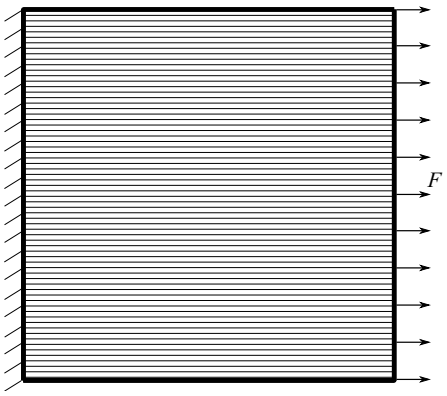

(b) Axial displacement contour for a square plate with uniform horizontal fibre orientation under the same boundary and loading condition as (a). The strain energy of the square plate with horizontally aligned fibres is 0.1575.

Figure 5.2: A square composite laminate with arbitrary fibre configuration. The Abaqus results on the right provide the solution of the maximum stiffness design problem for a square plate under an axial load.

After getting the theoretical solution for the maximum stiffness design problem for the square plate, the two gradient-based fibre angle optimizations, A and B, are performed. Both optimizations are set with the same convergence criteria, which determines convergence based on the magnitude of successive changes in the objective function, $f(\theta_i)$, falling under a user defined limit.

$$||f(\theta_{i+1}) - f(\theta_i)|| < \epsilon_a, \tag{5.20}$$

where ϵ_a is the absolute tolerance on the change in objective function value, which is set to 10^{-9}.

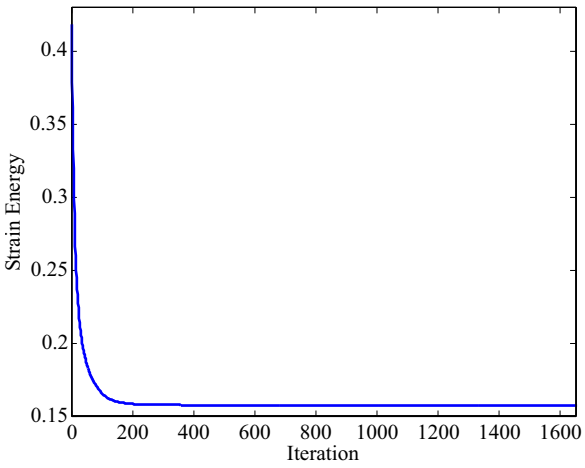

(a) Optimization A: convergence of the strain energy for a 25 elements ×25 elements conventional finite elements. The converged strain energy is 0.1575 and the elapsed time is 788.9 s.

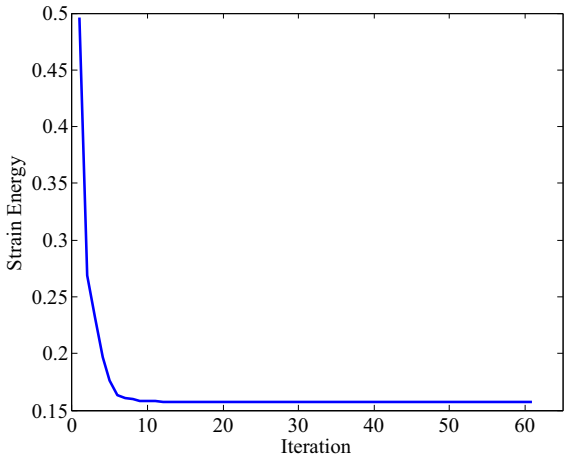

(b) Optimization B: convergence of the strain energy for a 7 elements ×7 elements finite elements with explicit fibre curvature. The converged strain energy is 0.1575 and the elapsed time is 36.7 s.

Figure 5.3: The convergence comparison between two optimizations. Optimization B reduces the computation time by 95.3%.

The optimal fibre configuration of the square plate should approach horizontal fibre orientations. It can be seen that optimization A, Fig. 5.3(a), takes more than 1600 iterations reach convergence, while 62 iterations are necessary for optimization B, Fig. 5.3(b). The norms of the gradient of optimization A and B reduce by 9 and 5 orders of the magnitude, respectively. Both optimizations reach the strain energy of 0.1575, which is same as the theoretical solution. The reduction in computation time R is evaluated as,

$$R = \frac{T_s - T_c}{T_s} \times 100\%, \tag{5.21}$$

where T_s and T_c are the computation time of optimizations using conventional finite elements and finite elements with curved fibres, respectively. Optimization B reduces the computation time by 95.3%. For the square plate example, optimization B, the gradient-based optimization with explicit fibre curvature, is more efficient than optimization A, the one without conventional finite element method. It is noticed that using fewer elements requires fewer iterations to converge. Fewer iterations, less grid generation plus curved finite element tends to converge more quickly than the conventional finite element, which is an advantage of using the new optimization method.

The L-shaped structure has been discussed in Chapter 3 and 4. Since the stress distribution in this structure is more complicated than in a square plate, it is difficult to know the fibre orientation for the maximum stiffness. Pedersen [88] found the collinearity between principal stress, strain and material directions. The extreme energy solutions are obtained with parallel principal directions for material, stresses and strains. This collinearity can help design for the fibre path by aligning fibres with the principal stress directions at each point of the structure to increase stiffness [89]. The collinearity between principal stress, strain and material directions can also be applied in the structural optimization. Hyer and Charette [8] optimized the strength of a plate with a hole uniformly loaded at its two ends. The fibres were initially aligned with the principal stress directions for an isotropic plate. Because of the anisotropy of composites, the principal directions of the stresses in a composite are not the same as the principal directions of the stresses for an isotropic material. Hence the principal directions of the stresses are modified at each optimization step. The fibres were realigned with the new principal stress directions in each iteration. The optimized laminate showed an improved tensile strength.

For the L-shaped composite structure, the optimal fibre distribution for maximum stiffness has the fibres oriented with the maximum principal stress. One can perform gradient-based fibre angle optimization to obtain the optimal fibre distribution, but it is easy to fall into a local minimum, because steepest descent method takes steps proportional to the negative of the gradient to reach the minimum of the objective function in the neighborhood. Avoiding a local minimum requires a good initial guess for the fibre orientations. A convenient method to generate a good initial guess is to calculate the directions of maximum principal stress for the same geometry with an isotropic material, which will be close to the directions of maximum principal stress for the composite structure. Then the initial fibre distribution is assigned as the directions of maximum principal stress for the L-shaped structure with an isotropic material. This gives a good initial guess, increasing the likelihood that the gradient-based optimization will reach a global minimum of strain energy for the L-shaped composite plate. It also accelerates the process dramatically.

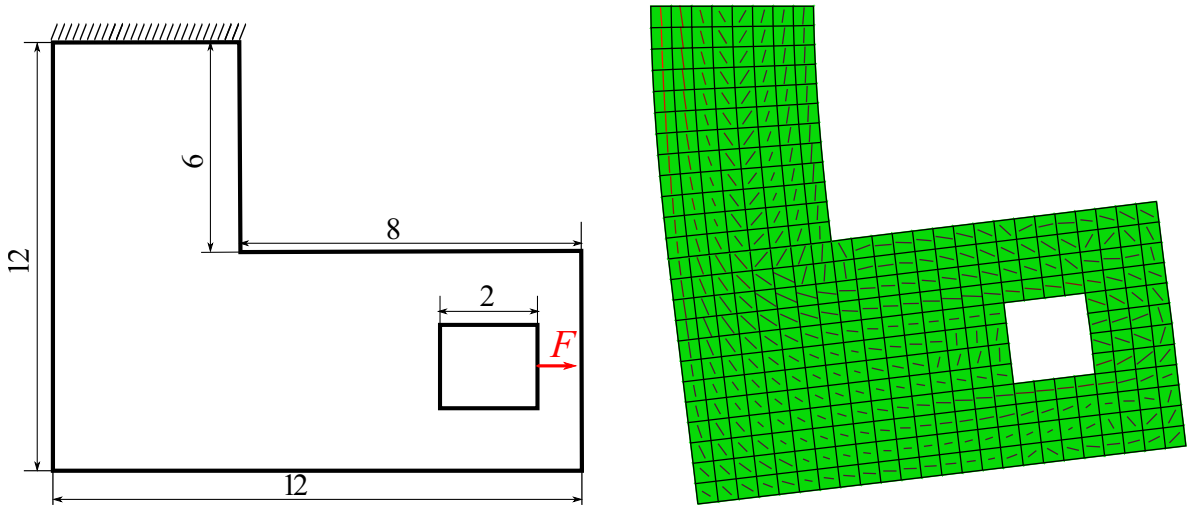

(a) An L-shaped structure with top edge fixed. The point load, F=10000, is applied in the middle of the right edge of the square hole.

(b) Maximum principal stress direction in each element of the isotropic structure from Abaqus simulation.

Figure 5.4: Geometric model of the L-shaped structure. The Abaqus model uses a isotropic material and applies the same load and boundary conditions on the L-shaped structure. The maximum principal stress directions are exported and assigned as the initial fibre configuration.

Two gradient-based fibre angle optimizations for maximum stiffness of the L-shaped structure using different analytical sensitivity analysis and finite element approach are performed, labeled as optimization C and D. Optimization C is the conventional gradient-based fibre angle optimization using the conventional finite element. Fibres are assumed to be straight in each element. The gradient of the objective function is calculated from Eq. (5.9). Optimization D applies the finite element with explicit fibre curvature for the analysis. Larger elements with curved fibres are used. The fibre curvature in each element is calculated by minimizing the fibre discontinuity between adjacent elements given their average fibre orientation. With the assumption that the curved fibres are circular arcs, the fibre orientation angle at each Gauss point is obtained based on that geometry. The stiffness matrix is formed using the fibre angle at each Gauss integration point. The finite element equation is solved and the derivative of the objective function is calculated by Eq. (5.18). Both optimizations will use the maximum principal stress directions of the L-shaped structure with isotropic material as the initial fibre distribution.

Fig. 5.4(a) shows the geometry of this L-shaped thin plate. The top edge is fixed, and

a point load, 10000, is applied on the middle of the right edge of the square hole. The L-shaped structure with isotropic material is modeled in Abaqus with the same boundary and loading conditions. Shell elements (S8R5) were employed to mesh the plate part. The Abaqus simulation is conducted to get the shear, horizontal and transverse stresses, τ_{xy}, σ_x and σ_y, respectively. They are interpolated to the element centres. The principal directions θ_p are calculated from

$$\tan 2\theta_p = \frac{2\tau_{xy}}{\sigma_x - \sigma_y}. \tag{5.22}$$

Then the principal stress directions are assigned to each element as the initial fibre orientation for the maximum stiffness optimization.

Fig. 5.5(a) shows the convergence for stiffness maximization for the L-shaped thin plate using optimization C. It takes 1680 iterations to reach convergence, while 210 iterations are required using optimization D, as shown in Fig. 5.5(b). Optimization D has reduces the computation time by 64.5%. The maximum curvature is 0.47. The converged strain energy for optimization C and D, calculated using Eq. (5.2), is 2.6326 and 2.7354, respectively. The norms of the gradient of the objective function with respect to the design variables for optimization C and D reduce by 3 and 2 orders of magnitude, respectively. The final norms of the gradient of the objective function for optimization C and D are 3.6103×10^{-7} and 1.6116×10^{-6}, respectively. The result from optimization D is higher than that of optimization C, because optimization D uses finite element with curved fibres. Fibre curvature causes the structure to have more compliance. As opposed to optimization A and B, there is no theoretical solution for the optimization of this complicated structure. This is a standard problem in the computation of optima for complicated systems, but it is possible to show that the optimization with finite elements with explicit curvature provides better results then the conventional approach, and is also more efficient. However, the fibres in the elements are straight in optimization C and curved in D. To make a fair comparison between the two optimization results, one can calculate the implied curvatures based on the optimized fibre orientations in the conventional optimization C, and run an analysis using the finite element with explicit curvature on the same mesh. This gives a new compliance, 2.7431, which is greater than the result of optimization D. This shows that optimization D, using

finite element with explicit fibre curvature, generated a better fibre angle configuration than optimization C, and greatly reduced computation time.

Fig. 5.6 shows the fibre layout of the L-shaped structure before and after optimization D. It can be seen that the strain energy of this optimized structure decreases by 3.9%. Fig. 5.6(b) also plots the curved fibre orientation in each element with the curvatures obtained from the optimization. Compared to optimization C, the maximum stiffness optimization with explicit fibre curvature not only improves the efficiency, but also illustrates how fibres are spatially varying in the laminate domain and reduces the fibre discontinuity between adjacent elements after optimization. However, there is still fibre discontinuity in the optimized fibre layout, and further work might include penalizing the discontinuity to get more continuous fibres, or even use an explicit physical model of discontinuity [90].

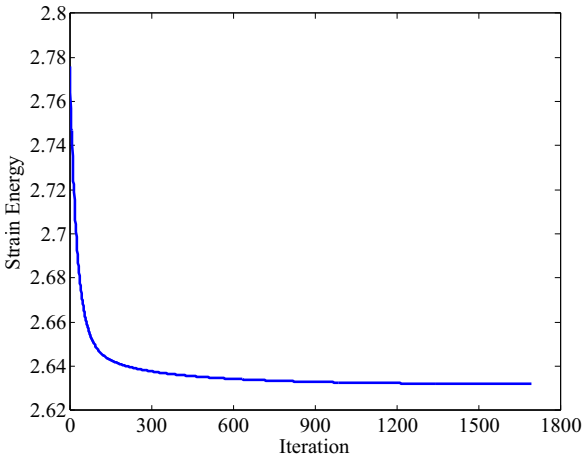

(a) Optimization C: convergence for maximizing the stiffness of the L-shaped structure using the conventional finite element method. The converged strain energy is 2.6326.

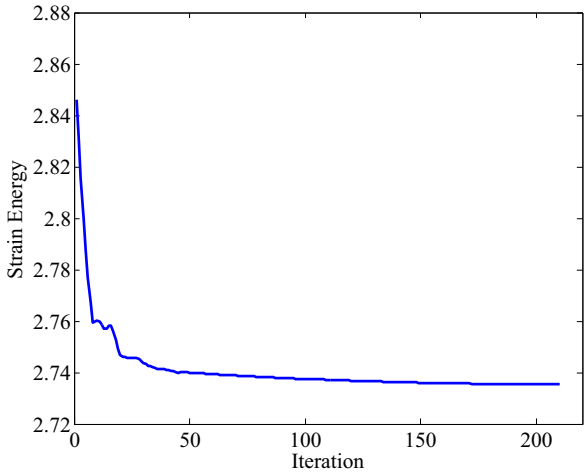

(b) Optimization D: convergence for maximizing the stiffness of the L-shaped structure using the finite element with explicit fibre curvature. The converged strain energy is 2.7354.

Figure 5.5: Convergence for the stiffness maximization for the L-shaped structure using optimizations C and D. Optimization D reduces the computation time by 64.5%.

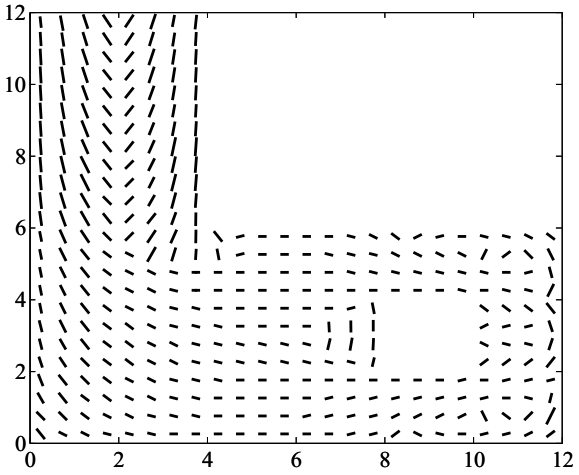

(a) The initial fibre configuration of the L-shaped structure. It is orientated with the maximum principal stress for the relevant geometry with an isotropic material. The corresponding initial strain energy is 2.8461.

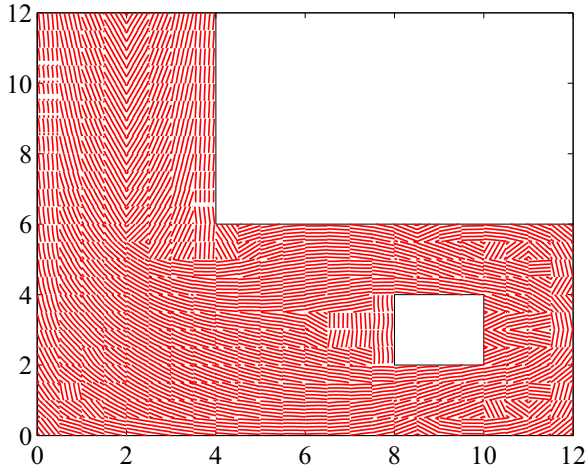

(b) The optimal curved fibre orientation after optimization D. The curves in each element represent how fibres are spatially varying in the element domain. The corresponding strain energy is 2.7354, which is 3.9% less than the initial one.

Figure 5.6: Fibre orientations before and after the stiffness maximization for the L-shaped composite thin plate using optimization D. The stiffness of this structure is improved by 3.9% after the optimization.

Another practical and realistic example is a T-shaped structure with five square holes on it, which is similar to a structure with bolt holes. The square holes are used since only structured meshes are considered in this work. The edges of the left four square holes are fixed, and the middle of the bottom edge of the right hole is subjected to a vertical point load, as shown in Fig. 5.7(a).

Two gradient-based fibre angle optimizations for stiffness maximization of the T-shaped structure using different analytical sensitivity analysis and finite element approach are performed, labeled as optimization E and F. Optimization E uses the conventional gradient-based fibre angle optimization process with straight fibres in each element. The objective function is a function of the fibre orientation and its derivative is calculated using Eq. (5.9). Optimization F applies finite elements with curved fibres. The total derivative of the objective function with respect to fibre orientation is calculated by Eq. (5.18). Both optimizations use the maximum principal stress directions for the T-shaped structure with isotropic material as the initial fibre configuration. An Abaqus simulation is conducted for the same T-shaped structure with isotropic material, as shown in . The shear, horizontal and transverse stresses are exported from the simulation results. The principal directions θ_p are calculated from

Eq. (5.22).

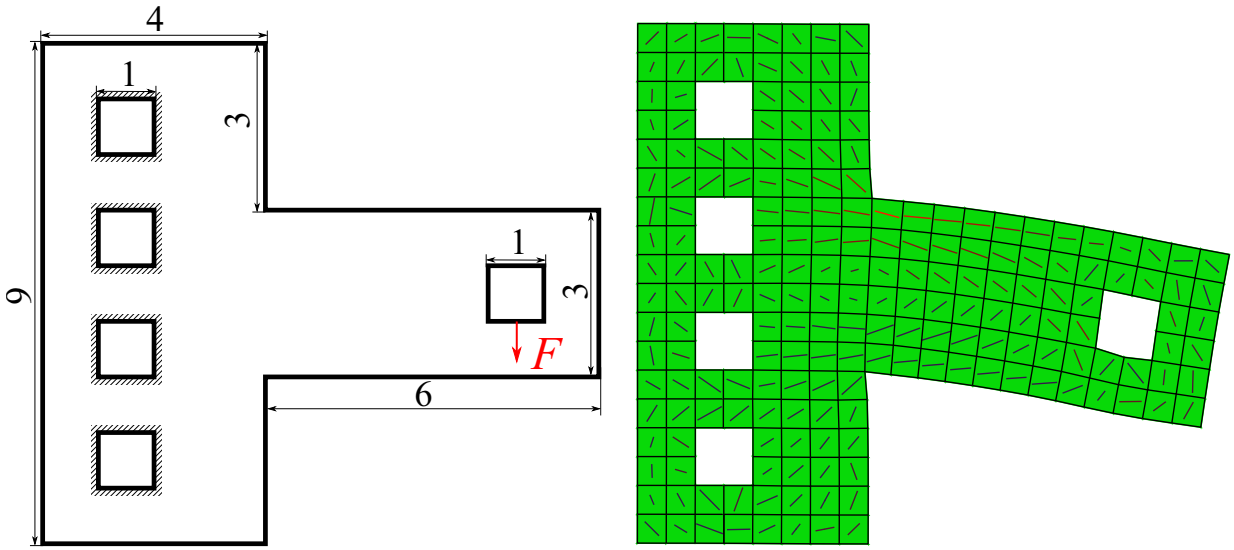

(a) A T shaped structure with edges of left four square holes fixed. The point load, F=10000, is applied in the middle of the bottom edge of the right square hole.

(b) Maximum principal stress direction in each element of the isotropic structure from an Abaqus simulation.

Figure 5.7: Geometric model of the T-shaped structure. The Abaqus model uses an isotropic material and apply the same load and boundary conditions on the T-shaped structure. Then the maximum principal stress direction are exported and assigned as the initial fibre orientation.

Fig. 5.8(b) shows the convergence of the maximum stiffness optimization with explicit fibre curvature. It only takes 74 iterations to converge, and 1950 iterations for optimization using the conventional finite element process, as shown in Fig. 5.8(a). Optimization D reduces the computation time by 69.6%. The maximum curvature is 0.73. The converged strain energy for optimization E and F are 1.5816 and 1.7515, respectively. The norms of the gradient of both optimizations reduce by 2 orders of the magnitude. The final norms of the gradient of the objective function with respect to the design variables for optimization E and F are 3.6188×10^{-7} and 1.2325×10^{-6}, respectively. Similar to the L-shaped structure, the conventional optimization E has lower compliance than that of optimization F, as the fibre curvature in the finite element with curved fibres reduce the structural stiffness. To show that the new optimization using larger elements with curved fibres is better than the conventional approach with straight fibres, the curvatures are calculated based on the optimized fibre orientations from optimization E, and a simulation employing the finite element with explicit curvature is conducted on the same mesh. The new compliance, 1.8064, is greater than

the result of the conventional optimization and greater than the result for optimization F. Table. 5.1 gives the summary of the optimization results for the L- and T-shaped thin composite plates. It shows that the new optimization gives lower compliance than that of the conventional optimization.

L-shaped structure	C	C*	D
Optimal compliance	2.6326	2.7431	2.7354
T-shaped structure	E	E*	F
Optimal compliance	1.5816	1.8064	1.7515

Table 5.1: Summary of the optimization results for the L- and T-shaped structures. The star sign denotes the compliance obtained by calculating the curvatures based on the optimized fibre orientations in the conventional optimization, and running the finite element with explicit curvature on the same mesh.

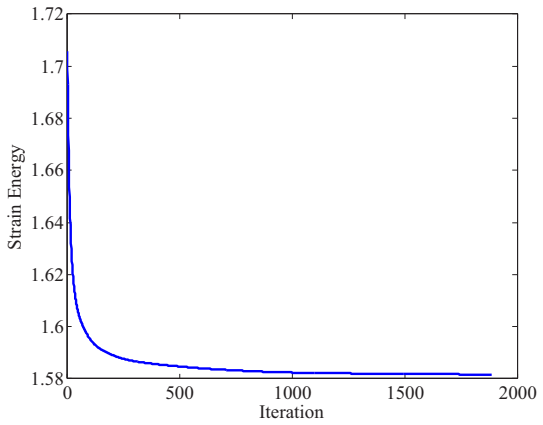

(a) Optimization E: convergence for the maximizing the stiffness of the T-shaped structure using the conventional finite element. The converged strain energy is 1.5816.

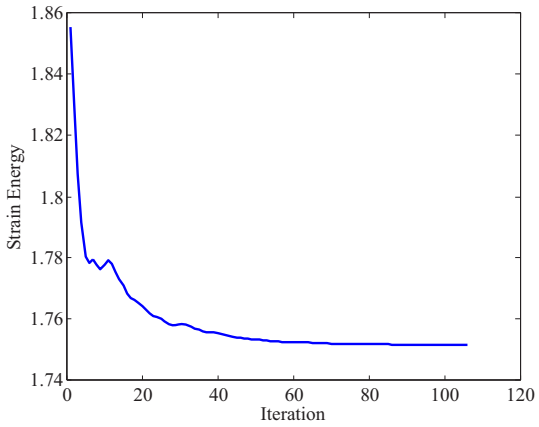

(b) Optimization F: convergence for the maximizing the stiffness of the T-shaped structure using the finite element with explicit fibre curvature. The converged strain energy is 1.7515.

Figure 5.8: Convergence for the stiffness maximization for the T-shaped structure using optimization E and F. Optimization F reduces the computation time by 69.6%.

Stiffness optimization using elements with explicit fibre curvature is performed on this structure. Fig. 5.9(a) shows the initial fibre arrangement that is aligned with the direction of the maximum principal stresses in each element as calculated for an isotropic material, and Fig. 5.9(b) shows the curved fibres in each element after the stiffness optimization with explicit fibre curvature. The strain energy of this optimized structure decreases by 5.6%.

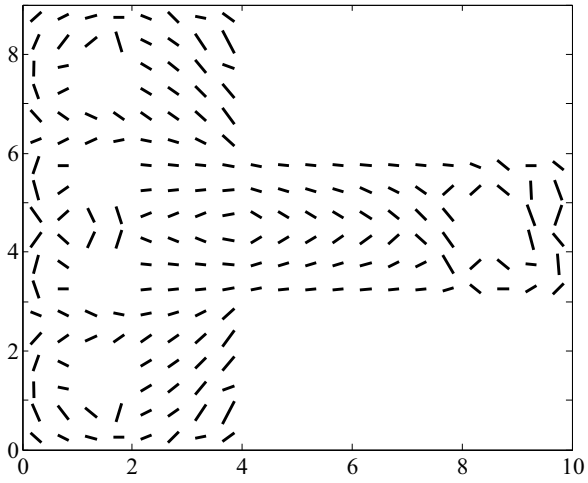

(a) The initial fibre angles of the L-shaped structure are the same as its maximum principal stresses direction. The corresponding initial strain energy is 1.8555.

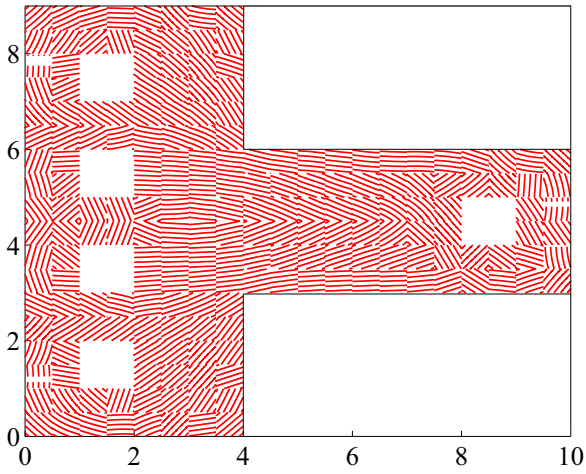

(b) The optimal curved fibre orientation after optimization F. The curves in each element denote the configuration of curved fibres. The corresponding strain energy is 1.7515, which is 5.6% less than the initial one.

Figure 5.9: Fibre orientations before and after the stiffness maximization for the T-shaped structure using optimization F. The stiffness of this structure is improved by 5.6% after the optimization.

5.4 Concluding Remarks

The stiffness maximization for the single-layer thin composite lamina is performed using a gradient descent algorithm integrated with the finite element formulation with explicit fibre curvature. The finite element formulation with explicit fibre curvature allows the use of larger elements while maintaining accuracy. Using larger elements reduce the computational expense, but involves fibre curvature. The curvature is a function of the fibre orientation and an intermediate variable to the objective function. Therefore, the total derivative of the objective function includes the derivative of objective function with respect to curvature and the derivative of curvature with respect to fibre orientation, while the optimization using conventional finite element is only a function of the fibre orientation. The derivative involving curvature was included by introducing a continuity constraint. The sensitivity analysis is performed analytically using the adjoint method. Two gradient-based fibre angle optimizations for stiffness maximization using different finite element approach are performed on a square, on L- and T-shaped thin composite lamina. One uses the conventional finite element method for the structural analysis, and the other one applies the finite element

with explicit fibre curvature. As the theoretical solution for maximizing the stiffness of a square plate with uniformly distributed load is that all fibres are aligned horizontally, it is convenient to verify the two optimizations using this square plate. Results show that this new optimization with explicit fibre curvature reaches the exact solution and is more efficient than the conventional approach. The gradient-based fibre angle optimizations for maximum stiffness are performed on L- and T-shaped structures. Both test cases show that the optimization with explicit fibre curvature converges faster than the optimization using conventional finite elements. Also, it can provide the curvature information in each element, which illustrates spatially varying fibres in the domain and reduces the fibre discontinuity for the whole structure. Therefore, it is shown that the proposed optimization method improves the computational efficiency for optimizing composite structures.

Chapter 6

Conclusions

This work develops an accurate, efficient finite element model for composite structures with complex fibre configurations, which can be used for optimizing the local fibre orientations in composite plates to maximize stiffness. In contrast to the conventional FE approach that requires fine meshes to attain high accuracy, the technique retains relatively large elements by modeling the fibre curvature explicitly to capture the changes in stiffness, and incorporate the elements into the gradient-based fibre angle optimization problem to improve the computational efficiency.

The behavior of interlayer slip between single fibres and fibre tows is studied by investigating the deformation of bonded curved elastic beams with initial curvature subjected to axial load. The results shows that the fibre curvature has a strong influence on the effective stiffness of a composite, while the slip effects between either individual fibres, or adjacent fibre tows, has little impact on the mechanical properties of such composites. As a result, perfect bonding between fibres is a reasonable assumption in composite structural analysis.

With the assumption of perfect bonding, a finite element with explicit fibre curvature is formulated for a single-layer thin composite lamina with curved fibres. The new FE method allows the use of larger elements with the desired level of accuracy. Fewer elements means smaller global stiffness matrices, reducing computation time. In the element with curved fibres, the fibre curvature changes the local stiffness. When performing the quadratures for determining the element stiffness matrices, the local fibre orientations at each Gauss point

are used. This gives a stiffness matrix that explicitly accounts for the varying orientations of the fibres within the element, while the conventional FE has a constant stiffness over the element domain. The comparison between the finite element with explicit fibre curvature and the conventional FE shows that the proposed method can greatly improve the computational efficiency with good accuracy.

The fibre curvature is calculated by minimizing the fibre discontinuity between adjacent elements given their average fibre orientation. This is a least square minimization problem and is solved through its normal equation. The curvatures obtained from this new method show good agreement with analytical solutions for the curvature of different continuous fibres, which indicates that it is an efficient way to generate the curvature.

Finally, a fibre angle optimization for the maximum stiffness of the single-layer thin composite lamina is performed using a gradient descent algorithm employing the new finite element method. The design variable is fibre orientation. The curvature itself is not a design variable, but instead is an intermediate variable in the objective function. As a consequence, in addition to the equilibrium constraint that is used in the conventional fibre angle optimization for maximum stiffness, a curvature constraint is added. It is necessary to calculate the derivative of the objective function with respect to the curvature and the derivative of curvature with respect to fibre orientation. The sensitivity analysis is conducted using the adjoint method, so that the gradient of the objective with respect to fibre orientation is derived analytically considering the influence of curvature. To accelerate the convergence, the initial fibre configuration in each element is chosen as the maximum principal stress for the relevant geometry with an isotropic material. Finally, the optimal solution is verified and compared to the results from gradient descent optimization using the conventional finite elements.

The optimization method developed in this work is helpful to improve the performance of a geometrically constrained composite component, such as maxmizing the stiffness, specific eigenfrequencies or eigenfrequency bandgaps. It provides an efficient way to find the optimal fibre configuration in the design of composite structures, and enable full exploitation the sophisticated manufacturing processes now available for composites. In addition, the finite element with explicit curvature is useful when confronted with the need for structural analysis

and optimization on complicated fibre configurations. Moreover, the calculation of curvature not only enables the optimization using curved fibres, but also provides a method to reconnect discretized fibres to reduce fibre discontinuity.

6.1 Contributions

The main contributions of the research are:

1. A novel finite element method for composite structures with complicated fibre configurations;
2. A new way of generating the curvature that minimizes the fibre discontinuity;
3. An analytical derivation of sensitivity analysis for gradient-based fibre angle optimization on thin composite plates;
4. An efficient gradient-based fibre angle optimization approach for thin composite plates;
5. A computer code for the structural analysis and optimization for thin composite plates.

6.2 Future Research Directions

Numerous directions of research remain open for further exploration and study. A few are listed here:

1. Extend the FE method to unstructured meshes and formulate a 3-D finite element with curved fibres, so that the FE method can be applied to more practical and realistic composite structures.
2. Apply the new FE method and optimization approach to multi-ply composite laminates. This is important because composite laminates nearly always contain more than one layer. However, it is difficult to extend the method from single layer to multiple layers. This is because the fibre orientations at one particular point with (x, y) coordinates are different along the z direction. Firstly, continuity of curvature across adjacent

elements for one layer may not lead to continuity of curvature for the adjacent layer. In addition, the Gauss points are difficult to select because each layer has a different fibre configuration. One way to solve this is to use one element per layer, but this would lead to a large number of elements and will be computationally expensive.

As a result, it is necessary to find efficient parallel computation algorithms for the multi-ply composite laminates optimization problems. This work enables the efficient calculations for the analysis of composites, and they bring the possibility of doing all the layers individually. Therefore, one option is to use parallel computing to run hundreds or thousands of cores to solve the optimization of complicated composites.

3. Employing composite configurations with curved fibres can improve the mechanical properties of the composites, such as strength, stiffness and vibrational properties. This work only performs fibre angle optimizations for maximum stiffness of composite structures. It is important to explore the fibre angle optimization of composite laminates using the finite element with curved fibres to improve other properties. For example, the objective function can be modified to a generalized eigenproblem to obtain a desirable vibrational frequency

4. Use more sophisticated optimization schemes instead of the steepest descent method for the stiffness maximization problem, such as the Quasi-Newton method. The primary concern in this work is to show that this curved finite element works well and can be used in the optimization algorithm to save a significant amount of time. It is necessary to concentrate on the detail of the optimization process and explore more efficient optimization approaches in the future work.

5. Fibre discontinuity have been reduced, but still exists in the optimization results. It is difficult to eliminate the fibre discontinuity to 0 in complicated composite structures. However, it is necessary to keep fibres as continuous as possible to ease manufacture of the laminates. Further work should be penalizing the discontinuity to get more smoothly connected fibres, or even finding an explicit physical model of discontinuity.

6. Manufacture composite plates with curved fibres and experimentally validate the

analytical results. This work develops a novel finite element approach that enables the use of larger elements with the desired level of accuracy, and a fibre angle optimization for maximum stiffness based on the finite element method. It is important to validate the results through experiments. For example, the displacement of the composite plates with curved fibres can be measured experimentally and compared to the analytical results. The experimental validation will make the results of the finite element with curved fibres more convincing.

Bibliography

[1] J Tomblin and W Seneviratne. Determining the fatigue life of composite aircraft structures using life and load-enhancement factors. *Final Report, Air Traffic Organization, Washington DC, USA*, 2011.

[2] H Ghiasi, K Fayazbakhsh, D Pasini, and L Lessard. Optimum stacking sequence design of composite materials part II: Variable stiffness design. *Composite Structures*, 93(1):1–13, 2010.

[3] I Kreja. A literature review on computational models for laminated composite and sandwich panels. *Central European Journal of Engineering*, 1(1):59–80, 2011.

[4] Z K Awad, T Aravinthan, Y Zhuge, and F Gonzalez. A review of optimization techniques used in the design of fibre composite structures for civil engineering applications. *Materials & Design*, 33:534–544, 2012.

[5] P Ribeiro, H Akhavan, A Teter, and J Warmiński. A review on the mechanical behaviour of curvilinear fibre composite laminated panels. *Journal of Composite Materials*, 48(22):2761–2777, 2014.

[6] P K Mallick. *Fibre-reinforced composites: materials, manufacturing, and design*. CRC press, 2007.

[7] H L Dirk, C Ward, and K D Potter. The engineering aspects of automated prepreg layup: History, present and future. *Composites Part B: Engineering*, 43(3):997–1009, 2012.

[8] M W Hyer and R F Charette. Use of curvilinear fibre format in composite structure design. *AIAA Journal*, 29(6):1011–1015, 1991.

[9] M M Abdalla, Z Gürdal, and G F Abdelal. Thermomechanical response of variable stiffness composite panels. *Journal of Thermal Stresses*, 32(1-2):187–208, 2008.

[10] C S Lopes, Z Gürdal, and P P Camanho. Tailoring for strength of composite steered-fibre panels with cutouts. *Composites Part A: Applied Science and Manufacturing*, 41(12):1760–1767, 2010.

[11] S Honda and Y Narita. Natural frequencies and vibration modes of laminated composite plates reinforced with arbitrary curvilinear fibre shape paths. *Journal of Sound and Vibration*, 331 (1):180–191, 2012.

[12] H Akhavan and P Ribeiro. Natural modes of vibration of variable stiffness composite laminates with curvilinear fibres. *Composite Structures*, 93(11):3040–3047, 2011.

[13] C S Lopes, Z Gürdal, and P P Camanho. Variable-stiffness composite panels: buckling and first-ply failure improvements over straight-fibre laminates. *Computers & Structures*, 86(9): 897–907, 2008.

[14] C S Lopes, P P Camanho, Z Gürdal, and B F Tatting. Progressive failure analysis of tow-placed, variable-stiffness composite panels. *International Journal of Solids and Structures*, 44(25): 8493–8516, 2007.

[15] Z Gürdal and R Olmedo. In-plane response of laminates with spatially varying fibre orientations: variable stiffness concept. *AIAA Journal*, 31(4):751–758, 1993.

[16] S Murugan and M I Friswell. Morphing wing flexible skins with curvilinear fibre composites. *Composite Structures*, 99:69–75, 2013.

[17] A W Blom, C S Lopes, P J Kromwijk, Z Gürdal, and P P Camanho. A theoretical model to study the influence of tow-drop areas on the stiffness and strength of variable-stiffness laminates. *Journal of Composite Materials*, 43(5):403–425, 2009.

[18] M Nik and K P Fayazbakhsh. Optimization of variable stiffness composites with embedded defects induced by automated fibre placement. *Composite Structures*, 107:160–166, 2014.

[19] A H Akbarzadeh, M Nik, and D Pasini. The role of shear deformation in laminated plates with curvilinear fibre paths and embedded defects. *Composite Structures*, 118:217–227, 2014.

[20] K Fayazbakhsh, M A Nik, D Pasini, and L Lessard. Defect layer method to capture effect of gaps and overlaps in variable stiffness laminates made by automated fibre placement. *Composite Structures*, 97:245–251, 2013.

[21] M Luersen, C A Steeves, and P B Nair. Curved fibre paths optimization of a composite cylindrical shell via kriging-based approach. *Journal of Composite Materials*, 49(29):3583–3597, 2015.

[22] A W Blom, P B Stickler, and Z Gürdal. Optimization of a composite cylinder under bending by tailoring stiffness properties in circumferential direction. *Composites Part B: Engineering*, 41(2):157–165, 2010.

[23] L Parnas, S Oral, and Ü Ceyhan. Optimum design of composite structures with curved fibre courses. *Composites Science and Technology*, 63(7):1071–1082, 2003.

[24] S Honda, T Igarashi, and Y Narita. Multi-objective optimization of curvilinear fibre shapes for laminated composite plates by using NSGA-II. *Composites Part B: Engineering*, 45(1): 1071–1078, 2013.

[25] M P Bendsoe and O Sigmund. *Topology optimization: theory, methods, and applications*. Springer Science & Business Media, 2013.

[26] A Panesar, I Ashcroft, D Brackett, R Wildman, and R Hague. Design framework for multifunctional additive manufacturing: coupled optimization strategy for structures with embedded functional systems. *Additive Manufacturing*, 16:98–106, 2017.

[27] A Sutradhar, J Park, D Carrau, T H Nguyen, M J Miller, and G H Paulino. Designing patient-specific 3-D printed craniofacial implants using a novel topology optimization method. *Medical & Biological Engineering & Computing*, 54(7):1123–1135, 2016.

[28] J P Blasques and M Stolpe. Multi-material topology optimization of laminated composite beam cross sections. *Composite Structures*, 94(11):3278–3289, 2012.

[29] J P Blasques. Multi-material topology optimization of laminated composite beams with eigenfrequency constraints. *Composite Structures*, 111:45–55, 2014.

[30] P G Coelho, J M Guedes, and H C Rodrigues. Multiscale topology optimization of bi-material laminated composite structures. *Composite Structures*, 132:495–505, 2015.

[31] Z B Zabinsky. *Stochastic adaptive search for global optimization*, volume 72. Springer Science & Business Media, 2013.

[32] M Walker and R E Smith. A technique for the multiobjective optimisation of laminated composite structures using genetic algorithms and finite element analysis. *Composite Structures*, 62(1):123–128, 2003.

[33] M Bagheri, A A Jafari, and M Sadeghifar. Multi-objective optimization of ring stiffened cylindrical shells using a genetic algorithm. *Journal of Sound and Vibration*, 330(3):374–384, 2011.

[34] O Erdal and F O Sonmez. Optimum design of composite laminates for maximum buckling load capacity using simulated annealing. *Composite Structures*, 71(1):45–52, 2005.

[35] M Akbulut and F O Sonmez. Optimum design of composite laminates for minimum thickness. *Computers & Structures*, 86(21):1974–1982, 2008.

[36] S N Omkar, J Senthilnath, R Khandelwal, G N Naik, and S Gopalakrishnan. Artificial Bee Colony (ABC) for multi-objective design optimization of composite structures. *Applied Soft Computing*, 11(1):489–499, 2011.

[37] C M C Roque and P Martins. Maximization of fundamental frequency of layered composites using differential evolution optimization. *Composite Structures*, 183(1):77–83, 2018.

[38] E Lund and J Stegmann. On structural optimization of composite shell structures using a discrete constitutive parametrization. *Wind Energy*, 8(1):109–124, 2005.

[39] J Stegmann and E Lund. Discrete material optimization of general composite shell structures. *International Journal for Numerical Methods in Engineering*, 62(14):2009–2027, 2005.

[40] E Lund, L Kühlmeier, and J Stegmann. Buckling optimization of laminated hybrid composite shell structures using discrete material optimization. In *6th World congress on structural and multidisciplinary optimization*, 2005.

[41] E Lund and J Stegmann. Eigenfrequency and buckling optimization of laminated composite shell structures using discrete material optimization. In *IUTAM Symposium on Topological Design Optimization of Structures, Machines and Materials*, pages 147–156. Springer, 2006.

[42] E Lindgaard, E Lund, and K Rasmussen. Nonlinear buckling optimization of composite structures considering "worst" shape imperfections. *International Journal of Solids and Structures*, 47(22):3186–3202, 2010.

[43] E Lindgaard and E Lund. Nonlinear buckling optimization of composite structures. *Computer Methods in Applied Mechanics and Engineering*, 199(37):2319–2330, 2010.

[44] K Svanberg. The method of moving asymptotes-a new method for structural optimization. *International Journal for Numerical Methods in Engineering*, 24(2):359–373, 1987.

[45] M M Abdalla, S Setoodeh, and Z Gürdal. Design of variable stiffness composite panels for maximum fundamental frequency using lamination parameters. *Composite Structures*, 81(2): 283–291, 2007.

[46] S Setoodeh, M M Abdalla, S T IJsselmuiden, and Z Gürdal. Design of variable-stiffness composite panels for maximum buckling load. *Composite Structures*, 87(1):109–117, 2009.

[47] C Bisagni and L Lanzi. Post-buckling optimisation of composite stiffened panels using neural networks. *Composite Structures*, 58(2):237–247, 2002.

[48] A L Araújo, P Martins, C M Mota Soares, C A M Soares, and J Herskovits. Damping optimization of viscoelastic laminated sandwich composite structures. *Structural and Multidisciplinary Optimization*, 39(6):569, 2009.

[49] M Kaufmann, D Zenkert, and P Wennhage. Integrated cost/weight optimization of aircraft structures. *Structural and Multidisciplinary Optimization*, 41(2):325–334, 2010.

[50] J Campen, C Kassapoglou, and Z Gürdal. Generating realistic laminate fibre angle distributions for optimal variable stiffness laminates. *Composites Part B: Engineering*, 43(2):354–360, 2012.

[51] M Montemurro and A Catapano. On the effective integration of manufacturability constraints within the multi-scale methodology for designing variable angle-tow laminates. *Composite Structures*, 161:145–159, 2017.

[52] D Haystead. Determining the optimal orientation of orthotropic material for maximizing frequency band gaps. Master's thesis, University of Toronto, 2012.

[53] N Challamel. On geometrically exact post-buckling of composite columns with interlayer slip-the partially composite elastica. *International Journal of Non-Linear Mechanics*, 47(3): 7–17, 2012.

[54] U A Girhammar. A simplified analysis method for composite beams with interlayer slip. *International Journal of Mechanical Sciences*, 51(7):515–530, 2009.

[55] S Schnabl and I Planinc. The effect of transverse shear deformation on the buckling of two-layer composite columns with interlayer slip. *International Journal of Non-Linear Mechanics*, 46(3): 543–553, 2011.

[56] Q H Nguyen, M Hjiaj, and P Le Grognec. Analytical approach for free vibration analysis of two-layer timoshenko beams with interlayer slip. *Journal of Sound and Vibration*, 331(12): 2949–2961, 2012.

[57] R Xu and D Chen. Variational principles of partial-interaction composite beams. *Journal of Engineering Mechanics*, 138(5):542–551, 2011.

[58] U A Girhammar and D Pan. Exact static analysis of partially composite beams and beam-columns. *International Journal of Mechanical Sciences*, 49(2):239–255, 2007.

[59] U A Girhammar and V K Gopu. Composite beam-columns with interlayer slip-exact analysis. *Journal of Structural Engineering*, 119(4):1265–1282, 1993.

[60] J Nie and C S Cai. Steel-concrete composite beams considering shear slip effects. *Journal of Structural Engineering*, 129(4):495–506, 2003.

[61] P Krawczyk, F Frey, and A P Zielinski. Large deflections of laminated beams with interlayer slips: Part 1: model development. *Engineering Computations*, 24(1):17–32, 2007.

[62] S P Timoshenko and J M Gere. *Theory of elastic stability*. Dover Publications, 2012.

[63] B K Lee and S J Oh. Elastica and buckling load of simple tapered columns with constant volume. *International Journal of Solids and Structures*, 37(18):2507–2518, 2000.

[64] K Garikipati, S Göktepe, and C Miehe. Elastica-based strain energy functions for soft biological tissue. *Journal of the Mechanics and Physics of Solids*, 56(4):1693–1713, 2008.

[65] A Magnusson, M Ristinmaa, and C Ljung. Behaviour of the extensible elastica solution. *International Journal of Solids and Structures*, 38(46):8441–8457, 2001.

[66] V V Kuznetsov and S V Levyakov. Complete solution of the stability problem for elastica of euler's column. *International Journal of Non-linear Mechanics*, 37(6):1003–1009, 2002.

[67] Hextow continuous carbon fibre products. `http://www.hexcel.com/Resources/Cont-Carbon-Fibre-Data-Sheets`.

[68] D D Samborsky, J F Mandell, and P Agastra. 3-D static elastic constants and strength properties of a glass/epoxy unidirectional laminate. *internal report. Department of Chemical and Biological Engineering, Montana State University*, 2012.

[69] V Srinivasa, V Shivakumar, V Nayaka, S Jagadeeshaiaih, M Seethram, R Shenoy, and A Nafidi. Fracture morphology of carbon fibre reinforced plastic composite laminates. *Materials Research*, 13(3):417–424, 2010.

[70] C L Nogueira, J M F Paiva, and M C Rezende. Effect of the interfacial adhesion on the tensile and impact properties of carbon fiber reinforced polypropylene matrices. *Materials Research*, 8 (1):81–89, 2005.

[71] H M Hsiao and I M Daniel. Elastic properties of composites with fibre waviness. *Composites Part A: Applied Science and Manufacturing*, 27(10):931–941, 1996.

[72] Z Gürdal, B F Tatting, and C K Wu. Variable stiffness composite panels: effects of stiffness variation on the in-plane and buckling response. *Composites Part A: Applied Science and Manufacturing*, 39(5):911–922, 2008.

[73] J N Reddy. *Mechanics of laminated composite plates and shells: theory and analysis*. CRC press, 2004.

[74] R D Cook. *Finite element modeling for stress analysis*. Wiley, 1995.

[75] T J R Hughes. *The Finite element method: linear static and dynamic finite element analysis*. Courier Corporation, 2012.

[76] O C Zienkiewicz, R L Taylor, and R L Taylor. *The finite element method: solid mechanics*, volume 2. Butterworth-heinemann, 2000.

[77] S Nagendra, S Kodiyalam, J Davis, and V N Parthasarathy. Optimization of tow fibre paths for composite design. In *Proceedings of the AIAA/ASME/ASCE/AHS/ASC 36th Structures, Structural Dynamics and Materials Conference, New Orleans, LA*, pages 1031–41, 1995.

[78] A Khani, S IJsselmuiden, and Z Gürdal. Design of variable stiffness panels for maximum strength using lamination parameters. *Composites Part B: Engineering*, 42(3):546–552, 2011.

[79] S Setoodeh, M M Abdalla, and Z Gürdal. Design of variable–stiffness laminates using lamination parameters. *Composites Part B: Engineering*, 37(4-5):301–309, 2006.

[80] E Lund. Buckling topology optimization of laminated multi-material composite shell structures. *Composite Structures*, 91(2):158–167, 2009.

[81] A W Blom, S Setoodeh, J M Hol, and Z Gürdal. Design of variable-stiffness conical shells for maximum fundamental eigenfrequency. *Computers & Structures*, 86(9):870–878, 2008.

[82] A Bjorck. *Numerical methods for least squares problems*. SIAM, 1996.

[83] C Canuto, M Y Hussaini, A Quarteroni, and T A Zang. *Spectral methods: fundamentals in single domains*. Springer Berlin Heidelberg, 2006.

[84] P Courrieu. Fast computation of Moore-Penrose inverse matrices. *Neural Information Processing-Letters and Reviews*, 8(2):25–29, 2005.

[85] V Klema and A Laub. The singular value decomposition: Its computation and some applications. *IEEE Transactions on Automatic Control*, 25(2):164–176, 1980.

[86] G H Golub and C Reinsch. Singular value decomposition and least squares solutions. *Numerische Mathematik*, 14(5):403–420, 1970.

[87] M B Giles and N A Pierce. An introduction to the adjoint approach to design. *Flow, Turbulence and Combustion*, 65(3-4):393–415, 2000.

[88] P Pedersen. Bounds on elastic energy in solids of orthotropic materials. *Structural Optimization*, 2(1):55–63, 1990.

[89] M W Tosh and D W Kelly. Fibre steering for a composite C-beam. *Composite Structures*, 53 (2):133–141, 2001.

[90] A Sabido, L Bahamonde, R Harik, and M van Tooren. Maturity assessment of the laminate variable stiffness design process. *Composite Structures*, 160:804–812, 2017.